EMERSON FERREIRA VILELA

SOIL GENESIS, MINERALOGY AND CHEMICAL COMPOSITION IN A STEATITE-SERPENTINITE OUTCROP UNDER TROPICAL HUMID CLIMATE IN BOM SUCESSO, BRAZIL

LAVRAS - MG
2019

EMERSON FERREIRA VILELA

SOIL GENESIS, MINERALOGY AND CHEMICAL COMPOSITION IN A STEATITE-SERPENTINITE OUTCROP UNDER TROPICAL HUMID CLIMATE IN BOM SUCESSO, BRAZIL

Tese apresentada à Universidade Federal de Lavras, como parte das exigências do Programa de Pós-Graduação em Ciência do Solo, área de concentração em Recursos Ambientais e Uso da Terra, para a obtenção do título de Doutor.

Prof. Dr. Yuri Lopes Zinn
Orientador

LAVRAS - MG
2019

Ficha catalográfica elaborada pelo Sistema de Geração de Ficha Catalográfica da Biblioteca Universitária da UFLA, com dados informados pelo(a) próprio(a) autor(a).

Vilela, Emerson Ferreira.
Soil genesis, mineralogy and chemical composition in a steatite-serpentinite outcropunder tropical humid climate in Bom Sucesso, Brazil / Emerson Ferreira Vilela. - 2019.
97 p.

Orientador(a): Yuri Lopes Zinn.

Tese (doutorado) - Universidade Federal de Lavras, 2019.
Bibliografia.

1. Rochas ultramáficas. 2. Gênese do solo. 3. Micromorfologia do solo. I. Zinn, Yuri Lopes. II. Título.

EMERSON FERREIRA VILELA

SOIL GENESIS, MINERALOGY AND CHEMICAL COMPOSITION IN A STEATITE-SERPENTINITE OUTCROP UNDER TROPICAL HUMID CLIMATE IN BOM SUCESSO, BRAZIL

Tese apresentada à Universidade Federal de Lavras, como parte das exigências do Programa de Pós-Graduação em Ciência do Solo, área de concentração em Recursos Ambientais e Uso da Terra, para a obtenção do título de Doutor.

APROVADO em 12 de fevereiro 2019.

Dr. Alberto Vasconcellos Inda	UFRGS
Dr. Zuy Maria Magriotis	UFLA
Dr. Carlos Alberto Silva	UFLA
Dr. Geraldo César de Oliveira	UFLA

Prof. Dr. Yuri Lopes Zinn
Orientador

LAVRAS - MG
2019

AGRADECIMENTOS

A Deus, por toda força concedida durante esta etapa.

A minha amada esposa Silvânia, que esteve sempre presente e dando suporte em todos os sentidos.

Aos meus pais, Devair e Cleuza e meus irmãos Wadson, Reggine, Junior e a minha sobrinha Maria Luiza que sempre me motivaram.

À minha nova família Antonio Pelinsari e Marleth Mól e aos seus filhos Antonio, Simone, Gustavo e Marleth, que me acolheu e apoiou.

À Universidade Federal de Lavras, especialmente ao Departamento de Ciência do Solo, pela oportunidade para a realização deste trabalho.

O presente trabalho foi realizado com o apoio do Conselho Nacional de Desenvolvimento Científico e Tecnológico (CNPq), da Fundação de Amparo à Pesquisa de Minas Gerais (FAPEMIG) e do Conselho de Aperfeiçoamento de Pessoal de Nível Superios – Brasil (CAPES).

Ao meu orientador e professor Dr. Yuri Lopes Zinn pela orientação, paciência, incentivo, confiança e ensinamentos.

Ao professor Alberto Vasconcellos Inda e a Universidade Federal do Rio Grande do Sul, por me receberem e pela valiosa contribuição no trabalho da tese e na minha formação e toda ajuda no trabalho.

Ao bolsista de iniciação científica Nathan Vicente Almeida, pelo auxilio com as análises.

Aos professores do Departamento de Ciência do Solo da UFLA pelos ensinamentos compartilhados durante o meu doutorado.

Aos colegas de departamento pela convivência e amizade.

Aos funcionários do Departamento de Ciência do Solo, em especial aos técnicos Dulce, Doroteo (Teo), Geila, Mariene, Lívia e Alexandre pelo apoio na realização das análises e pela enorme atenção e ajuda em todos os momentos necessários.

Aos obreiros e pastores da Igreja Universal que me receberam muito bem em Lavras.

Agradeço a todos que de alguma forma contribuíram para a realização deste trabalho.

RESUMO

Serpentinito e esteatito são rochas ultrabásicas metamorfizadas, constituídas de proporções variáveis de serpentina, talco e magnetita, dentre outros minerais incomuns. Solos derivados dessas rochas são tipicamente improdutivos devido ao excesso de Mg, baixo teor de P e elevados níveis de metais pesados, mas em países tropicais esses solos são ainda pouco estudados. Este trabalho visou compreender o processo de formação de oito solos derivados de esteatito-serpentinito no complexo ultramáfico do Morro das Almas, em Bom Sucesso - MG, e avaliar sua composição mineral e geoquímica. Os solos foram estratificados em quatro tipos básicos, em grau crescente de intemperismo: a) Neossolos Litólicos (3 perfis); b) Cambissolos (2 perfis); c) Latossolos (2 perfis) e b) Plintossolo Pétrico (1 perfil). Todos os solos apresentaram elevada densidade de partículas, mas baixa densidade de solo, devido à elevada porosidade de empilhamento associada à estrutura granular. O pH e teor de Mg trocável foram relativamente elevados, e houve ainda baixos teores de P e Al. A suscetibilidade magnética aumentou fortemente com o grau de intemperismo, devido a concentração de magnetita. Análises de fluorescência de raios-X mostraram que os Neossolos e Cambissolos possuem altos teores de MgO total (94 a 200 g kg^{-1}) e teores ainda maiores de Fe_2O_3, enquanto os Latossolos e Plintossolo são ainda mais concentrados em Fe_2O_3, embora também possuam teores significativos de MgO (6 a 30 g kg^{-1}). Os teores de SiO_2 e Al_2O_3 são relativamente baixos, embora a sílica seja mais expressiva nos Neossolos e Cambissolos, pobres em alumina, e nos Latossolos e Plintossolo a alumina predomina sobre a sílica. Tal composição incomum se deve à mineralogia das frações granulométricas, incluindo argilas, que possuem importante quantidade de talco nos Cambissolos e Neossolos, com presença bem menor de caulinita e óxidos secundários de Fe, enquanto os demais solos possuem concentrações expressivas de hematita. A serpentina não foi encontrada nos solos, embora presente na rocha, e o quartzo ocorre em baixa quantidade na areia, e provavelmente alóctone. O alto teor de MgO é devido a fragmentos de esteatito-serpentinito estarem preservados por uma crosta de óxido de ferro, visível macro- e microscopicamente. Altos teores totais de Cr_2O_6 (até 50 g kg^{-1} de solo) sugerem que parte dos picos de difração atribuídos à hematita se devem à cromita ($FeCrO_4$), enquanto os teores de NiO (até 6 g kg^{-1} de solo) são provavelmente devidos à substituição de Mg por Ni no talco, formando garnierita e co-precipitação em óxidos de Fe. O declive e aspecto influenciam fortemente a formação do solo e sua composição, e essa interação complexa resulta em formações variadas de floresta ombrófila de cânion, floresta semi-decidual e cerrado numa área pequena de 3,1 km^2.

Palavras-chaves: Rochas ultramáficas. Micromorfologia do solo. Gênese do solo. Laterita.

ABSTRACT

Serpentinite and steatite are metamorphic ultrabasic rocks, consisting of variable proportions of serpentine, talc and magnetite, among other unusual minerals. Soils derived from these rocks are typically unproductive due to excess Mg, low P content and high levels of heavy metals, but in tropical countries these soils are still poorly studied. This work aimed to understand the process of formation of eight steatite-serpentinite soils in the ultramafic complex of Morro das Almas, Bom Sucesso, Brazil, and to its mineral and geochemical composition. The soils were stratified into three basic types, in increasing degree of weathering: a) Lithic Udorthents (3 profiles); b) Oxic Dystrudepts (2 profiles); c) Acrudoxes (3 pedons). All soils presented high particle density, but low soil density due to the high packing void porosity associated to the granular structure. Soil pH and exchangeable Mg were relatively high, and there were low P and Al contents. Magnetic susceptibility increased strongly with the degree of weathering due to the concentration of magnetite. X-ray fluorescence analysis showed that Lithic Udorthents and Oxic Dystrudepts have high levels of total MgO (94 to 200 g kg^{-1}) and higher Fe_2O_3 contents, while Acrudoxes are even more concentrated in Fe_2O_3, although they also have levels of MgO (6 to 30 g kg^{-1}). The SiO_2 and Al_2O_3 contents are relatively low, although silica is more concentrated in the Lithic Udorthents and Oxic Dystrudepts, poor in alumina, whereas alumina predominates over silica in the other soils. This unusual composition is due to the mineralogy of the granulometric fractions, including clays, which have an important amount of talc in Lithic Udorthents and Oxic Dystrudepts, with much lower presence of kaolinite and secondary oxides of Fe, whereas the other soils have massive concentrations of hematite. Serpentine was not found in soils, although present in the rock, and quartz occurs in low quantity in the sand, and probably. The high contentes allochtone of MgO are due to fragments of steatite-serpentinite preserved by an iron oxide crust, visible macro- and microscopically. High levels of Cr_2O_6 (up to 50 g kg^{-1} soil) suggest that part of the diffraction peaks attributed to hematite are due to chromite ($FeCrO_4$), while higher NiO (up to 6 g kg^{-1} soil) was due to the substitution of Mg by Ni in the talc, forming garnierite and co-precipitation in Fe oxides. Slope and aspect strongly influence the formation of the soil and its composition, and this complex interaction results in varied formations of canyon cloud forest, semi-deciduous forest and savannas in a small area of 3.1 km^2.

Keywords: Ultramafic rocks. Soil micromorphology. Soil Genesis. Laterite.

LISTA DE ILUSTRAÇÕES

LISTA DE TABELAS

SUMÁRIO

1. INTRODUÇÃO

Esteatito e serpentinito são rochas ultrabásicas (muito pobres em sílica) metamorfizadas, com baixos teores de alumínio e elevados teores de Mg, Fe, e metais pesados como Cr e Ni. Devido a essa composição, solos derivados dessas rochas tendem a apresentar elevado teor de Cr e Ni, dentre outros metais pesados, e um predomínio de Mg em relação ao Ca, além de baixa fertilidade em geral (ALEXANDER; WILDMAN, 1985). O teor de Mg^{+2} trocável frequentemente ocupa mais de 60% da capacidade de troca de cátions, e além disso esses solos tendem a ser rasos e sujeitos à erosão (WHITE; DIXON, 2002). Como consequência, essas áreas possuem baixa aptidão para agricultura, com condições desfavoráveis para o pleno crescimento de plantas. O sistema Soil Taxonomy (SOIL SURVEY STAFF, 2010) considera que qualquer solo com mais de 40% de sua massa composta de minerais magnesianos, tal como serpentina, talco ou olivina, pertence à família de mineralogia magnésica, mas não se sabe se tal critério seria útil para solos brasileiros.

Rochas ultrabásicas / ultramáficas ocupam em geral menos de 1% da superfície terrestre (ECHEVARRIA, 2018). Na região de Lavras - Minas Gerais, as áreas com rochas ultramáficas correspondem a 1,6 % da superfície (Figura 1), mas sabe-se muito pouco sobre os solos formados a partir desses materiais de origem nas condições climáticas locais.

Figura 1 - Áreas com ocorrência de rochas ultramáficas na folha Lavras - Minas Gerais

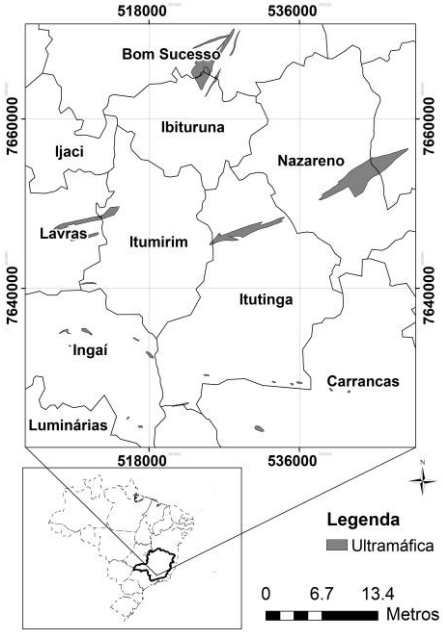

Fonte: Adaptado de CODEMIG, 2005 e IBGE. http://www.portalgeologia.com.br/index.php/mapa/#downloads-tab/. Acesso em 10/01/2019.

2. REFERENCIAL TEÓRICO

2.1 Rochas ultramáficas

As rochas ultramáficas são compostas por mais de 90 % de minerais máficos, isto é, silicatos ricos em ferro e magnésio, tais como olivina, piroxênio e serpentina (SZABÓ et al., 2009). As rochas ultramáficas normalmente também são ultrabásicas, ou seja, possuem menos de 45 % de sílica (SZABÓ et al., 2009). A sua composição apresenta poucos elementos essenciais para o crescimento e desenvolvimento das plantas, tais como, K, Ca e P, mas por outro lado, são importantes fontes de Ni e Co para o ecossistema terrestre (ECHEVARRIA, 2018). Essas rochas podem sofrer um processo de metamorfismo conhecido por serpentinização, o que leva a formação do mineral serpentina, e outros minerais como magnetita, brucita e talco (ECHEVARRIA, 2018).

Devido a essa composição pouco comum, os solos derivados de rochas ultramáficas não são recomendados para a agricultura, mas ocorrem sobre formações geológicas ricas em minerais que as tornam importantes para a mineração de produtos de importância industrial. Por exemplo, o serpentinito é resistente a altas temperaturas, possui baixa condutividade elétrica, e a cor verde o torna interessante para a ornamentação, embora a crisotila, polimorfo da serpentina, seja potencialmente cancerígena (WHITE; DIXON, 2002). O talco é usado em plásticos de propileno para aumentar a resistência e a temperatura de deformação, em computadores, tintas, automóveis, materiais refratários, indústria farmacêutica e de cosméticos, dentre outros (ZELAZNY et al., 2002).

O processo de formação de esteatito e serpentinito é o metamorfismo hidrotermal metassomático do peridotito, rocha ígnea do manto (ERNESTO et al., 2009). A serpentina e o talco não são formados por processos pedogenéticos, mas apenas por hidratação de minerais máficos. Esse processo de formação ocorre com a subducção da crosta oceânica por baixo da crosta continental (Figura 2).

Figura 2 - Formação de serpentina e talco.

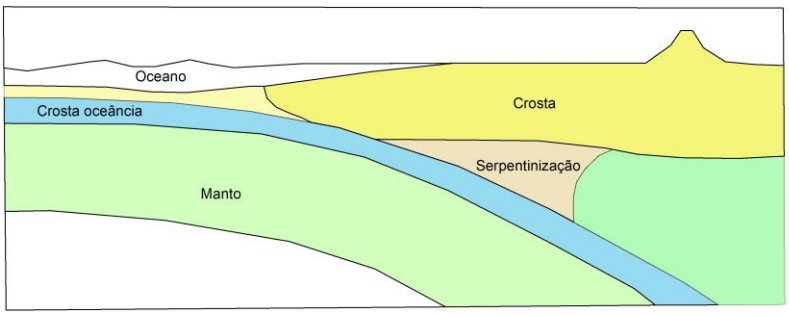

Fonte: Adaptado de Hyndman e Peacock (2003)

No processo de serpentinização, a olivina e o piroxênio são transformados em serpentina, um filossilicato trioctaedral 1:1 de magnésio (Figura 3), cujos principais polimorfos são a antigorita, crisotila e lizardita (RAJAKARUNA et al., 2009). O processo de formação da serpentina ocorre segundo a equação proposta por Pinti (2011): $(Fe,Mg)_2SiO_4 + nH_2O + CO_2 \rightarrow Mg_3Si_2O_5(OH)_4 + Fe_3O_4 + CH_4$.

A magnetita (Fe_3O_4) formada neste processo pode ser encontrada na fração grosseira dos solos formados, e a oxidação da magnetita forma a maghemita (Υ-Fe_2O_3) (SHAETZL; ANDERSON, 2005). Uma das principais características que a magnetita e maghemita conferem aos solos é alta suscetibilidade magnética.

Figura 3- Estrutura cristalina da lâmina octaedral da caulinita (dioctaedral) e da serpentina / talco (trioctaedral).

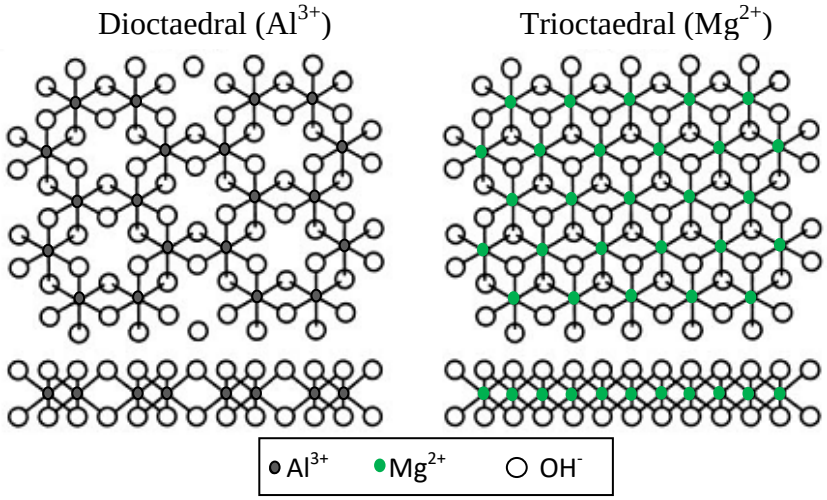

Fonte: Adaptado de Shaetzl e Anderson (2005)

Ao contrário da caulinita (filossilicato 1:1 dioctaedral), a lâmina octaedral da serpentina é formada por cátions divalentes, principalmente o Mg^{2+} (Figuras 3 e 4). Outro mineral formado por esse processo é o talco, que é um filossilicato trioctaedral 2:1, que tem como subgrupo o talco, quando a folha trioctaedral contém principalmente o Mg^{2+}, e willemseita, em que a folha trioctaedral contém principalmente o Ni^{2+}. Assim, o talco distingue-se dos outros filossilicatos comuns em solos, como vermiculita, esmectita e micas, pela ausência de carga nas camadas devido a ausência de substituição isomórfica nas camadas 2:1 (Figura 3). As camadas 2:1 no talco são mantidas juntas por fracas forças de van der Waals, levando, assim, o talco a ter uma escala de dureza de Mohs de 1 a 2, uma baixa condutividade elétrica e alta condutividade termal.

Figura 4 - Estrutura da camada de filossilicatos 1:1, dioctaedral (caulinita), 1:1 trioctaedral (serpentina) e 2:1 trioctaedral (talco).

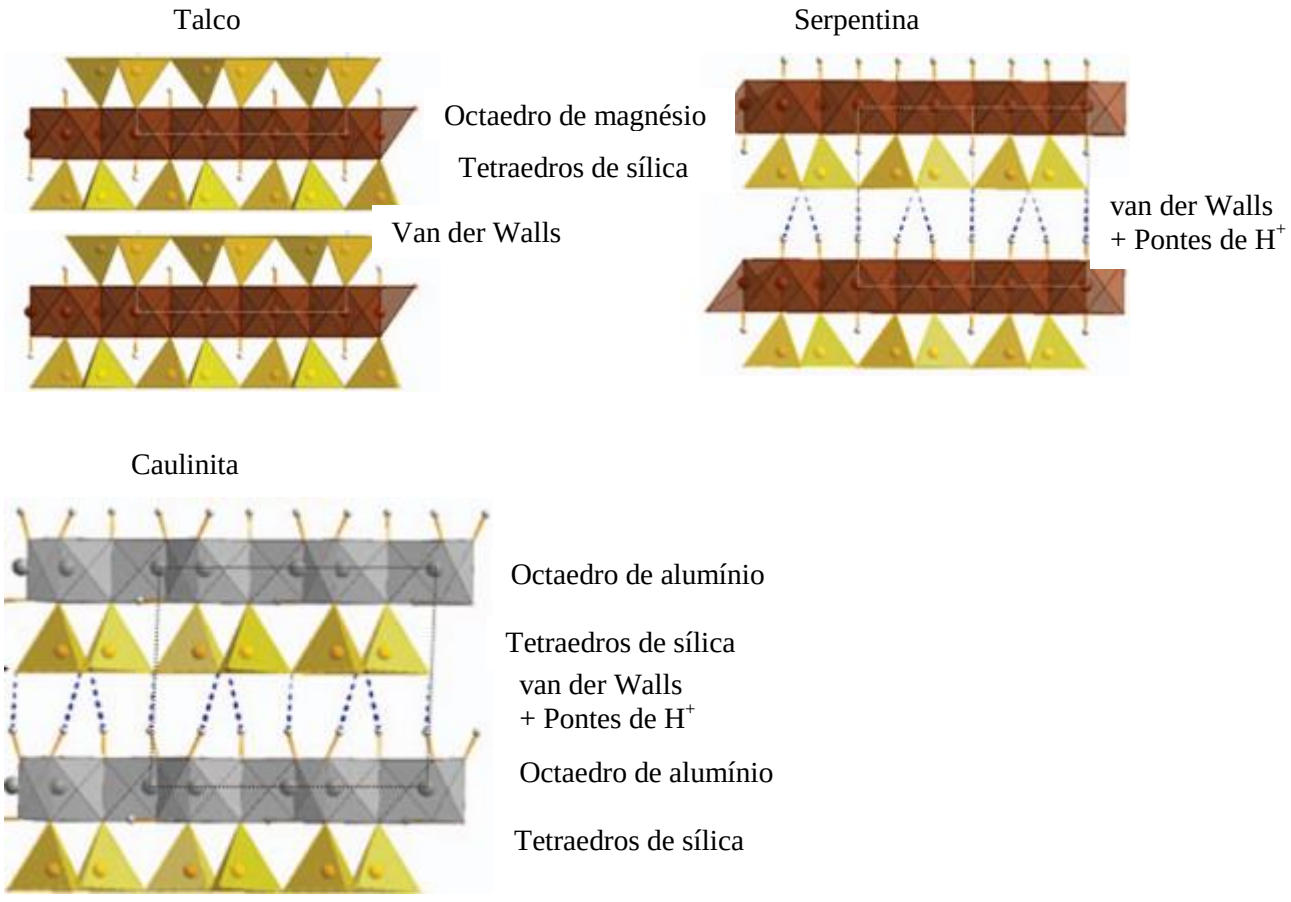

Fonte: adaptado de Tunega et al. (2012)

No Brasil, há poucos estudos sobre solos derivados de esteatito, sendo mais estudados os formados sobre serpentinito e rochas ultrabásicas não-metamorfizadas (VIDAL-TORRADO et al., 2007; GARNIER et al., 2009). No prolongamento mais a sudoeste do Supergrupo Minas, na região de Bom Sucesso – MG, ocorre uma grande diversidade litológica, que pode ser dividida em dois blocos distintos. A oeste, afloram unidades arqueanas, constituída por gnaisses, granitóides, anfibolitos, rochas máficas e ultramáficas, xistos e quartzitos (MACHADO FILHO et al. 1983), enquanto no bloco leste afloram rochas vulcano-sedimentares do tipo *greenstone belt* (Greenstone Belt Rio das Mortes, Nazareno e Dores do Campo) (NERI, 2013). O complexo ultramáfico Morro das Almas está localizado a oeste da Serra (Fig. 1), apresentando xistosidade paralela à orientação do Supergrupo Minas. As rochas do maciço incluem principalmente serpentinitos com raros vestígios de olivina (QUÉMÉNEUR et al., 2003). Contudo, o complexo ultramáfico Morro das Almas apresenta uma grande diversidade de materiais de origem, como esteatito, dunito, ortopiroxenito, zonas com acamamento ígneo, foliação metamórfica, fraturas, camadas nodulares de magnetita e cromita, crisotila, diques de diabásio e autólitos dúniticos (BARBOSA, 1998).

2.2 Intemperismo e formação de solo

O intemperismo de uma rocha depende dos seus minerais constituintes, sua textura e estrutura. Rochas com muitos minerais facilmente intemperizáveis são mais suscetíveis ao intemperismo (SHAETZL; ANDERSON, 2005). Além da composição química dos minerais constituintes, a suscetibilidade da rocha também depende do tamanho dos minerais formados. Rochas ígneas com textura fanerítica, ou seja, formadas por minerais com textura grosseira (visíveis ao olho nu), tendem a ser menos resistentes ao intemperismo do que rochas com os mesmos minerais em tamanho menor, afaníticas (textura fina). Isso se deve ao fato de ser mais fácil separar fisicamente os minerais maiores (SHAETZL; ANDERSON, 2005). O grau de cimentação dos minerais também influencia o intemperismo das rochas, sendo mais importante que a mineralogia.

A serie de Goldich (1938) compara a estabilidade dos minerais de tamanho >silte (tabela 1). Essa sequência indica que os primeiros minerais formados com o resfriamento do magma, em maiores temperaturas, são geralmente mais suscetíveis ao intemperismo. Esse comportamento se deve ao maior número de ligações iônicas formadas, pois o magma tem uma maior quantidade de metais disponíveis (FONTES, 2012). À medida em que o magma

vai esfriando, a quantidade de metais diminui, ocasionando um maior grau de condensação da estrutura, isto é, compartilhamento dos oxigênios entre os tetraedros de sílica. Com essa diminuição da razão Si/O, aumenta a quantidade de ligações com forte caráter covalente na estrutura, o que confere maior estabilidade (KÄMPF et al., 2016).

Tabela 1 - Série adaptada de Goldich: ordem de estabilidade dos minerais mais comuns frente ao intemperismo

Estabilidade dos minerais	Velocidade de intemperismo
Mais estável	Menor
Óxido de ferro (hematita)	
Hidróxido de alumínio (gibbsita)	
Quartzo	
Argilominerais	
Muscovita	
K-feldspato	
Biotita	
Albita	
Anfibólio	
Piroxênio	
Anortita	
Olivina	
Calcita	
Halita	
Menos estável	Maior

Minerais primários ricos em Fe e Mg se intemperizam mais rápido do que outros minerais pobres nesses elementos (GOLDICH, 1938). O Mg se hidrata facilmente e o ferro se oxida com facilidade, o que aumenta sua carga positiva, o que é equilibrado pela saída de cátions como Ca^{2+}, Mg^{2+} ou do Fe^{3+}, tornando a estrutura do mineral instável (KÄMPF et al., 2016). Dentre os filossilicatos, minerais trioctaedrais como a serpentina se intemperizam mais facilmente que os dioctaedrais, como a caulinita (Figura 4). Isso ocorre devido à repulsão dos H e OH para a cavidade vazia nos dioctaedrais, enquanto nos trioctaedrais o H e o OH se posicionam perpendicularmente à lâmina trioctaedral (AZEVEDO; VIDAL-TORRADO, 2016), o que a torna mais instável.

3. CONSIDERAÇÕES FINAIS

No Brasil, existem poucos trabalhos com solos derivados de rochas ultramáficas/serpentinito. Solos derivados de rochas ultramáficas serpentinizadas podem possuir composições mineralógicas pouco comuns ricas em talco, tremolita, olivina, serpentina e clorita (VIDAL-TORRADO et al., 2007). Essas áreas, mesmo em clima tropical, normalmente geram solos com características morfológicas e mineralógicas semelhantes àquelas em regiões de clima temperado (VIDAL-TORRADO et al., 2006). Uma característica comum desses solos é a cor muito avermelhada, devido ao alto teor de óxidos de ferro (GARNIER et al., 2009), principalmente hematita (ARAUJO, 2014).

Este trabalho visou descrever e compreender a composição geoquímica, mineral e física do solo e envolver os processos de formação em um afloramento esteatito-serpentinito no sudeste do Brasil. Este estudo pode também servir de subsidio para a avaliação da qualidade ambiental visando o desenvolvimento sustentável da região, e teve como hipóteses: 1) talco e serpentina são propensos a intemperismo rápido, e os solos deles formados não mais os possuem como componentes minerais; e 2) devido a esse intemperismo acelerado, os solos não mais possuem Mg como um dos componentes principais, apenas como o íon predominante do complexo de troca.

REFERÊNCIAS

ALEXANDER, E. B.; WILDMAN, W. E.; LYNN, W. C. Ultramafic (Serpentinitic) Mineralogy Class. In: Kittrick, J. A., ed. **Mineral Classification of Soils**. SSSA Spec. Publ. 16. SSSA and ASA, Madison, WI, 1985, p. 135-146.

ARAUJO, M. A. et al. Paragênese mineral de solos desenvolvidos de diferentes litologias na região sul de Minas Gerais. **Revista Brasileira de Ciência do Solo**, Viçosa, v.38, n.1, p. 11-15, 2014.

BARBOSA, M. I. M.. **Complexo ultramáfico acamadado Morro das Almas, região de Bom Sucesso e Ibituruna (MG):** Geologia, magmatismo e metamorfismo. 1998, 215 p. Tese (Doutorado em Geologia)-Universidade Federal do Rio de Janeiro - Instituto de Geociências, Rio de Janeiro, 2014.

CODEMIG, 2005. **Mapa Geológico de Minas Gerais.** Disponível em: <http://www.codemig.com.br/atuacao/mineracao/mapeamento-geologico/2013-mapa geologico-de-minas-gerais/>. Acesso em: 1 jan. 2019.

ECHEVARRIA, G. Genesis and behaviour of ultramafic soils and consequences for nickel biogeochemistry. In: **Agromining: Farming for Metals**. Springer, Cham. p.135-156, 2018.

ERNESTO et al., 2009. O interior da terra. In: Teixeira, W. et al. (Eds). **Decifrando a Terra**. São Paulo: IBEP, v. 98, p.50-77, 2009.

GARNIER, J. et al. Understanding the genesis of ultramafic soils and catena dynamics in Niquelândia, Brazil. **Geoderma**, v. 151, n.3/4, p. 204-214, 2009.

HYNDMAN, R. D.; PEACOCK, S. M. Serpentinization of the forearc mantle. **Earth and Planetary Science Letters**, v. 212, n. 3/4, p. 417-432, 2003.

MACHADO FILHO, L. et al. Geologia das Folhas 23/24 Rio de Janeiro e Vitória. In: OLIVEIRA, A. H., CARNEIRO, M. A. Campo Belo Metamorphic Complex: evolution of an Archean sialic crust of the Southern São Francisco Craton in Minas Gerais (Brazil). **Anais** da Academia Brasileira de Ciências, v. 73, n.3, p. 397-415, 2001.

NERI, M. E. N. V., ROSIÈRE, C. A., DE CARVALHO L. C. Supergrupo Minas na Serra de Bom Sucesso, extremo sudoeste do Quadrilátero Ferrífero-MG: Petrografia, geoquímica e isótopos de U-Pb. **Geologia USP**. Série Científica, v. 13, n. 2, p. 175-202, 2013.

PINTI, D. L. Serpentinization. In: GARGAUD, Muriel; AMILS, Ricardo; Cleaves, Henderson James (Ed.). **Encyclopedia of astrobiology**. Springer Science & Business Media, 2011.

QUÉMÉNEUR, J. J. G. et al. 2003. Geologia da folha Lavras 1: 100.000. In: Antônio Carlos Pedrosa Soares. (Org.). **Projeto Sul de Minas**, Belo Horizonte, p. 259-316.

RAJAKARUNA, N., HARRIS, T. B., ALEXANDER, E. B. Serpentine Geoecology of eastern north america: A review. **Rhodophora**, v.111, n. 945, p. 21-108, 2009.

SCHAETZL, R. ANDERSON, S. **Soils Genesis and Geomorphology**. Cambridge. 833 pp 2005.

TUNEGA, D.; BUCKO, T.; ZAOUI, A. Assessment of ten DFT methods in predicting structures of sheet silicates: Importance of dispersion corrections. **The Journal of Chemical Physics**, v. 137, n. 11, p. 114105, 2012.

VIDAL-TORRADO, P. et al. Gênese de solos derivados de rochas ultramáficas serpentinizadas no sudoeste de Minas Gerais. **Revista Brasileira de Ciência do Solo**. v.30, p.523-541, 2006.

VIDAL-TORRADO, P. et al. Evolução geoquímica e mineralógica em perfis de alteração sobre rochas serpentinizadas no sudoeste de Minas Gerais. **Revista Brasileira Ciência do Solo**, v.31, p.1069-1083, 2007.

WHITE GN.; JB DIXON 2002. Kaolin-serpentine minerals. In: Dixon, J.B. and Schulze, D. G. (eds.) **Soil Mineralogy with Environmental Applications**. Soil Sci. Soc. Amer. Inc. Madison, Wisconsin. pp. 389-412.

ZELAZNY, L. W., THOMAS, P. J., LAWRENCE, C. L. 2002. Pyrophyllite—Talc Minerals. In: Dixon, J.B. and Schulze, D. G. (eds.) **Soil Mineralogy with Environmental Applications**. Soil Sci. Soc. Amer. Inc. Madison, Wisconsin. p. 415-430.

SEGUNDA PARTE – ARTIGO

Artigo elaborado de acordo com as normas do periódico Catena (versão submetida).

Soil genesis, mineralogy and chemical composition in a steatite-serpentinite outcrop under tropical humid climate in Bom Sucesso, Brazil

Emerson Ferreira Vilela[1], Alberto Vasconcellos Inda[2], Yuri Lopes Zinn[1*]

[1] Graduate Program in Soil Science, Federal University of Lavras. Campus, Lavras MG, Brazil, P.O. Box 37200-000, Brazil.

[2] Graduate Program in Soil Science, Federal University of Rio Grande do Sul. Av. Bento Gonçalves 7712, Porto Alegre RS, P.O. Box 91540-000, Brazil.

* Corresponding author: ylzinn@dcs.ufla.br

Abstract

Serpentinite and steatite are metamorphic, ultrabasic rocks composed by variable proportions of serpentine, talc, magnetite and other unique minerals. Soils developed from weathering of these rocks are typically unproductive due to excess Mg and low P contents, aside with high levels of heavy metals, but the extent of such limitations in the humid tropics is still poorly known. Here, we aimed to study pedogenesis, morphology and composition of eight soils formed from steatite-serpentinite in the Morro das Almas ultrabasic complex in Bom Sucesso, Brazil. These soils were classified in three basic groups, in increasing stage of weathering: a) Lithic Udorthents (3 pedons); b) Oxic Dystrudepts (2 pedons); and c) Acrudoxes (3 pedons). All soils presented high particle density but low bulk density due to high packing void porosity associated to granular structure. Soil pH and exchangeable Mg^{+2} were relatively high, whereas Mehlich-I P and exchangeable Al^{+3} were very low. X-ray fluorescence data showed that Entisols and Inceptisols have high (94 a 200 g kg^{-1}) MgO contents, whereas Oxisols are highly enriched in Fe_2O_3, although still bearing MgO contents as high as 30 g kg^{-1}. Such unusual chemical composition is explained by the mineralogy of all particle sizes, composed by important amounts of talc in Entisols and Inceptisols, which also had Fe oxides

and small amounts of kaolinite, whereas the dusky red Oxisols are highly concentrated in hematite. Although present in the parent material, serpentine was not detected in soils, and quartz occurred in low amounts as sand, probably allochtonous. The considerable amounts of MgO in Oxisols can be explained by rock fragments preserved by a dark Fe oxide coating, visible in thin sections and also in the field. High Cr_2O_6 contents, reaching 50 g kg^{-1}, suggesting that part of the X-ray diffraction peaks ascribed to hematite are actually due to chromite ($FeCr_2O_4$), whereas NiO contents reaching 6 g kg^{-1} are probably due to substitution for Mg in talc, forming garnierite, aside with co-precipitation within Fe oxides. Magnetic susceptibility was high and increased strongly the weathering stage as indicated by total Fe_2O_3. Local topography, especially slope and aspect, strongly controlled soil formation and composition, in a complex interaction that allowed for the existence of three climax vegetations: canyon cloud forests, semi-deciduous forests and Cerrado savannas, suggesting that soil limitations to growth of native plants are lower than previously expected.

Keywords: soils of extreme environments, magnesic mineralogy class, magnetic susceptibility, soil micromorphology.

1. Introduction

There is increasing need to study soil formation processes occurring through alteration of unusual parent materials, which range from anthropogenic residues and rubble to natural but rare rocks such as metallic ores (e.g., banded iron formations) and ultrabasic rocks. Unlike acid, intermediate and basic rocks, which are typical of the Earth´s crust, ultrabasic rocks are chemically similar to the Earth's mantle (MacGregor, 1979). Such rocks are composed mainly by Mg and Fe silicates, are marked by low contents of light elements such as Al and P, and contain high levels of heavy metals such as Co, Cr and Ni (Echevarria, 2018; Rajakaruna et al., 2009). Many of the world´s ultrabasic rocks are found in very old, typically Proterozoic terranes, and thus have underwent widespread metamorphism. A common metamorphic process of ultrabasic rocks is hydrothermal alteration or serpentinization, which consists of infiltration of hot water (~ 350 ^{o}C) into rock fractures and hydration of pre-existent mafic minerals (Ruberti et al., 2009; USDA, 2018). Under these conditions, hot water enriched in Mg and heavy metals (Vidal-Torrado et al., 2007) transforms olivines and pyroxenes into serpentine and talc (Evans, 2004), among other minerals such as Mg hydroxides and carbonates. During the serpentinization process, Fe^{2+} can be partly retained in the structure of

talc and serpentine, or released and partially oxidized, forming magnetite (Fe_3O_4) and H_2 (Syverson et al., 2017). The most common metamorphic rocks thus formed, typically from peridotite and dunite protoliths (Ernesto et al., 2009), are talc-schists and serpentinites.

In regard to pedogenesis, all ultrabasic rocks decompose into unique soils, due to their unusual major and minor chemical composition, coupled to their often rapid weathering. Crystalline ultrabasic rocks are typically composed by olivines and pyroxenes, which are highly weatherable (Kampf et al., 2016), but also hard (> 5 in the Mohs scale) minerals (Schumann, 2008). However, most minerals in talc-schists and serpentines have low Mohs hardness values (<2), and thus are expectably more weatherable than their predecessors, which can result in very fast release of Si, Mg and other ions during pedogenesis. Serpentines are a group of 1:1 magnesium phyllosilicate minerals with three polymorphs of $Mg_3Si_2O_5(OH)_4$: antigorite, chrysotile (a type of asbestos) and lizardite (Rajakaruna et al., 2009), in addition to garnierite, a Ni-rich variety (Mottana et al., 1987). Serpentines have a crystalline structure similar to that of kaolinite, although trioctahedral, and yield similar diffraction peaks, which are stable upon heating at 550 ^{0}C, unlike kaolinite. The term "serpentine" was coined due to its similarity to snake scales (Barbosa, 1998). Talc ($Mg_3Si_4O_{10}(OH)_2$) is a 2:1 trioctaedral mineral containing Mg in the trioctaedral sheet, with little or no isomorphic substitution able to generate surface charges, and talc-like species with trioctahedral Ni^{2+} and Fe^{2+} are also known (Zelazny et al., 2002). Talc-schists and serpentinites often include the same main minerals talc and serpentine, only varying in their respective predominance, and a common variety of whitish, soft talc-schist is known as soapstone or steatite (Mottana et al., 1987).

Serpentine soils have since long been recognized as unique not only in genesis and composition, but also on the vegetation associated with them (e.g., Alexander et al., 1985; Krukeberg, 1992). Under Mediterranean climates such as in parts of California, soils derived from serpentinite and peridotite are often shallow, occur on barren and steep slopes, have poor water retention capacity and show red colors due to the formation of secondary Fe oxides, despite their abundant serpentine, olivine and pyroxene (Alexander, 2004; Rajakaruna et al., 2009; Kierczark et al., 2016). Under warm, humid climates, serpentinite is rapidly weathered, and thus magnetite and chromite are the main primary minerals found in soils due to their higher resistance to weathering (Alexander, 2010). Thus, in most areas of Brazil, serpentine soils on gentle slopes are highly weathered, very deep and rich in Fe-oxides due to residual concentration, which can result in lateritic Ni ores (Garnier et al., 2009). However, on steep

slopes or under cooler climate, where weathering is slower and erosion/rejuvenation is stronger, shallow soils with abundant talc and amphiboles in the clay fraction have also been described (Vidal-Torrado et al., 2006, 2007). Another remarkable feature of the mineralogy of serpentine or ultramafic soils is that kaolinite, often considered the most widespread clay mineral in the world, is usually absent (Araujo et al., 2014), which can be ascribed to the low Al levels in the parent material.

In regard to chemical composition and exchangeable cations, soils derived from serpentine and crystalline ultrabasic rocks are characterized by the excess of Mg relatively to Ca, high concentrations of Cr, Ni and other heavy metals, and generally low fertility (Alexander et al., 1985). In consequence, these areas have low agricultural aptitude, but can be economically important due to mining activities, especially of Ni (Alexander, 2010; Garnier et al., 2009; Siebecker et al., 2017), and some have been developed for housing and other purposes. There are relatively much fewer data on soils derived from steatites or other talc-rich rocks, especially in the humid tropics (e.g., Santana et al., 2001; Guerra, 2015), but it is generally expected that these soils are similar to serpentine soils.

Despite the relatively small area occupied by ultrabasic rock outcrops, their unique composition poses not only agricultural limitations but also environmental hazards, and thus efforts for the study of their soils and properties are critical to proper sustainable development. In the present work, we aim to describe and understand soil physical, mineral and geochemical composition and involved formation processes on a steatite- serpentinite outcrop in southeastern Brazil. The hypotheses tested are: 1) since talc and serpentine are prone to rapid weathering under the local tropical humid climate, these minerals will be mostly absent from a suite of soils; and 2) in consequence of the former hypothesis, Mg removal from soil components will be nearly complete, thus Mg excess would occur only in exchangeable forms.

2. Materials and Methods

2.1 Environmental setting and sampling

The study area is located in the state of Minas Gerais, Brazil, in the district of Aureliano Mourão, near Bom Sucesso (Figure 1). The ultramafic complex of *Morro das Almas* occupies ca. 8.17 km², and is located at the foothills of an itabirite range that actually is the southernmost extension of the Iron Quadrangle (*Quadrilátero Ferrífero*), which ranks

among the largest mining provinces of the world. The regional geology is dominated by Archean acid and basic rocks (Queméneur e Noce, 2000), although the main elevations are the itabirite and ultrabasic hills. A full petrographic characterization of the ultramafic complex showed the occurrence of serpentinite, steatite, and also dunite, pyroxenite, Fe-oxide nodules, chrysotile, and diabase dikes (Barbosa, 1998). However, in the area specifically sampled of *Morro Paraíso*, we found only fresh steatite and serpentinite, their saproliths and tafoni, a highly porous saprolith with honeycomb-weathering pits (Bloom, 1998), all occurring in sizes from boulder to gravel. In addition, phenocrysts of massive talc and fibrous magnetite also occur scattered in the area, as well as black obsidian, associated to mafic dykes (Barbosa, 1998). Fragments of all these parent materials were collected for some of the analyses described below.

According to the Köppen classification, the regional climate is Cwa, warm temperate (mesothermic) with dry winters and rainy summers, with mean annual temperature and rainfall of 19.4^{o}C and 1,530 mm, respectively (Dantas et al., 2007). In regard to vegetation, the area is on the transition between the Atlantic Forest (*Mata Atlântica*) and Central Savanna (*Cerrado*) biomes, and despite the small area, three different native vegetations occur: 1) on the summit and W-NW aspects of Morro das Almas, the dominant vegetation is a sparse savanna interspersed on a boulder field (Fig. 2); 2) on the N and NE aspects, as well as along a drainageway on the piedmont, a semi-deciduous forest occurs; and 3) on the S and SW aspects, facing the *Rio das Mortes* canyon, the dominant vegetation is a cloud rainforest probably fed by moisture condensation retained within the narrow canyon. The only agricultural land use is a pasture, in the W-SW slopes and on the piedmont.

After a series of visits to the site, which is of very difficult access even by foot due to boulders and often steep slopes, we selected eight representative soils for this study. Soil profiles were excavated to a minimal depth of 1 m or reaching lithic or petroferric contact, described and sampled by horizon. Each profile was georeferenced and classified according to Soil Taxonomy (Soil Survey Staff, 2010). Table 1 summarizes soil classification, position on landscape and aspect, land cover and geographical information. Slope was determined with a clinometer and ranged from 5 to 90%. Fig. 2 shows the location of each soil and the elevation plot of two transects passing through the summit and the canyon. In all cases, soils developed from the weathering of steatite and/or serpentinite, except for the soil on the drainageway, which can be considered as forming from ironstone after steatite-serpentinite.

In each described profile, undisturbed samples were taken for determination of bulk by the core method of each horizon, and also for micromorphological description with PVC Kubiena boxes, in the B horizon when available. In addition, bulk samples of each horizon were taken for chemical, physical and mineralogical analyses. Soil samples were passed through 2 mm sieves and the percentage of gravel and pebbles (> 2 mm) was calculated based on weight. Interestingly, gravels and pebbles were often black and hard on their surface, but light-colored and soft inside, and thus could be easily cut with a spade or knife. However, in the soil on the drainageway/ironstone, all stones, gravels and pebbles were very hard and were cut only with difficulty.

<<<<<INSERT FIG. 1. AND FIG.2. HERE >>>>>

2.2 Physical and chemical characterization

Soil particle-size distribution was determined by the pipette method (Gee and Or, 1986), using dispersion with NaOH (1 mol L^{-1}), slow shaking for 16 hours, sieving the slurry < 53 μm and using 2-53 μm as the size limit for silt. Soil bulk density was determined by weighing after drying undisturbed soil cores for 24 hours at 105^{o}C (Blake and Hartge, 1986). Soil particle density was determined by the pycnometer method (Blake and Hartge, 1986), and the same method was also used for finely ground parent materials.

Soil fertility characterization was assessed using the following methods compiled by Teixeira et al. (2017), except when noted otherwise: pH was measured in H_2O and KCl 1 mol L^{-1} at a 1: 2.5 soil-liquid ratio (v / v). Exchangeable Ca^{2+}, Mg^{2+} and Al^{3+} were extracted with 1 mol L^{-1} KCl; Ca^{2+} and Mg^{2+} were determined by atomic absorption spectrophotometry and Al^{3+} by titration with NaOH 0.025 mol L^{-1}. Available K and P were extracted with Mehlich-I solution (HCl 0,05 mol L^{-1} + H_2SO_4 0,025 mol L^{-1}), with K^{+} determined by flame photometry and P by colorimetry at 725 nm. Exchangeable H + Al was determined indirectly by potentiometric decrease of a buffered SMP solution at pH 7.5 (Quaggio & van Raij, 2001). Total soil carbon was determined in finely ground (<105 μm) samples by dry combustion in a Vario TOC Cube (Elementar Americas, Hanau, Germany) analys.

Finely ground (<105 μm) samples of soils were also analyzed by selective extractions of poorly crystalline or amorphous Fe and Al hydroxides with acid ammonium oxalate (Schwertmann, 1973; Jackson et al., 1986) and of total Fe oxides and hydroxides pedogenic with Na-dithionite-citrate-bicarbonate (DCB, Mehra and Jackson, 1960). The extracts were

analyzed by plasma optical emission spectrometry inductively coupled (ICPOES) - Spectro – Blue, Germany, aiming to determine not only Fe and Al but all elements detectable in each sample. In order to determine total chemical composition, samples of parent materials and bulk soils were finely ground (<105 μm), mixed with wax to form a pat and analyzed by semi-quantitative X-ray fluorescence on a WDXRF – S8 Tiger (Bruker), working at 4kW, 60 kV and 170 mA.

2.3 Parent material and soil mineralogy, micromorphology and magnetic susceptibility

Mineralogical characterization of parent materials, and soil size separates was performed by X-ray diffraction in finely ground samples. Soil samples (20 g) were previously treated with hydrogen peroxide at 80^{o}C for the oxidation of organic matter, then were dispersed with 0.1 N NaOH, as described above for particle-size analysis. The sand fraction was collected with a 53 μm sieve, and the clay fraction was separated from the silt + clay suspension by siphoning, according to Stokes' law. The identification and characterization of the minerals were carried out by means of X-ray diffractometry in a Bruker D2 Phaser apparatus using Cu-α radiation filter (λ = 1,54 Å) operating at 30kV and with a Lynxeye^{TM} fast linear detector module, using the software DiffracSuite^{TM}. The scanning amplitude employed in the silt and sand samples was 4 to 50^{o}2θ, at an angular velocity of 0.02^{o}2θ s^{-1} oriented with a scanning speed of 2 °2θ min^{-1} to silt and sand fractions and 1 °2θ min^{-1} to clay fraction. Likewise, ground samples of the sampled source materials were treated.

Undisturbed soil samples in Kubiena boxes were air-dried for 60 days, then oven-dried at 60 ^{o}C for 24 hours prior to at 24 hours at 105 ^{o}C, for impregnation with an epoxy resin. The impregnated samples were kept at a vacuum for 72 h, then heated for 4 hours at 100 ° C and 4 hours at 140 ° C for hardening and curing, respectively. The resin blocks were cut with diamond saw, polished with sandpaper and glued on glass slides with Thin Section epoxy Hillquist® resin in a resin/hardener rate of 7: 3. Due to the unusual nature of the sampled soils, the mounted slides were easily destroyed during cutting, so after many trial-and-error steps, the slides were diamond-cut sequentially at the decreasing thicknesses of 300, 200, 150 and 100 μm, and then lapped carefully by hand to 30 μm with a fine corundum paper. The thin sections were cleaned from abrasive remnants with an ultrasonic bath and described according to Stoops (2003) with a petrographic microscope coupled to a digital camera.

Magnetic susceptibility (χ) of ground parent materials, fine earth and clay fractions was measured using a Bartington MS2 magnetometer device at low (0.47 KHz, χlf) and high frequency (4.7 kHz, χhf). The percentage of frequency dependence on magnetic susceptibility

(χfd) was calculated by the following equation (Dearing, 1999): χfd (%) = 100 x [(χlf - χhf) / χlf]. The amount of maghemite was estimated as the χlf in the clay fraction (Poggere et al., 2018).

3. Results

3.1 Characterization of soil parent materials

The main parent material found at the study area was originally identified in the field as serpentinite, since it was very similar and at short distances from the serpentinite described earlier by Araujo et al. (2014), for which X-ray diffraction showed only serpentine and spinel minerals. However, in the present study, fresh samples of the main rock collected showed large peaks of serpentine but also smaller peaks of talc (Fig. 3a). In addition, massive phenocrysts of a fibrous mineral initially suspected to be asbestos, found scattered in the area, were shown by X-ray diffraction to be actually highly crystalline, elongated talc (Fig. 3b), with no serpentine. Two samples of massive saprolites, removed from soil profiles, showed only peaks of talc, and small peaks of amphiboles and magnetite (Fig. 3a), but no serpentine, similarly to the highly porous tafoni saprolites (Fig. 3b). Due to the complex pattern of occurrence of serpentine and talc in fresh rocks and saprolites, for simplicity the main parent material in this work will be referred to as steatite-serpentinite, as it cannot be exactly identified in every sampled location. Coarse obsidians showed as expected no diffraction peaks, whereas large fibrous magnetite phenocrysts where highly crystalline, although containing pedogenic gibbsite (Fig. 3c). Nearly all these parent materials showed peaks of goethite deriving from weathering of Fe-bearing phases, as well as some peaks of hematite-like minerals that can both be secondary or primary (see next paragraphs).

In terms of geochemical composition, X-ray fluorescence results showed that the steatite-serpentinite and massive talc showed <45% SiO_2 and <4% Al_2O_3, aside with MgO contents > 18% (Table 2). In addition, Cr_2O_3 and NiO generally occurred in higher contents than K_2O and CaO, and Mg/Ca rates were very high, in consistence with ultrabasic rocks. Similar results were noted for the common and tafone saproliths. The magnetite phenocrysts showed 77% Fe_2O_3 and 20% Al_2O_3, and the highest NiO contents. The composition of the obsidian contrasts sharply with those of the other parent materials, with high CaO, K_2O and

Al_2O_3 contents, in accord to its formation in narrow mafic dikes crossing the ultramafic complex (Barbosa, 1998), from which obsidian is the only non-weathered remnant.

The fresh rock and massive talc presented particle densities of ca. 2.75 g cm^{-3}, whereas particle densities of saproliths reached 3.05 g cm^{-3} (Table 2). The magnetite phenocrysts presented a density of 4.58 g cm^{-3}, a little lower than the standard values of 5.2 g cm^{-3} (Mottana et al., 1987), which may be due to partial hydration. The magnetic susceptibility was as expected very high in magnetite phenocrysts (ca. 360 m^3 kg^{-1}x 10^{-6}), and very low in the steatite-serpentinite and massive talc, increasing > 20-fold in the saprolites, due to weathering and formation of secondary Fe-oxides (Table 2).

<<<<< INSERT TABLE 2, FIG 3 HERE>>>>>

3.2 Soil morphology, physical and chemical characterization

The eight studied soils were stratified into 3 basic types: 1) Lithic Udorthents, shallow (<30 cm depth) soils found at the summit and in the two steepest slopes (35 and 90%, respectively of NE and S aspect); 2) Oxic Dystrudepts, deep (>100 cm depth) soils on slopes of 15% (NW) and 30% (SW); and 3) Acrudoxes, deep soils on slopes < 20%, piedmont and drainageway (Tables 1,3, Fig. 2). Although such stratification disposed soils into contrasting groups of limited and advanced weathering stages, all soils and most horizons were remarkably similar in regard to some key properties.

A brief morphological and physical characterization description of the sampled soils is presented in Table 3. All soils and horizons presented granular structure, with ped size varying from medium to very fine, and with friable or very friable moist consistency. Clods from Entisols, Inceptisols and the Oxisol on the W face presented a marked greasy feel when manipulated, as well as some hydrophobicity. Munsell colors varied from yellowish red (hues 2.5 to 5YR) in Entisols and Inceptisols, and from 2.5YR to dusky red (5R) in Oxisols. All soils presented considerable gravel contents (18 to 797 g kg^{-1}), and with exception of two organic-matter rich A horizons, presented high particle densities, reaching 3.8 g cm^{-3}. However, due to the granular structure and thus high packing void porosity, bulk densities were in most cases in the 1.0-1.3 g cm^{-3} range, except in some organic-rich A1 horizons, reaching 0.3 g cm^{-3}, and in some bottom horizons, ranging from 1.3 to 1.8 g cm^{-3}. Clay contents were generally high, typically ranging from 300 to 642 g kg^{-1}, except for the Petroferric Acrudox, in which clay contents were <190 g kg^{-1}, since most of this soil is composed by concretionary ironstone (Araujo et al., 2014; Zinn et al., 2015).

In terms of chemical properties, many similarities were also noted (Table 4). Soil pH in water (pH_{H2O}) was variable, but generally high for tropical humid soils, reaching 6.7. More importantly, pH values above 6.0 were noted in unexpected horizons, such as in the organic-rich A1 of the Inceptisol under cloud forest, and A and B horizons of Oxisols. Soil pH_{H2O} increased with increasing depth in Oxisols and in the deeper NW Inceptisol, a pattern noted earlier by other soils on ultrabasic rocks (e.g., Vidal-Torrado et al., 2007; Hseu et al., 2015). This pattern is likely due to higher contents of organic C and thus carboxylic groups in surface horizons, and to active weathering of serpentine and talc near the weathering front, releasing proton-consuming SiO_4^{-4} and $Mg(OH)_6^{-4}$. Such high pH values also suggested the possible presence of carbonates, but no reaction with HCl 10% occurred at room temperature (negative for calcite) and even at 80 ^{0}C only the deeper horizons of two soils showed a slight bubbling (Table 4), indicative of magnesite ($MgCO_3$) and/or siderite ($FeCO_3$). Values of pH in KCL 1 mol L^{-1} (pH_{KCl}) in Oxisols were mostly >5.0 and >pH_{H2O}, indicating a predominance of positive vs. negative surface charges, i.e. an acric character (Soil Survey Staff, 2010), also noted in the deeper Inceptisol. Also not common in most tropical humid soils, exchangeable Al^{+3} content in all soils was very low or zero, even in the more acidic Oxisols. The sum of exchangeable bases (Ca^{+2}, Mg^{+2} and K^+) was < 4 $cmol_c$ kg^{-1} in the Oxisols, but also in the Entisol on summit and the deeper Inceptisol, suggesting these less weathered soils underwent pronounced base leaching. Conversely, two Entisols and one Inceptisol presented higher base levels and eutrophic horizons, as well as high-activity clays. In most soils and horizons, Mg^{+2} was the predominant exchangeable cation: the average Mg/Ca ratio was 2.7, and reached 9.9 in one Inceptisol. In addition, the Mg/Ca ratio increased with increasing depth in most cases, probably due to the lesser distance to the weathering front (Table 4).

Soil organic carbon contents were moderate to high, and decreased with increasing depth in most soils (Table 4). As expected, soils under the cloud forests (Entisol on S aspect and Inceptisol on SW) presented the highest organic carbon levels, reaching 13.7%, which can be attributed to higher biomass production in these sites. The levels of Mehlich-1 P were always low, and only in the superficial horizons they exceeded 1 mg kg^{-1}.

<<<<<INSERT TABLES 3, 4 HERE >>>>>

3.3 Geochemical, mineralogical and micromorphological characterization

The semi-quantitative X-ray fluorescence was able to determine an average 87% of the total sample mass as expressed in oxide form, with lower recovery values for organic-rich topsoils and higher rates for Fe-rich soils (Table 5). In comparison to the main soil parent materials, i.e. steatite/serpentinite (Table 2), all soils, except for the Entisols on the steep slopes, were greatly depleted in SiO_2, especially the Petroferric Acrudox (Table 5). Similarly, MgO contents also decreased in all soils except for the Entisol on the steeper slope, and interestingly, even in the Oxisols MgO reached values of ca. 30 mg kg^{-1}. Conversely, in comparison to the parent material, Al_2O_3 and Fe_2O_3 contents increased in all soils by residual accumulation, again with the exception of the steepest-slope Entisol, and especially for Fe_2O_3, which reached 670 g kg^{-1} in the Petroferric Acrudox. This value is very similar to the 720 g kg^{-1} determined with electron-dispersion spectroscopy by Araujo et al. (2014). The contents of CaO, K_2O, P_2O_5 and especially MnO were also higher than those in the parent material. Although the Cr_2O_3, NiO, TiO_2 and ZrO_2 contents varied greatly in the main parent materials, in soils these elements were generally enriched, except for the steepest Entisol, and were especially high in the Petroferric Acrudox (Table 5), due to residual accumulation. The Fe_2O_3 contents across all soils and horizons were positively correlated with contents of Al_2O_3, Cr_2O_3, ZrO_2, TiO_2, NiO and MnO, and negatively correlated with SiO_2, MgO and CaO (Figure 4).

Fe oxides contents extractable with dithionite (Table 6) comprised in average half of the total Fe_2O_3 as determined by X-ray fluorescence (Table 5), except for the two Oxisols with the highest total Fe_2O_3 contents, where this rate is ca. 40%. Considerable amounts of the total concentrations of other major elements were also extractable by dithionite: an average 11% of total soil SiO_2 and 37% of Al_2O_3 were present in the lattice of soil Fe oxides. The percentage of total MgO (as determined by X-ray fluorescence) released from Fe oxides was low in Mg-rich Entisols and Inceptisols (3-12%), whereas in Mg-poor Oxisols ca. 50% of total MgO was comprised within Fe oxides. The amounts of K and Ca extractable with dithionite were similar or greater than those of Mn, a common co-precipitate in Fe oxides. The levels of Cr, Ni and Ti extractable by dithionite were low, but still much greater than those of P, which has great affinity for Fe oxides.

Much lower contents of all these elements, but especially Fe, were extracted with acid oxalate from amorphous or short-range order Fe oxides. The Fe-oxalate/Fe-dithionite ratio was <0.04 (Table 7), indicating that Fe oxides are highly crystalline, and this ratio varied little among all soils. The only element to be found mostly in short-range order oxide phases was

Mn, since MnO extractable by oxalate was in most cases >50% of MnO-dithionite. This pattern of very small crystal size and high surface area of Mn oxides is well known, even for soils developed from common soil parent materials (White and Dixon, 2002). CaO-oxalate contents were below the detection limit of the device.

<<<<< INSERT FIG.4., TABLES 5, 6 HERE>>>>>

Due to the complexity of the local geological formation, we calculated several ratios between elemental contents as determined by different analyses to better assess variability of parent materials and soils (Table 7). Total Ti/Zr ratios, as determined by X-ray fluorescence, were generally >30 in Entisols and Inceptisols but not in Oxisols, and varied little along depths of an individual soil profile. Conversely, Ti/Zr rates in dithionite and oxalate extracts were higher in Oxisols than in Entisols and Inceptisols. These combined results suggest that the steatite-serpentinite was relatively homogeneous in Morro das Almas, since the lower total Ti/Zr ratios in Oxisols can be explained by partial weathering of Ti-bearing minerals, less resistant than those of Zr (Fitzpatrick & Chittleborough, 2002), and partial leaching from soils. The higher Ti/Zr ratios in dithionite and oxalate are explained by incorporation of part of the released Ti as short-range order oxides within Fe-oxides. The Ni/Cr ratios calculated from X-ray fluorescence data, both elements common in ultrabasic rocks, varied little (0.06-0.26) among soils, supporting the idea of parent material homogeneity in the area. When calculated for dithionite extracts, Ni/Cr ratios were higher (0.1-0.65), especially in the more weathered Oxisols, whereas for oxalate data these ratios were mostly >1 and higher in less weathered soils or horizons. Such affinity of released Ni for Fe-oxides was reported earlier (Siebecker et al., 2017). The total Mg/Ca ratio, which in steatite-serpentinite and talc was >1,800 (Table 2), and dropped starkly to <110 in A horizons, although increased strongly with depth within the same soil, near the weathering front. However, in dithionite extracts the Mg/Ca ratios were much lower, <3 in dithionite extracts, and could not be calculated in oxalate extracts since Ca was below detection limits. The higher solubility of Mg in comparison to Ca was responsible for this marked decreasing trend, noted also in the exchangeable forms (Table 4).

All Entisols presented strong peaks of talc in the clay fraction, which intensity decreased in the order S> NE> summit (Figure 5). Strong talc peaks were also noted in the Inceptisols (Figs. 5,6), but only as traces on the Oxisol of the W slope, and were absent in the

other Oxisols (Fig.6). The Entisol on the S slope show narrow, small peaks of 14.5 Å in the sand and silt frations, that can be ascribed to chlorite (not shown, see Vilela, 2019). Small or very small peaks of 7.2 Å were observed in five soils, and were initially ascribed to serpentine. However, their collapse after heating at 550 ^{o}C for 2 hours suggests that the peaks were actually of kaolinite, i.e. that serpentine is more unstable than talc, under the regional climate. In the Entisols, the strongest kaolinite peaks were noted on the NE and S slopes, whereas the summit showed no kaolinite, as well as the Inceptisol on the NW slope. In the other soils, kaolinite was less frequent and with smaller peaks, whereas the Plinthic Acrudox did not present kaolinite, as noted earlier (Araujo et al., 2014).

Hematite showed strong diffraction peaks in all soils, although peak width was variable and the peak of 2.5 Å was greatly increased in soils with talc, which has a coincident secondary peak. Diffraction peaks for goethite were noted in all soils, and in Entisols they were larger in the summit soil, followed by the S and NE slopes. The Inceptisol on the SW slope presented the strongest goethite peak, followed by the soils on slopes W, NW, and piedmont. The Plinthic Acrudox presented the weakest goethite peaks. Entisols and the NW Inceptisol did not present gibbsite peaks, which occurred in the other soils, with stronger peaks in the Oxisol in the W slope.

Peaks for magnetite / maghemite were visible only in the clay of the Plinthic Acrudox (Fig. 6). However, all soils showed very high magnetic susceptibility (9.7-210.0 $m^3\ kg^{-1}.10^{-6}$, Table 8) in comparison to the low values of steatite-serpentinite (0.2 $m^3\ kg^{-1}.10^{-6}$, Table 2) and the magnetite phenocrysts (360 $m^3\ kg^{-1}.10^{-6}$). The lowest magnetic susceptibility occurred in the Entisol of the S slope, and the highest in Plinthic Acrudox. This pattern also occurred in the sand and silt fraction (not shown, see Vilela, 2019) and in the clays (Table 8), which showed even higher susceptibility values than the bulk soil. The contents of maghemite in soils, estimated from magnetic susceptibility data of the clay fractions (Poggere et al., 2018), suggest that a considerable part of total soil magnetism is composed by this mineral. Magnetic susceptibility was also strongly correlated with total Fe_2O_3 (r^2=0.80).

The main geochemical and mineralogical data are reflected in soil thin sections (Fig. 7). The microstructure of Entisols and the Inceptisol on the SW slope was in subangular to angular blocks, partially separated and partially accommodated along planar pores, consistent with predominance of face-to-face arrangements of platelike phyllosilicates, i.e. talc and to a much lesser degree, kaolinite. Conversely, the microstructure of the NW Inceptisol and the Oxisols is granular, consistent with predominance of hematite droplets, surrounded by highly

interconnected packing voids, which favor excessive drainage. Nevertheless, all soils showed a red micromass indicative of the important presence of clay-sized hematite, so the thin sections had to be lapped to 15-20 µm to be transparent enough for description. The b-fabrics in most soils were stipple-speckled, granostriated and crystallitic (Stoops, 2003), the latter being only caused by talc domains. A very similar fabric was noted chlorite-talc saprolites near the study area (Guerra, 2015), although this author reported Fe-rich clay coatings not observed in the present study. The only pedofeatures observed were nodules of Fe-oxides, and some showed effervescence with diluted H_2O_2, due to Mn oxides. Most importantly, all soils show fragments of steatite-serpentinite or saprolite coated with dark Fe-oxides, even in the most weathered soil, the Plinthic Acrudox. Such coatings, also visible macroscopically in gravels, were certainly involved in the preservation of Mg in soils, not only as talc but probably also within its alteromorphs of goethite or amorphous hydrated oxides, noted by yellowish-brown colors (Fig. 7), or hematite.

4. Discussion

4.1 On soil genesis and composition

The main parent material at the site study site has been identified either as steatite (Barbosa, 1998) or serpentinite (Araujo et al. 2014). However, in the field these rocks were very similar morphologically and can only be identified by X-ray diffraction. In Fig. 3, serpentinite shows larger peaks for serpentine than talc, whereas the massive talc shows no serpentine peaks, and the serpentinite diffraction by Araujo et al. (2014) showed no talc peaks. This is the reason why the area is referred to as an ultramafic complex (Barbosa, 1998), implying that it is very difficult to map exactly where each rock occurs, and thus in the present work we chose to refer to steatite-serpentinite as the main parent material. The preliminary alteration of these rocks into saprolites and tafoni has apparently resulted in rapid destruction of serpentine, which disappeared from diffraction patterns whereas talc was preserved and goethite peaks appeared of increased (Fig. 3). The tafoni saprolite, a very unusual feature in tropical humid climates, is commonly attributed to hemispherical exfoliation by evaporation-driven salts (Bloom, 1998) in Mediterranean or drier climates. In the present study, the tafoni saprolites (not shown, see pictures in Vilela, 2019) were found only in the drier sites under savanna vegetation, and probably result from corrosion due to excess magnesia ($Mg(OH)_6^{-4}$) liberated from talc-serpentine weathering on the boulders.

Working with pyroxene-serpentine-olivine ultrabasic rocks in a warmer environment, Garnier et al. (2009) noted the presence of Ni-rich smectites (nontronite), which is consistent with fast weathering of those minerals. Interestingly, smectites were not observed in the present study, suggesting that either talc is more resistant to weathering or that a talc-smectite direct alteration or neoformation is not viable in the well-drained soils. However, as weathering proceeds into Oxisol formation, talc is eventually altered, although its coating by Fe-oxides (Fig. 7) can effectively delay this decomposition and the ensuing Mg release.

As noted already in the saprolites, serpentine was absent from even the less weathered soils (Figs. 5,6). The mechanisms for kaolinite formation in these soils are unclear as no Al-rich silicate minerals were present in the parent materials, but it is possible that Al included as contaminant in magnetite, talc and serpentine was liberated after their weathering and substituted Mg within serpentine or talc alteromorphs. Alternatively, kaolinite could form from direct alteration of amphiboles as reported by Guerra (2015) in chlorite-talc schists, and in fact these minerals occur in the ultramafic complex as the last product of the hydrothermal alteration of olivines (Barbosa, 1998). Finally, Al released from all these minerals can combine with released silica in neoformed kaolinite. The latter mechanism is perhaps more likely due to the rather weak and broad kaolinite peaks, but the main point is that kaolinite is a minor to trace mineral in the studied soils, which is unusual since most soils in the region, formed from non-ultrabasic rocks, are rich in kaolinite (e.g., Araujo et al., 2014). In any case, it remains clear that talc is much more stable than serpentine under tropical humid climate, which can be due to the presence of only siloxane on basal surfaces, when compared with the siloxane-magnesia surfaces of serpentine. The instability of serpentine was apparently not attenuated by coating of rock fragments with Fe-oxides (Fig. 7). Thus, our first hypothesis was confirmed for serpentine, which was obliterated from all soils, but it was only partially confirmed for talc, which in the highly weathered Oxisols has nearly disappeared.

Figure 4 shows the accumulation and depletion patterns of major and minor elements as Fe is residually accumulated as secondary, but probably also primary oxides. The unusual geochemical composition of the studied soils can be explained by their mineralogy rich in talc, present in all particle sizes (Fig. 7, see also X-ray diffractions for sand and silt in Vilela, 2019). With the increasing stage of weathering, magnesia and silica are eventually leached away, and residual accumulation of Fe and Al ensued in all soils, but especially in the Oxisols. Total Fe_2O_3 > 60% occurred in the deep, well-drained piedmont Oxisol, and especially in the Plinthic Acrudox on the drainageway, where dissolved Fe from uplands

probably was conveyed into and Fe oxides coalesced, forming a continuous ironstone that is currently being hydrated and disintegrating into soil material (Zinn et al., 2015; Fig. 7p,q). In addition, the high Cr_2O_3 content of all soils, reaching 5% in the Plinthic Acrudox (Table 5) suggests the important presence of chromite ($FeCr_2O_4$) as the main stable Cr phase, noted earlier by Barbosa (1998). However, this mineral is of difficult observation since, aside with hematite and magnetite, it is opaque in this sections and its diffraction peaks coincide with those of the hematite. Ni also underwent residual accumulation, but it is more likely contained in talc (garnierite variation or willemseite) and co-precipitated the secondary oxides of Fe (Table 7, Siebecker et al., 2017). Quartz, absent from the parent materials, was rarely seen in thin sections, and occurred more frequently in the piedmont and drainageway Oxisols. This paucity of quartz is another unusual feature of the studied soils, and probably the quartz contained in these soils came transported from the surrounding areas either by wind or sediment flow, the latter onto the piedmont and drainageway Oxisols. Ti and Zr are also residually accumulated in this weathering sequence adequately described by Fe accumulation.

Although the classification of the Entisols and Oxisols was relatively straightforward in the field, such was not the case for the Inceptisols, which due to their thickness >1 m, red colors and granular structure were initially thought to be Oxisols. This initial classification was questioned by analytical data showing large peaks of talc (Figs. 5,6) and MgO contents ranging from ca. 9 to 14% (Table 5), which according to Table 2 would correspond to >40% of talc in the soil mass, exceeding by far the maximum amount of weatherable minerals for Oxisols (Soil Survey Staff, 2010). In fact, > 40% talc is among the the criteria for the magnesic mineralogy family in Soil Taxonomy (Soil Survey Staff, 2010). Although this percentage in Soil Taxonomy refers to serpentine, talc and other Mg-rich silicates, and a small part of the Mg in the studied soils is apparently included in Fe oxides lattices, the percentage of MgO in the present work is enough to include all Entisols and Inceptisols as in the magnesic family. Therefore, the second hypothesys was rejected, since high levels of Mg were preserved in Entisols and Inceptisols, and even the Oxisols showed residual Mg forms. In addition, the present work shows an untapped potential of using X-ray fluorescence, or other total chemical composition methods, as a much easier tool to identify magnesic soils than counting grains on a petrographical microscope, which anyway can only be done for sand, but not for silt and clay separates.

The effect of local topography was critical in determining soil genesis. The less weathered soil, either by criteria of Fe accumulation, limited Mg depletion or macro- and

micromorphology, was the Entisol on the steep (90%) slope carved by the Rio das Mortes canyon, which undergo strong rejuvenation and constant exposure of fresh rock to weathering. Conversely, the Entisol on the summit, although being the shallowest (< 10 cm) of all soils, presented a composition richer in Fe and poorer in Si and Mg compared to othe Entisols, suggesting pronounced leaching. The Entisol on the 35% NE slope presented intermediate properties between those two extreme Entisols. In regard to the Inceptisols, their thicker profiles either resulted from gentler slopes, i.e. less erosion (NW slope), or deposition from upland (SW slope), resulting in a great depth more typical of Oxisols, despite their current weathering stage more similar to the Entisols. It is also evident that Oxisols only form in slopes <20%, which allowed for limited erosion, excessive drainage and strong leaching (piedmont and W slopes). The formation of ironstones along drainageways, which gave rise to the Plinthic Acrudox, probably results from dissolved Fe inputs from the wider uplands and their precipitation as hematite.

4.2 On soil fertility and other environmental aspects

The base saturation is generally >25% (Table 4), which is relatively high in comparison to most soils in the study region (e.g. Araujo et al., 2014). In fact, four out of eight soils presented euthrophic horizons, including an Oxisol, but can not be interpreted as chemically fertile soils due to the magnesic mineralogy and the excess Mg in comparison to Ca. Although most Mg was effectively removed from saprolites and soils, Mg^{+2}/Ca^{+2} rates in KCl extracts were seldom <1.0 and often exceed 2.0. It is not known to what extent such imbalance would affect cultivated plants in the study area, although the literature often refers that such conditions are not favorable (e.g., Alexander, 2010). Other hindrances may occur due to very low available P levels (Table 4), not only due to the inherently low P in the parent material, but to its fixation in pedogenic Fe-oxides, which abound even in the less weathered soils. Those limitations can be perhaps more consequential to plant growth than likely benefits from the low or nil exchangeable Al^{+3} levels.

However, it is important to note that, despite the unusual soil properties and limitations described above, a rather diverse and productive forest and savanna vegetation was nevertheless established in the area. The cloud forests in the S and SW slopes receive a continuous moisture flow from condensation along the river canyon, and the biomass produced is enough to provide thick soil coverage (Fig. 2) and high (>10%) total soil organic carbon in topsoils. Not distant from this canyon, the climax vegetation are semi-decidual

forests currently covering the Entisol on the NE slope and the Plinthic Acrudox, which have soil carbon contents > 2%. The savannas on the summit, W and NW slopes are the most limited plant formations, marked by short trees and sparse grass and herbs which provide only ca. 50% soil coverage. These savannas were vegetation which more closely resemble the serpentine barrens and low-biomass communities typically described under Mediterranean or drier climates (e.g., Alexander 2004; Rajakaruna et al., 2009; Kierczark et al., 2016). However, it is possible that these features are more due to excessive insolation and high soil temperature on the shallow summit soils, and to thick soil depth in W and NW slopes, promoting low water availability, than to inherent soil fertility limitations. In fact, the diversity in vegetation in serpentine soils has been reported earlier and ascribed to water availability (e.g., Alexander, 2014), but in the present study such large variation occurred inexpectedly in a very small area.

Total carbon contents in topsoils under savanna range between 2.0 and 3.7 %, which are high compared to other Cerrado soils with comparable clay contents under more productive savanna vegetations (e.g., Zinn et al., 2011). This higher carbon content can also be attributed to imbalanced ratios of nutritional elements that can also affect decomposing organisms. The thick Oxisol on the piedmont is currently under a fairly-productive *Urochloa* sp. pasture, which was never fertilized or limed. However, soils derived from ultrabasic rocks are known for having high concentrations of hazardous heavy metals such as Co, which were not assessed in the present study and deserve further attention.

Conclusions

In the present study, we presented physical, chemical, mineralogical and micromorphological data showing a wide variety of soils occur in a small area, and that these soils have unique properties that set them apart from tropical humid soils developed from common rocks. Furthermore, the soils studied here also contrast with others developed from ultrabasic rocks, under tropical climate or not. The considerable presence of talc in all particle size fractions of the less weathered soils, aside with high to moderate Mg contents and predominance of Fe oxides in the more weathered soils, are particular features of the studied soils that is not often reported in the literature, which raises interest in potential studies about environmental services and soil processes.

Although most soil properties in soils with both limited and advanced stages of weathering are typically considered not consistent with adequate plant growth, the study area

actually showed diverse plant formations within a small area, suggesting that the soils developed from ultrabasic rocks under tropical humid climate are perhaps not the extreme environments commonly reported under drier or cooler climates.

Acknowledgments

This research was funded by the Brazilian National Research Council (CNPq), which provided a scholarship grant and bench fees to E.F. Vilela, and research grants to A.V. Inda and Y.L. Zinn. We thank Geila Carvalho and Luiz R.G. Guilherme (Univ. Fed. Lavras) for supplies and help with the X-ray fluorescence apparatus. Finally, we thank Carlos A. Silva (Univ. Fed. Lavras) for the C analyses.

References

Alexander, E. B., 2004. Serpentine soil redness, differences among peridotite and serpentinite materials, Klamath Mountains, California. International Geology Review, 46(8), 754-764.

Alexander, E. B., 2010. Old Neogene summer–dry soils with ultramafic parent materials. Geoderma 159 (2), 02-08. https://doi.org/ 10.1016/j.geoderma .2010.06.006.

Alexander, E.B. 2014. Arid to humid serpentine soil, mineralogy and vegetation, Klamath Mountains, USA. Geoderma 116, 114-122.

Alexander, E. B., Wildman, W. E., Lynn, W. C., 1985. Ultramafic (Serpentinitic) Mineralogy Class. in: Kittrick, J. A., (Ed.), Mineral Classification of Soils. SSSA Spec. Publ. 16. Soil Science Society of America, American Society of Agronomy, Madison, WI. pp. 135-146. doi:10.2136/sssaspecpub16.c12

Araujo, M. A., Pedroso, A. V., Amaral, D., Zinn, Y., 2014. Paragênese mineral de solos desenvolvidos de diferentes litologias na região sul de Minas Gerais. Rev. Bras. Ciênc. Solo 38 (1), 11-15 (in Portuguese).

Blake, G.R., Hartge, K.H., 1986. Particle density. In: Klute, A. (Ed). Methods of soil analysis. 2.ed. Madison, American Society of Agronomy,. Part 1. pp.377-382.

Barbosa, M. I. M., 1998. Complexo ultramáfico acamadado Morro das Almas, região de Bom Sucesso e Ibituruna (MG): Geologia, magmatismo e metamorfismo. (Thesis). Universidade Federal do Rio de Janeiro - Instituto de Geociências, 215 pp. (in portuguese).

Bloom, A. L., 1998. Geomorphology – a systematic analysis of late Cenozoic landforms. Upper Saddle River, NJ, Prentice Hall (3rd ed.).

Codemig, 2005 http://www.codemig.com.br/atuacao/mineracao/mapeamento-geologico/2013-mapa geologico-de-minas-gerais/. (accessed March 11th, 2018).

Dantas, A. A. A., Carvalho, L. D., Ferreira, E., 2007. Classificação e tendências climáticas em Lavras, MG. Ciênc. Agrotec., Lavras, 31 (6), 1862-1866.

Dearing, J. A. Environmental magnetic susceptibility: using the Bartington MS2 system. 2.ed. Kenilworth: Chi Publishing, 1999. 54 p.

Echevarria, G. 2018. Genesis and behaviour of ultramafic soils and consequences for nickel biogeochemistry. In: Agromining: Farming for Metals. Springer, Cham. p. 135-156.

Embrapa, Centro Nacional de Pesquisa em Solos, 2011. Manual de métodos de análise de solo, 2th Ed. Embrapa- CNPS, Rio de Janeiro 230 pp. (in Portuguese).

Ernesto, M., Marques, L. S., McReath, I., Ussami, N., Pacca, I. I. G., 2009. O interior da terra. In: Teixeira, W., Fairchild, T. R., Toledo, M. C. M., Taioli, F. (Eds). Decifrando a Terra. 2ed. São Paulo: IBEP. 98, pp 50-71 (in portuguese).

Evans, B. W. 2004. The serpentinite multisystem revisited: chrysotile is metastable. International Geology Review. 46 (6), 479-506.

Fitzpatrick, R. W., Chittleborough, D. J. 2002. Titanium and zirconium minerals. In: Dixon, J.B. and Schulze, D. G. (eds.) Soil Mineralogy with Environmental Applications. Madison, Soil Sci. Soc. Am. pp. 667-690.

Garnier, J., Quantin, C., Guimarães, E., Garg, V. K., Martins, E. S., Becquer, T., 2009. Understanding the genesis of ultramafic soils and catena dynamics in Niquelândia, Brazil. Geoderma, 151 (3/4), 204-214. https://doi.org/10.1016/j.geoderma.2009.04.0 20

Gee, G.W., and D. Or. 2002. Particle-size analysis. In: J.H. Dane and G.C. Topp (eds.) Methods of soil analysis. Part 4. Physical methods. SSSA Book Series No. 5. Madison, Soil Sci. Soc. Am. p. 255–289.

Guerra, A.R. 2015. Saprolitos na região Sudeste do Brasil: morfologia, classificação e evolução física-geoquímica-mineralógica. Ph.D. thesis (in Portuguese). Piracicaba, Esc. Sup. Agric. Luiz de Queirós. Available at http://www.teses.usp.br/teses/disponiveis/11/11140/tde-13042015-095939/pt-br.php (acessed Feb. 28th, 2019).

Hseu, Zeng-Y., Zehetner, F., Ottner, F., Iizuka, Y., 2015. Clay-mineral transformations and heavy-metal release in paddy soils formed on serpentinites in eastern Taiwan. Clay Clay Miner. 63 (2), 119-131. https://doi.org/10.1346/ CCMN.2015.0630204.

Jackson, M. L., Lim, C. H., Zelazny, L. W., 1986. Oxides, hydroxides and aluminosilicates. Section 6-3, in: A. Klute. (Ed). Methods of soil analysis. Part 1 - Physical and mineralogical methods. 2 ed. Agronomy 9, 113-118.

Kampf, N., Curi, N., Marques, J. J. 2016. Intemperismo e ocorrência de minerais no ambiente do solo. In: Melo, F. V, Alleoni, L. R. (Eds.) Química e mineralogia do solo. p. 333-379

Kierczak, J., Pędziwiatr, A., Waroszewski, J., Modelska, M., 2016. Mobility of Ni, Cr and Co in serpentine soils derived on various ultrabasic bedrocks under temperate climate. Geoderma, 268, 78–91. https://doi.org/10.1016/j.geoderma.2016.01.025

Krukeberg, A.R., 1992. California serpentines – flora, vegetation, geology, soils & management problems. U. California Press. pp. 196.

Macgregor, I. D., 1979. Mineralogy of model mantle compositions. In: P. J. Wyllie (Ed.). Ultramafic and Related Rocks. John Wiley and Sons, Inc., New York. pp. 382–393.

Mehra, O. P., Jackson, M. L., 2013. Iron oxides removal from soils and clays by a dithionite-citrate system buffered with sodium bicarbonate. Clay Clay Miner. 7. 317-327. https://doi.org/10.1016/B978-0-08-009235-5.50026-7.

Mottana, A., Crespi R., Liborio G. 1987. Guide to rocks and minerals. New York, Simon & Schuster. pp. 607.

Poggere, G. C., Inda, A. V., Barrón, V., Kämpf, N., de Brito, A. D. B., Barbosa, J. Z., Curi, N., 2018. Maghemite quantification and magnetic signature of Brazilian soils with contrasting parent materials. Applied Clay Science, 161, 385-394. https://doi.org/10.1016/j.clay.2018.05.014

Quaggio, J. A., van Raij, B., 2001. Determinação do pH em cloreto de cálcio e da acidez total. In: van Raij, B., Andrade, J.C., Cantarella, H., Quaggio, J.A., (Eds.). Análise química para avaliação da fertilidade de solos tropicais. Campinas, Instituto Agronômico de Campinas. pp.181-188. (in portuguese).

Quemeneur, J. J. G., Noce, C. M. (2017). Geochemistry and petrology of felsic and mafic suites related to the Paleoproterozoic Transamazonian orogeny in Minas Gerais, Brazil. Revista

Rajakaruna, N., Harris, T. B., Alexander, E. B., 2009. Serpentine geoecology of eastern north america: A review. Rhodophora. 111 (945), 21-108. https://doi.org/10.3119/07-23.1.

Ruberti, E., Szabó G. A. J., Machado, R., 2009. Metamorfismo: processo e produtos. In: Teixeira, W., Fairchild, T. R., Toledo, M. C. M., Taioli, F. (Eds). Decifrando a Terra. 2ed. São Paulo: IBEP. 98, pp 400-417. (In Portuguese)

Santana, G. P., Fabris, J. D., Goulart, A. T., Santana, D. P., 2001. Magnetite and its transformation to hematite in a soil derived from steatite. Rev. Bras. Ciênc. Solo, 25(1), 33-42. (In Portuguese)

Siebecker, M. G., Chaney, R. L., Sparks, D. L. 2017. Nickel speciation in several serpentine (ultramafic) topsoils via bulk synchrotron – based techniques. Geoderma, 298, 35-45. https://doi.org/10.1016/j.geoderma.2017.03.008.

Schumann, W. Minerals of the World. Sterling Publishing Company, Inc., 2008.

Schwertmann, U. 1973. Use of oxalate for Fe extraction from soils. Can. J. Soil Science. 53 (2), 244-246.

Soil Survey Staff, 2010. Keys to Soil Taxonomy, eleventh ed. USDA-Natural Resources Conservation Service, Washington, DC.

Syverson, D. D., Tutolo, B. M., Borrok, D. M., Seyfried Jr, W. E., 2017. Serpentinization of olivine at 300 °C and 500 bars: An experimental study examining the role of silica on the reaction path and oxidation state of iron. Chemical Geology, v. 475, p. 122-134, 2017. https://doi.org/10.1016/j.chemgeo.2017.11.006

Stoops, G. 2003. Guidelines for Analysis and Description of Soil and Regolith Thin Sections. Soil Sci. Soc. Am. Madison.

Teixeira, P.C., Donagemma, G, K., Fontana, A., Teixeira, W. G. Manual de métodos de análise de solo. 3. ed. rev. Brasília, DF: Embrapa, 2017. 230 p.

United States Department of Agriculture – USDA. Serpentine soils and plant adaptations. Forest Service. https://www.fs.fed.us/wildflowers/beauty/ serpentines/ adaptations.shtml. (accessed March, 11th, 2018).

Vidal-Torrado, P., Macias, F., Calvo, R., Carvalho, S. G. D., Silva, A. C., 2006 Gênese de solos derivados de rochas ultramáficas serpentinizadas no sudoeste de Minas Gerais. Rev. Bras. Ciênc. Solo. 30, 523-541. (In Portuguese).

Vidal-Torrado, P., Calvo, R., Macias, F., Carvalho, S. G., Silva, A. C., 2007. Evolução geoquímica e mineralógica em perfis de alteração sobre rochas serpentinizadas no sudoeste de Minas Gerais. Rev. Bras. Ciênc. Solo. 31, 1069-1083. (In Portuguese).

Vilela, E. F. 2019. Soil genesis, mineralogy and chemical composition in steatite-serpentinite outcrop under tropical humid climate in Bom Sucesso, Brazil. (Ph.D. Thesis). Universidade Federal de Lavras, 92 pp.

White, G. N., Dixon, J. B. 2002. Kaolin-serpentine minerals. In: Dixon, J.B. and Schulze, D. G. (eds.) Soil Mineralogy with Environmental Applications. Madison, Soil Sci. Soc. Am. pp. 389-412.

Zelazny, L. W., Thomas, P. J., Lawrence, C. L., 2002. Pyrophyllite-Talc Minerals. In: Dixon, J.B. and Schulze, D. G. (eds.) Soil Mineralogy with Environmental Applications. Madison, Soil Sci. Soc. Am. pp. 415-430.

Zinn, Y. L., Carducci, C. E., Araujo, M. A. 2015 Internal structure of a vermicular ironstone as determined by X-ray computed tomography scanning. Rev. Bras. Ciênc. Solo 39 (2), 345-349

Zinn, Y. L., Lal, R., Resck D. V. S. 2011. Eucalypt plantation effects on organic carbon and aggregation of three different-textured soils in Brazil. Soil Research 49 (7), 614-624.

Table 1. Location and geographic data of sampled soil profiles

Location (Fig. 2)	Soil	Position/ Aspect	Slope	Latitude S	Longitude W	Vegetation	Elevation (m)
1	Lithic Udorthent	Summit/-	< 5%	21°06'38.3"	44°46'09.4"	Savanna	1,018
2	Lithic Udorthent	Hillslope/ NE	35%	21°06'19.1	44°46'01.3"	Semi-deciduous forest	873
3	Lithic Udorthent	Hillslope at Canyon/S	90%	21°06'53.3"	44°46'03.8"	Cloud forest	846
4	Oxic Dystrudept	Hillslope at Canyon/ SW	30%	21°07'00.1"	44°46'20.7"	Cloud forest	840
5	Oxic Dystrudept	Hillslope/ NW	15%	21°06'25.7"	44°46'17.4"	Savanna	963
6	Anionic Acrudox	Hillslope/W	14%	21°06'45.5"	44°46'22.9"	Grazed savanna	947
7	Humic Rhodic Acrudox	Piedmont /N	20 %	21°06'00.6"	44°46'18.1"	*Urochloa* Pasture	898
8	Petroferric Acrudox	Drainageway on piedmont	16 %	21°06'13.2"	44°46'19.2"	Semi-deciduous forest	909

Table 2. Particle density, semi-quantitative geochemical composition and magnetic susceptibility in high (X-HF) and low frequency (X-LF) of soil parent materials

Parent material	**Particle density**	**SiO_2**	**Fe_2O_3**	**Al_2O_3**	**MgO**	**CaO**	**K_2O**	**P_2O_5**	**MnO**	**Cr_2O_3**	**NiO**	**TiO_2**	**ZrO_2**	**Recovery**	**Mg/Ca**	**X-LF**	**X-HF**
	($g\ cm^{-3}$)	---------- $g\ kg^{-1}$ ----------														$-(m^3.kg^{-1}).10^{-6}$ -	
Steatite-serpentinite	2.75	361.6	194.8	33.5	189.1	0.1	0.2	0.2	1.4	23.6	2.0	1.1	0.04	808.0	1891	0.23	0.25
Massive talc	2.74	444.4	46.1	2.1	228.9	0.0	0.0	6.5	0.3	1.0	2.3	6.9	0.02	725.0	> 2000	0.12	0.11
Common saprolite	3.06	407.0	81.4	13.9	215.6	5.8	0.2	0.0	1.5	7.3	1.1	0.9	0.02	736.0	37.2	5.52	5.42
Tafoni saprolite	3.05	317.4	264.6	33.0	166.8	1.5	0.2	0.3	6.7	12.8	2.8	1.2	0.03	821.0	111.2	2.88	2.81
Obsidian	2.86	260.7	2.7	104.5	11.0	303.1	26.8	0.0	1.1	8.9	3.2	7.4	0.53	724.0	0.04	0.53	0.55
Magnetite	4.58	7.7	774.0	200.2	4.5	0.2	0.0	0.2	5.9	3.1	8.2	0.6	0.02	1008.0	22.5	360.52	356.08

Table 3. Morphological and physical characterization of the studied soils and horizons

Soil-aspect		Depth cm	Ped size	Consistence dry	Consistence moist	Consistence wet	Wet color	Gravel	Sand	Silt	Clay	Pd	Bd
								---------- g kg^{-1} ----------				------- g cm^{-3} -----	
Lithic Udorthent-summit	A	0-6	vf/f	lo	lo	mpl/ss	5YR 3/4	144	194	382	424	3,19	1,15
Lithic Udorthent-NE	A	0-30	med	sh/h	lo	mpl/ms	5YR 3/4	549	149	431	420	2,96	1,06
Lithic Udorthent-S	A1	0-7	vf /f	lo	fr	npl/ns	-	364	177	515	308	2,36	0,85
	A2	7-21	f	lo	lo	spl/ss	5YR 4/3	509	253	443	304	2,74	0,99
	A3	21-25	f	lo	lo	mpl/ss	5YR 3/4	567	328	438	234	2,85	1,85
Oxic Dystrudept-SW	A1	0-16	vf	so	lo	npl/ns	5YR 3/4	246	114	411	475	2,58	0,30
	A2	17-36	vf /f	sh	lo	mpl/ss	2,5YR 3/4	258	124	365	511	2,99	0,82
	B	36-100	vf /f	so	lo	mpl/ms	5YR 4/4	103	120	416	464	3,08	1,02
Oxic Dystrudept-NW	A	0-16	mf/med	sh	lo	spl/ss	5 YR 4/4	341	153	355	492	3,24	0,89
	AB	16-57	vf	sh	lo	spl/ms	5YR 3/3	797	230	340	430	3,08	1,56
	B1	57-105	vf /med	sh	lo	spl/ss	2,5YR 3/6	171	109	320	571	3,25	1,08
	B2	105-150	vf /med	vh	lo	mpl/ms	5YR 4/6	150	128	379	493	3,30	1,29
	B3	150+	f	vh	lo	spl/ss	7,5YR 4/6	110	141	282	577	3,51	1,27
Anionic Acrudox-W	A	0-15	p /med	so	lo	mpl/ms	10R 3/2	30	95	503	402	3,34	1,17
	AB	15-95	p /med	so	lo	mpl/ms	2,5YR 2,5/4	18	84	453	463	3,44	1,28
	B1	95-110	med	so	lo	mpl/ss	10R 2.5/2	81	93	333	574	3,43	1,05
	B2	110-170+	med	so	lo	mpl/ms	2,5YR 2,5/4	91	91	267	642	3,53	–
Humic Rhodic Acrudox - piedmont	AP	0-5	vf /f	so/lo	lo	mpl/ss	2,5 YR 2,5/4	62	280	350	370	3,44	1,24
	A2	6-36	vf /f	so	lo	mpl/ss	2,5 YR 2,5/4	80	330	322	348	3,58	1,11
	BW1	36-140	vf /f	so/lo	lo	mpl/ss	2,5YR 2,5/4	55	292	318	390	3,70	1,38
	BW2	140-200+	vf /f	sh	lo	mpl/ss	10R 2,5/2	83	313	277	410	3,78	1,51
Petroferric Acrudox-drainageway	A	0-8	f	lo	lo	npl/ns	10R 2,5/2	73	510	307	183	3,82	1,26
	Bc	8-100	f	lo	lo	spl/ns	5R 2,5/3	483	446	373	181	3,81	1,32

vf = very fine; f= fine; med = medium; s= soft; lo= loose; fr=friable; npl= non-plastic; spl= slightly plastic; mpl= moderately plastic; ns= non sticky; ss = slightly sticky; ms = moderately sticky; lo= loose; so= soft; sh = slightly hard; h= hard; vh= very hard; Pd: particle density Bd = bulk density;

Table 4. Chemical characterization of studied soils and horizons

Soil-aspect	Horizon	pH		P	K	Ca	Mg	Al	H+Al	SB	t	T	Base Sat	Mg $_{Sat}$	Total C	Clay act.	Mg/Ca ratio
		H_2O	KCl	--mg kg^{-1}--		----------$cmol_c kg^{-1}$ ----------							----------%		----------		
Lithic Udorthent-summit	A*	5.90	4.93	0.8	42.5	0.46	1.16	0.07	4.83	1.7	1.80	6.6	26	18	2.86	low	2.5
Lithic Udorthent-NE	A*	5.90	4.89	0.9	38.2	2.01	3.77	0.08	5.64	5.9	5.96	11.5	51	33	2.89	High	1.9
Lithic Udorthent-S	A1*	6.30	5.45	5.0	87.5	8.10	6.40	0.06	3.87	14	14.7	18.6	79	34	13.76	High	0.8
	A2	5.60	4.77	1.9	59.7	2.23	4.77	0.11	5.90	7.1	7.26	13.0	55	37	4.21	High	2.1
	A3	5.60	4.78	0.7	27.6	0.52	3.79	0.09	3.10	4.4	4.47	7.48	59	51	1.41	High	7.3
Oxic Dystrudept-SW	A1	5.70	4.94	2.9	70.4	4.77	5.47	0.07	4.57	10	10.4	14.9	70	37	10.98	High	1.1
	A2	5.60	4.75	1.5	55.4	1.57	3.01	0.11	7.05	4.7	4.83	11.8	40	26	4.54	low	1.9
	B	4.70	4.47	0.7	21.1	0.10	0.57	0.18	5.64	0.7	0.90	6.36	11	9	2.49	low	5.7
Oxic Dystrudept-NW	A	5.70	4.81	2.1	70.4	1.30	2.47	0.11	5.58	3.9	4.06	9.53	41	26	3.74	low	1.9
	AB	5.80	5.06	0.9	36.1	0.10	0.99	0.04	3.62	1.2	1.22	4.8	25	21	2.23	low	9.9
	B1	5.80	6.72	0.7	6.1	0.10	0.23	0.00	1.35	0.3	0.35	1.7	20	14	0.73	low	2.3
	B2	6.20	6.93	0.4	4.0	0.10	0.32	0.00	1.39	0.4	0.43	1.82	24	18	0.70	low	3.2
	B3**	6.70	6.77	0.7	4.0	0.10	0.42	0.00	1.39	0.5	0.53	1.92	28	22	0.40	low	4.2
Anionic Acrudox-W	A	6.50	6.18	1.3	57.6	1.89	1.59	0.00	2.62	3.6	3.63	6.25	58	25	2.00	low	0.8
	AB	5.60	5.77	0.6	16.9	0.36	0.29	0.03	2.59	0.7	0.72	3.28	21	9	1.44	low	0.8
	B1	6.20	6.61	0.4	8.3	0.10	0.11	0.03	1.70	0.2	0.26	1.93	12	6	0.64	low	1.1
	B2**	6.40	6.86	0.5	6.1	0.17	0.27	0.03	1.64	0.5	0.49	2.1	22	13	0.50	low	1.6
Humic Rhodic Acrudox - piedmont	AP	5.30	5.30	0.8	48.9	1.61	1.33	0.40	4.04	3.1	3.47	7.11	43	19	2.87	low	0.8
	A2	6.30	5.42	2.5	19.0	1.73	0.35	0.03	3.62	2.1	2.16	5.75	37	6	2.26	low	0.2
	BW_1	6.20	6.10	0.8	8.3	0.24	0.28	0.03	2.15	0.5	0.57	2.69	20	10	0.96	low	1.2
	BW_2*	6.60	6.54	0.7	8.3	0.12	0.20	0.05	1.66	0.3	0.39	2	17	10	0.63	low	1.7
Petroferric Acrudox-drainageway	A	5.10	5.4	2.1	62	0.3	1.3	0.2	5.0	1.7	1.9	6.7	26	19	3.07	low	4.3
	B	5.80	6.1	0.9	8	0.1	0.2	0.1	2.1	0.3	0.4	2.5	13	8	1.71	low	2.0

*tested negative for carbonates; **positive for carbonates ($MgCO_3$/$FeCO_3$); Base Sat. = Base Saturation, Mg_{Sat} = Mg saturation => (Mg/T)*100

Table 5. Soil geochemical composition, as determined by semi-quantitative X-ray fluorescence.

Soil-aspect	Hor.	SiO_2	Fe_2O_3	Al_2O_3	MgO	CaO	K_2O	P_2O_5	MnO	Cr_2O_3	NiO	TiO_2	ZrO_2	Recovery %
		---------- g kg^{-1} ----------												
Lithic Udorthent-summit	A	225.9	411.4	67.3	106.7	1.24	0.21	0.93	4.46	32.64	1.76	4.87	0.10	86.1
Lithic Udorthent-NE	A	311.8	306.5	76.8	97.5	1.66	0.31	0.83	6.85	15.98	1.87	10.27	0.23	83.3
Lithic Udorthent-S	A1	292.4	151.8	26.5	136.4	14.3	0.84	0.94	4.93	7.66	1.68	1.89	0.05	64.2
	A2	372.8	163.7	26.3	188.4	2.39	0.21	0.52	3.54	7.60	1.77	1.56	0.04	77.0
	A3	396.8	153.5	24.8	204.7	0.73	0	0.31	3.12	6.75	1.77	1.04	0.03	79.5
Oxic Dystrudept-SW	A1	218.5	354.2	67.1	94.4	7.38	0.52	0.94	4.68	22.57	1.98	5.10	0.11	78.1
	A2	241.5	377.6	80.3	107.8	1.35	0.31	0.83	5.49	24.26	2.07	5.49	0.14	85.0
	A3	251.1	378.1	84.2	114.2	0.21	0.21	0.62	5.18	23.72	2.07	5.59	0.15	86.9
Oxic Dystrudept-NW	A	295.1	303.0	42.4	145.9	1.35	0.21	0.62	4.36	22.73	2.28	2.59	0.05	82.3
	AB	275.9	350.8	46.1	140.7	0.62	0.21	0.52	4.04	25.19	2.28	2.59	0.06	85.0
	B1	236.5	407.7	64.4	122.6	0.21	0.1	0.41	3.52	25.17	2.80	2.80	0.05	86.8
	B2	253.5	389.1	55.5	132.2	0	0	0.31	4.04	27.14	3.21	2.38	0.04	87.0
	B3	206.1	505.3	60.0	102.8	0	0	0.41	7.13	36.07	4.75	2.27	0.04	92.7
Anionic Acrudox-W	A	116.9	574.0	131.7	29.9	1.55	0.31	0.83	6.52	32.37	2.59	8.58	0.24	90.9
	AB	112.0	589.1	134.4	26.7	0.21	0.21	0.83	4.65	32.05	2.27	8.79	0.24	91.5
	B1	93.8	608.0	149.9	15.3	0	0.21	0.93	4.45	30.60	1.86	9.61	0.28	91.8
	B2	89.3	615.1	159.7	11.4	0.21	0.21	0.93	5.37	29.76	1.86	10.23	0.31	92.8
Humic Rhodic Acrudox - N	Ap	92.4	605.2	143.9	9.4	0.93	0.52	1.45	5.27	34.43	5.27	9.51	0.25	91.3
	A2	95.0	602.2	154.9	6.1	1.03	0.41	1.34	5.48	35.87	4.96	10.34	0.29	92.2
	BW1	94.0	631.2	137.9	11.3	0.21	0.31	0.93	5.68	36.57	5.89	8.57	0.25	93.7
	BW2	81.2	637.4	136.8	8.0	0.1	0.21	1.03	5.89	37.31	5.58	8.68	0.24	92.7
Petroferric Acrudox-drainageway	A	54.4	670.8	119.6	13.8	0.21	0.41	1.34	8.37	50.11	6.10	5.48	0.16	93.5
	B	50.3	689.4	129.8	10.0	0.09	0.31	1.24	7.85	47.91	5.89	5.99	0.19	95.3

Table 6. Element concentrations as extracted with dithionite and oxalate

		SiO_2	Fe_2O_3	Al_2O_3	MgO	CaO	K_2O	P_2O_5	MnO	Cr_2O_3	NiO	TiO_2	ZrO_2	Fe_2O_3	Al_2O_3	MgO	CaO	K_2O	P_2O_5	MnO	Cr_2O_3	NiO	TiO_2	ZrO_2
		dithionite (g/kg)												oxalate (g/kg)										
Lithic Udorthent-summit	A	24.2	232.8	40.0	13.0	5.5	29.1	<LQ	2.4	6.6	0.69	0.59	0.06	5.6	3.6	0.4	<LQ	1.0	0.2	1.5	0.1	0.066	0.027	0.010
Lithic Udorthent-NE	A	24.7	172.9	15.3	11.6	5.8	29.5	<LQ	3.0	3.5	0.66	0.77	0.06	6.0	3.1	0.8	<LQ	2.3	0.2	2.7	0.1	0.237	0.039	0.012
Lithic Udorthent-S	A_1	23.7	63.3	7.5	15.1	10.0	28.3	<LQ	1.7	0.8	0.25	0.05	0.04	2.2	4.2	3.1	<LQ	0.6	0.2	1.5	0.0	0.139	0.006	0.007
	A_2	21.4	72.6	6.3	12.9	6.3	27.1	<LQ	1.4	0.9	0.28	0.08	0.04	1.9	2.3	1.0	<LQ	<LQ	0.2	0.7	0.0	0.077	0.010	0.006
	A_3	18.5	77.7	5.4	10.8	5.2	26.0	<LQ	1.3	0.9	0.33	0.10	0.04	1.5	1.3	0.7	<LQ	0.8	0.1	0.5	0.0	0.069	0.007	0.007
Oxic Dystrudept-SW	A_1	27.2	180.6	29.7	14.4	7.9	29.0	<LQ	1.6	4.4	0.55	0.40	0.05	3.7	3.5	2.0	<LQ	1.6	0.2	1.1	0.1	0.087	0.023	0.010
	A_2	24.5	206.8	35.1	12.6	6.2	29.9	<LQ	2.4	5.3	0.72	0.60	0.06	4.6	4.2	0.8	<LQ	0.8	0.2	1.5	0.1	0.117	0.025	0.008
	A_3	21.9	212.5	35.6	11.0	5.6	29.3	<LQ	2.4	5.3	0.75	0.63	0.06	5.4	4.2	0.3	<LQ	1.3	0.2	1.5	0.1	0.122	0.032	0.011
Oxic Dystrudept-NW	A	19.8	158.4	23.1	8.3	2.8	27.4	<LQ	2.0	4.3	0.70	0.31	0.05	4.4	2.6	0.7	<LQ	1.5	0.2	1.5	0.1	0.180	0.020	0.008
	AB	18.2	203.1	28.4	7.8	2.8	29.5	0.1	1.7	5.7	0.68	0.35	0.05	4.6	2.6	0.4	<LQ	0.8	0.1	0.7	0.1	0.095	0.020	0.008
	B_1	14.1	240.1	41.2	4.5	2.6	29.4	0.1	2.0	6.1	1.16	0.47	0.06	2.6	2.3	0.2	<LQ	1.9	0.1	1.2	0.1	0.238	0.022	0.007
	B_2	14.4	237.7	34.2	4.5	2.8	30.3	<LQ	2.0	6.3	1.35	0.38	0.05	2.0	1.8	0.2	<LQ	2.1	0.1	1.0	0.1	0.202	0.014	0.007
	B_3	23.2	293.5	31.1	9.7	5.1	29.6	<LQ	5.0	8.5	2.88	0.39	0.06	5.8	2.4	0.7	<LQ	3.1	0.1	3.3	0.1	0.665	0.006	0.007
Anionic Acrudox-W	A	15.4	328.7	43.7	3.1	2.3	31.8	1.3	2.4	8.5	1.27	1.33	0.07	2.8	3.0	0.5	<LQ	<LQ	0.2	1.1	0.1	0.086	0.026	0.009
	AB	15.0	325.5	43.8	3.0	2.2	32.1	1.1	2.8	8.0	1.17	1.31	0.07	4.2	3.6	0.1	<LQ	2.8	0.1	1.4	0.1	0.123	0.042	0.008
	B_1	19.1	357.3	40.8	8.9	5.3	32.2	<LQ	2.0	8.5	0.96	1.50	0.08	3.3	2.7	0.1	<LQ	2.0	0.1	0.6	0.2	0.054	0.029	0.008
	B_2	18.7	377.2	41.6	9.0	5.5	32.9	<LQ	2.7	8.8	0.99	1.62	0.09	3.9	2.9	0.1	<LQ	2.7	0.1	1.1	0.4	0.073	0.031	0.010
Humic Rhodic Acrudox - N	Ap	16.1	263.1	37.7	4.8	3.2	31.6	0.8	1.8	4.0	1.98	1.22	0.07	3.6	4.3	0.3	<LQ	2.9	0.2	1.1	0.1	0.124	0.034	0.010
	A2	18.7	269.3	44.7	4.2	3.1	31.9	0.6	1.7	4.2	1.95	1.31	0.07	4.8	6.6	0.1	<LQ	1.3	0.3	1.2	0.1	0.154	0.063	0.009
	BW_1	13.1	266.0	35.3	3.5	2.4	31.5	0.9	1.9	4.1	2.09	1.26	0.06	5.8	4.2	0.1	<LQ	1.1	0.2	1.2	0.1	0.156	0.051	0.008
	BW_2	10.5	276.4	30.9	2.7	2.0	30.7	1.3	2.0	4.5	2.05	1.21	0.07	4.3	3.5	0.1	<LQ	2.3	0.1	1.1	0.2	0.120	0.045	0.009
Petroferric Acrudox-drainageway	A	17.7	256.5	29.8	10.2	5.6	30.1	<LQ	2.5	3.7	2.11	0.83	0.06	5.3	4.0	0.1	<LQ	1.6	0.1	1.2	0.2	0.142	0.042	0.007
	B	17.8	272.3	35.7	9.7	5.5	29.6	<LQ	2.2	4.0	2.00	0.98	0.06	5.6	4.5	0.3	<LQ	1.4	0.2	1.5	0.2	0.186	0.044	0.009

Table 7. Ratios between the element concentrations, determined by different methods

		----------FRX ----------			----------DCB----------			----------Oxalate----------			
		Mg/Ca	Ni/Cr	Ti/Zr	Mg/Ca	Ni/Cr	Ti/Zr	Mg/Ca	Ni/Cr	Ti/Zr	Fe_{ox}/Fe_{DCB}
Lithic Udorthent-summit	A	85.8	0.06	40.54	2.4	0.12	8.47	-	1.10	2.19	0.024
Lithic Udorthent-NE	A	58.8	0.11	36.64	2.0	0.22	10.07	-	4.49	2.74	0.035
Lithic Udorthent-S	A1	9.6	0.16	31.44	1.5	0.35	1.09	-	3.69	0.75	0.035
	A2	78.7	0.21	33.41	2.0	0.35	1.72	-	3.79	1.29	0.027
	A3	281.4	0.26	27.08	2.1	0.44	2.26	-	2.61	0.85	0.019
Oxic Dystrudept-SW	A1	12.8	0.07	36.80	1.8	0.14	6.35	-	1.38	1.90	0.020
	A2	80.0	0.08	32.28	2.0	0.16	8.74	-	1.57	2.62	0.022
	A3	551.5	0.09	30.20	2.0	0.16	8.98	-	2.28	2.38	0.025
Oxic Dystrudept-NW	A	108.2	0.10	42.03	3.0	0.19	5.19	-	2.55	2.07	0.028
	AB	226.2	0.09	36.98	2.8	0.14	5.25	-	1.06	2.08	0.023
	B1	592.0	0.11	45.30	1.7	0.22	6.70	-	3.26	2.57	0.011
	B2		0.12	44.62	1.6	0.25	5.67	-	2.78	1.60	0.008
	B3		0.13	52.41	1.9	0.39	5.51	-	8.14	0.70	0.020
Anionic Acrudox-W	A	19.3	0.08	29.06	1.3	0.17	15.05	-	1.07	2.38	0.009
	AB	129.0	0.07	29.26	1.4	0.17	14.48	-	1.01	4.19	0.013
	B1		0.07	27.97	1.7	0.13	15.39	-	0.35	3.10	0.009
	B2	55.0	0.07	27.13	1.6	0.13	14.95	-	0.24	2.51	0.010
Humic Rhodic Acrudox - N	Ap	10.1	0.16	30.65	1.5	0.57	15.17	-	2.09	2.75	0.014
	A2	5.9	0.15	28.55	1.4	0.53	14.55	-	2.36	5.65	0.018
	BW1	54.5	0.17	28.24	1.5	0.58	15.78	-	1.55	4.87	0.022
	BW2	77.0	0.16	29.23	1.4	0.52	14.99	-	0.92	4.23	0.015
Petroferric Acrudox-drainageway	A	67.0	0.13	28.54	1.8	0.65	12.04	-	0.79	4.60	0.021
	B	116.9	0.14	25.82	1.8	0.57	13.62	-	1.12	4.10	0.021

Table 8. Magnetic susceptibility in high (X-HF) and low frequency (X-LF) of soil and clay.

		Bulk soil			Clay			
		X-LF	**X-HF**	**X-FD**	**X-LF**	**X-HF**	**X-FD**	**Mh**
		$(m^3.kg^{-1}).10^{-6}$		%	$(m^3.kg^{-1}).10^{-6}$		%	$g.kg^{-1}$
Lithic Udorthent-summit	A	63.7	58.7	7.9	77.1	67.6	12.3	77.1
Lithic Udorthent-NE	A	39.1	36.3	7.0	56.5	50.5	10.7	56.5
Lithic Udorthent-S	A1	11.5	10.7	6.8	18.6	15.8	15.4	18.6
	A2	11.1	10.3	7.2	19.6	16.7	14.6	19.6
	A3	9.7	8.9	8.4	22.2	18.5	16.5	22.2
Oxic Dystrudept-SW	A1	30.8	28.4	7.9	46.7	40.2	14.0	46.7
	A2	41.8	38.1	8.8	48.4	41.9	13.4	48.4
	A3	43.7	39.7	9.3	51.8	44.6	13.9	51.8
Oxic Dystrudept-NW	A	33.4	30.6	8.5	38.6	33.4	13.3	38.6
	AB	37.4	34.4	8.0	39.5	34.3	13.0	39.5
	B1	26.3	23.9	9.0	29.3	25.0	14.8	29.3
	B2	24.9	22.9	8.2	25.3	21.5	15.0	25.3
	B3	28.0	25.5	8.9	31.3	26.4	15.7	31.3
Anionic Acrudox-W	A	56.8	51.1	9.9	61.3	53.0	13.5	61.3
	AB	62.0	55.6	10.3	64.6	56.1	13.2	64.6
	B1	68.5	60.9	11.0	68.7	59.7	13.1	68.7
	B2	72.6	64.6	11.1	76.3	66.3	13.1	76.3
Humic Rhodic Acrudox - N	AP	156	151	3.2	76.0	65.3	14.0	76.0
	A2	156	150	3.7	70.0	60.8	13.2	70.0
	BW1	175	169	3.5	95.8	82.9	13.4	95.8
	BW2	168	162	3.6	88.1	77.5	12.1	88.1
Petroferric Acrudox-drainageway	A	207	201	2.8	173	155	10.6	173
	B	210	204	3.0	160	142	11.3	160

Mh = maghemite concentration (Poggere et al., 2018)

Figure captions

Fig. 1. Location of Morro das Almas (*Maciço Ultramáfico do Morro das Almas*), in Bom Sucesso, Brazil, alongside itabirite rocks of *Supergrupo Minas* (adapted from CODEMIG, 2005).

Fig. 2. Aerial photograph of the study area (Morro das Almas) and soil profiles sampled (numbers reflect soil profiles as listed in Table 1). Note topographic profiles of the area, elaborated from transects from profiles 7-3 and 2-4.

Fig. 3. X-ray diffraction patterns of soil parent materials.

Fig. 4. Influence of total soil Fe_2O_3 contents in Al_2O_3, MgO, SiO_2, Cr_2O_3, CaO, MnO, TiO_2, K_2O, P_2O_5 and ZrO_2 contents.

Fig. 5. X-ray diffraction patterns of the studied soils.

Fig. 6. X-ray diffraction patterns of the studied soils.

Fig. 7. Thin sections of soils on: a,b) Entisol, summitt; c,d) Entisol, NE; e,f) Entisol, S, A2 horizon; g,h) Inceptisol, SW, B horizon; i,j) Inceptisol, NW, B1 horizon; l,m) – Oxisol, W, B horizon; n,o) Oxisol, piedmont, Bw1 horizon; p,q) Oxisol, drainageway, B horizon. Images on the left under plane polarized light, images on the right between crossed polars. Note blocky microstructure in a-h, granular microstructure in i-q, and Fe-coated saprolites.

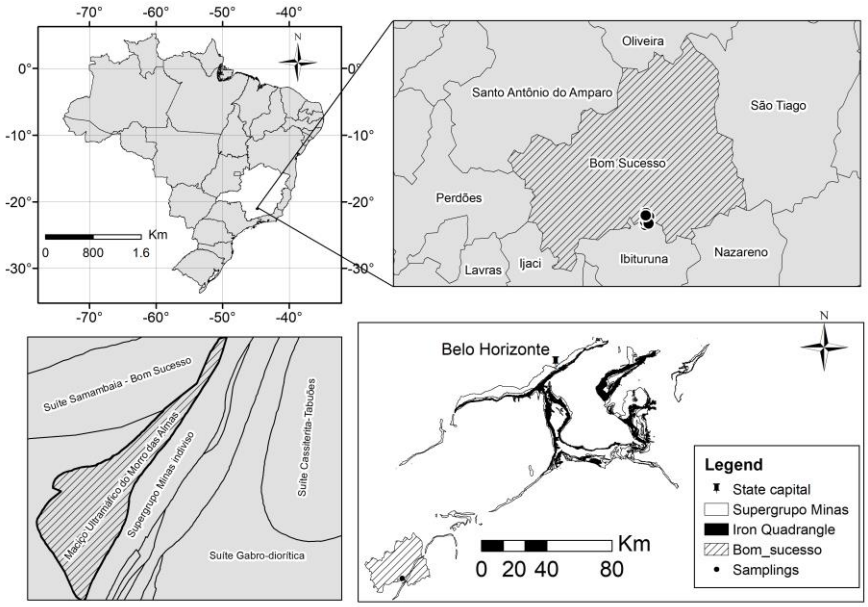
-70°
-60°
-50°
-40°
0°
-10°
-20°
-30°
N
Km
0 800 1.6
Oliveira
Santo Antônio do Amparo
São Tiago
Bom Sucesso
Perdões
Lavras
Ijaci
Ibituruna
Nazareno
Suíte Samambaia - Bom Sucesso
Maciço Ultramáfico do Morro das Almas
Supergrupo Minas indiviso
Suíte Gabro-dioritica
Suíte Cassiterita- Tabuões
Belo Horizonte
Km
0 20 40 80
Legend
State capital
Supergrupo Minas
Iron Quadrangle
Bom_sucesso
Samplings

Fig. 1

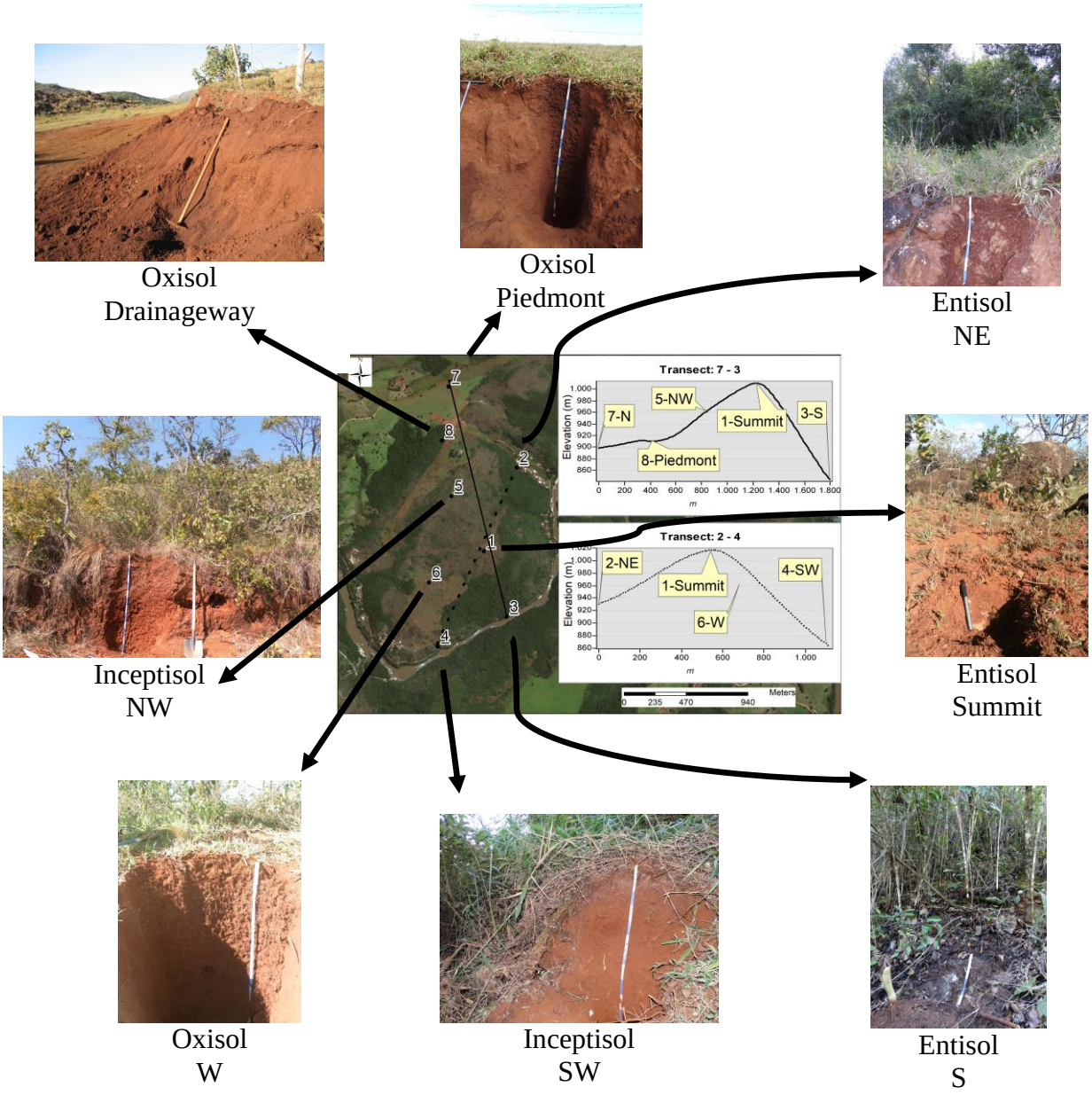
Oxisol
Drainageway
Oxisol
Piedmont
Entisol
NE
Inceptisol
NW
Entisol
Summit
Oxisol
W
Inceptisol
SW
Entisol
S
Transect: 7 - 3
7-N
5-NW
1-Summit
3-S
8-Piedmont
Transect: 2 - 4
2-NE
1-Summit
4-SW
6-W
Elevation (m)
m
Meters

Fig. 2

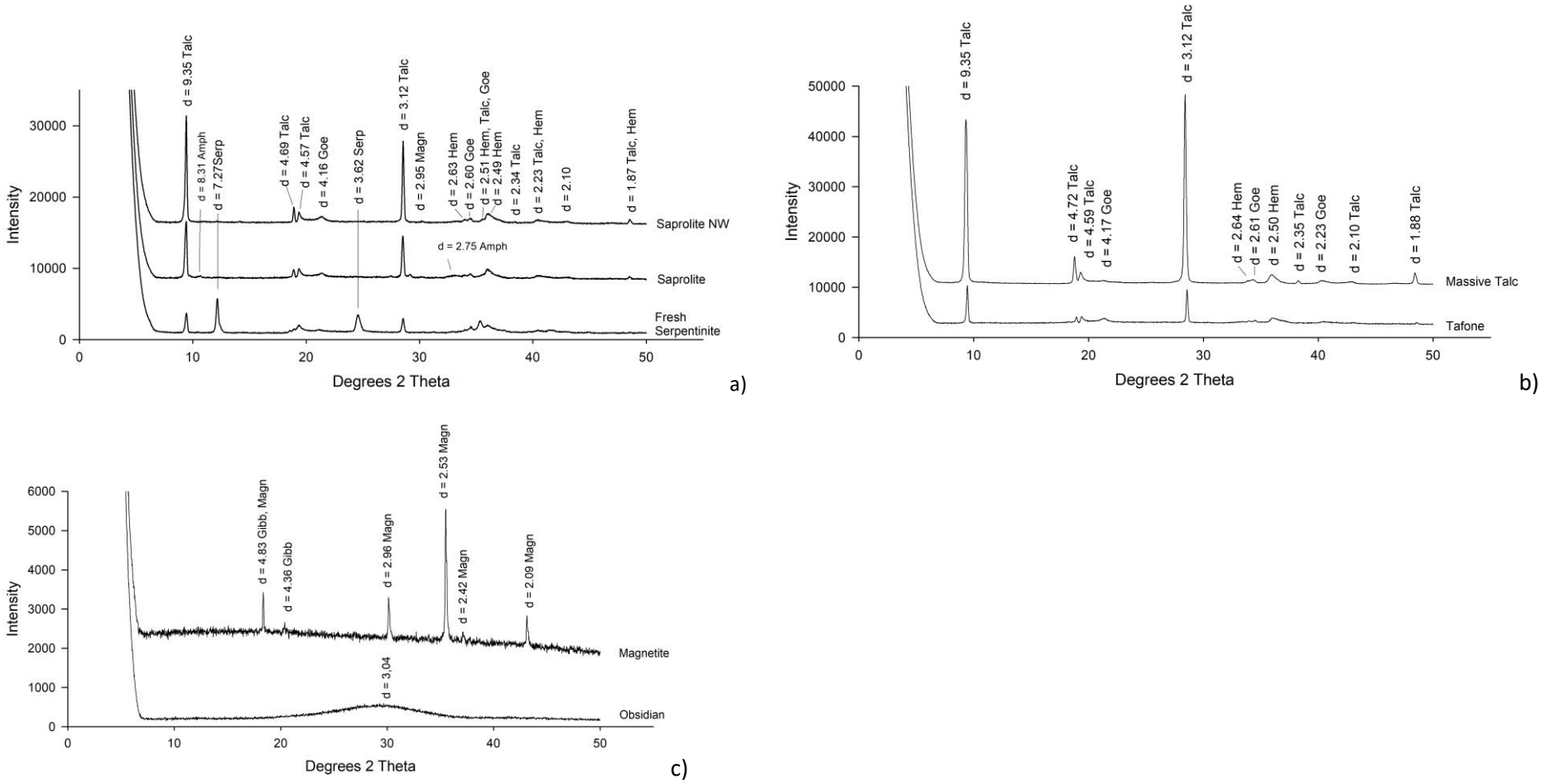
d = 9.35 Talc
d = 8.31 Amph
d = 7.27Serp
d = 4.69 Talc
d = 4.57 Talc
d = 4.16 Goe
d = 3.62 Serp
d = 3.12 Talc
d = 2.95 Magn
d = 2.63 Hem
d = 2.60 Goe
d = 2.51 Hem, Talc, Goe
d = 2.49 Hem
d = 2.34 Talc
d = 2.23 Talc, Hem
d = 2.10
d = 1.87 Talc, Hem
Saprolite NW
d = 2.75 Amph
Saprolite
Fresh Serpentinite
Intensity
Degrees 2 Theta
a)
d = 9.35 Talc
d = 3.12 Talc
d = 4.72 Talc
d = 4.59 Talc
d = 4.17 Goe
d = 2.64 Hem
d = 2.61 Goe
d = 2.50 Hem
d = 2.35 Talc
d = 2.23 Goe
d = 2.10 Talc
d = 1.88 Talc
Massive Talc
Tafone
Intensity
Degrees 2 Theta
b)
d = 4.83 Gibb, Magn
d = 4.36 Gibb
d = 2.96 Magn
d = 2.53 Magn
d = 2.42 Magn
d = 2.09 Magn
Magnetite
d = 3,04
Obsidian
Intensity
Degrees 2 Theta
c)

Fig. 3.

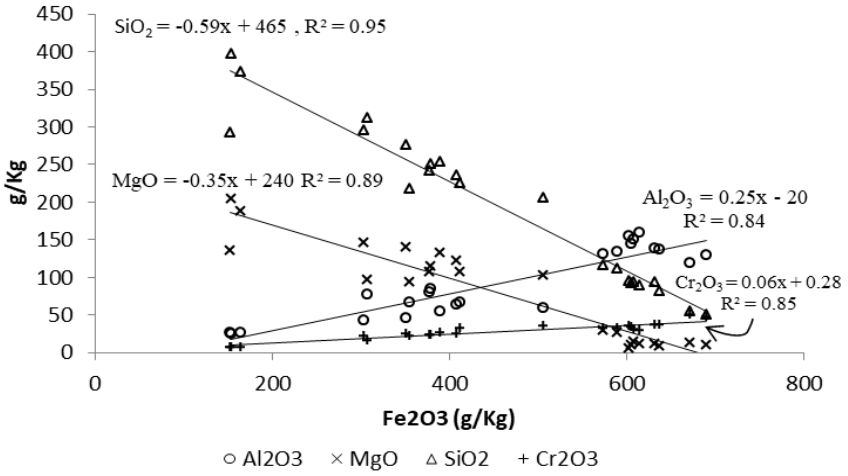
SiO2 = -0.59x + 465 , R² = 0.95
MgO = -0.35x + 240 R² = 0.89
Al2O3 = 0.25x - 20
R² = 0.84
Cr2O3 = 0.06x + 0.28
R² = 0.85
g/Kg
Fe2O3 (g/Kg)
Al2O3 MgO SiO2 Cr2O3

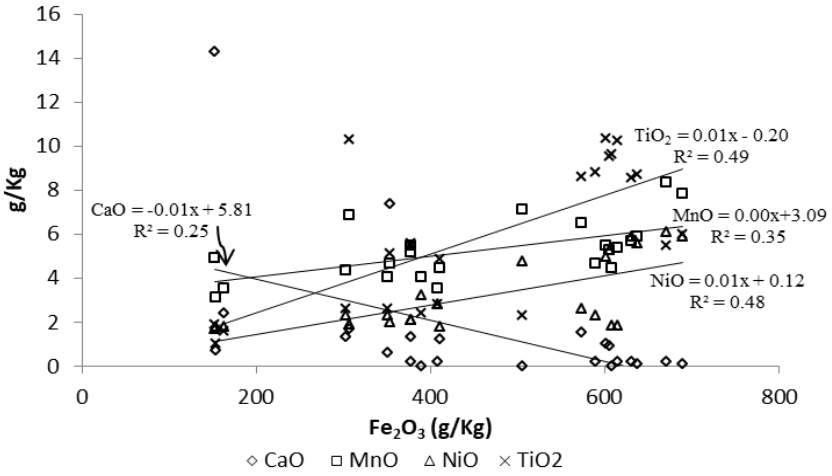
TiO2 = 0.01x - 0.20
R² = 0.49
CaO = -0.01x + 5.81
R² = 0.25
MnO = 0.00x+3.09
R² = 0.35
NiO = 0.01x + 0.12
R² = 0.48
g/Kg
Fe2O3 (g/Kg)
CaO MnO NiO TiO2

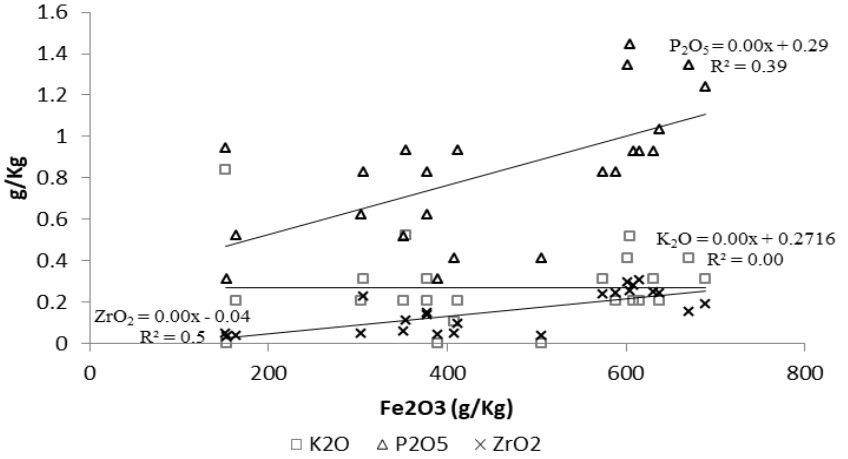
P2O5 = 0.00x + 0.29
R² = 0.39
K2O = 0.00x + 0.2716
R² = 0.00
ZrO2 = 0.00x - 0.04
R² = 0.5
g/Kg
Fe2O3 (g/Kg)
K2O P2O5 ZrO2

Fig 4.

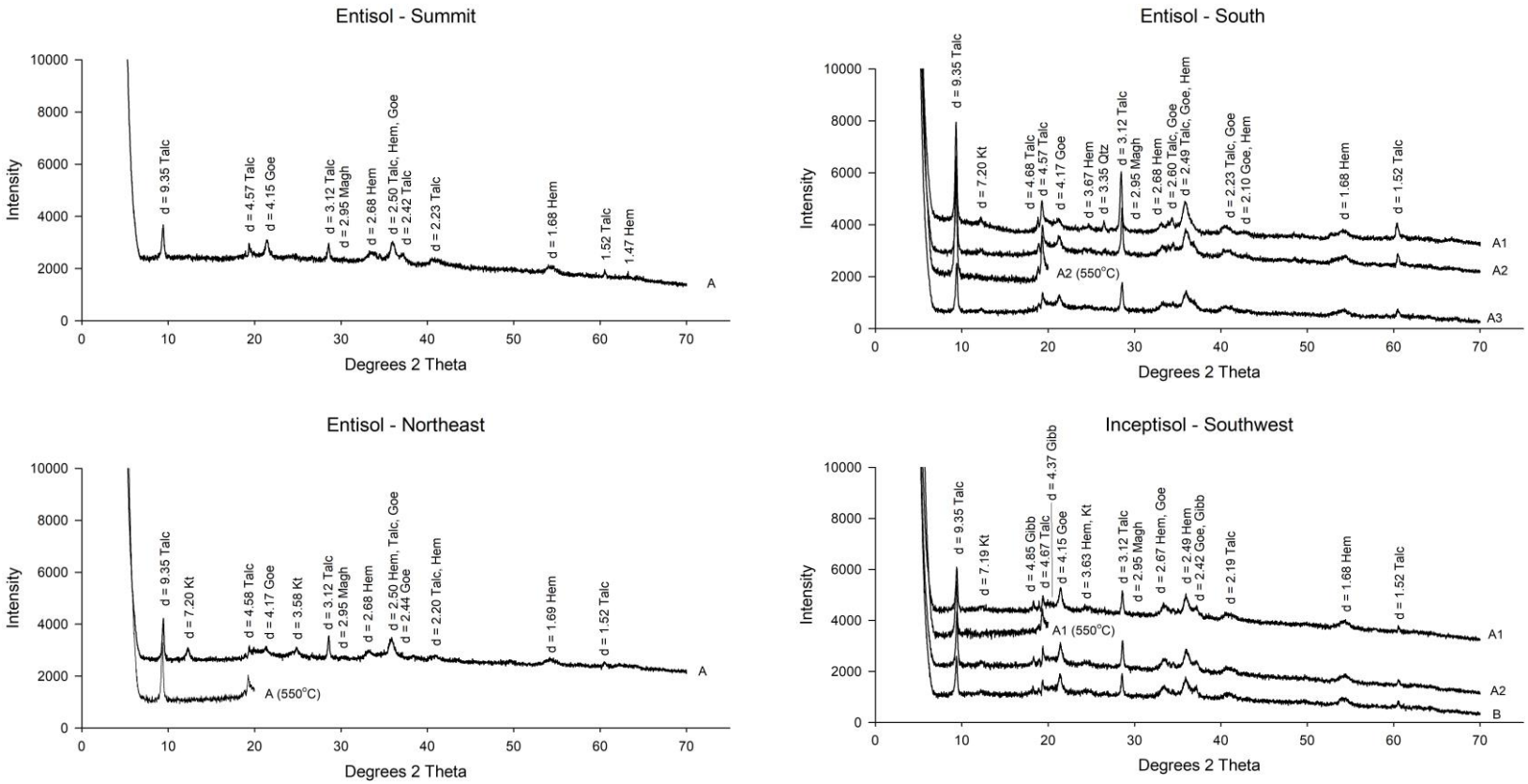
Entisol - Summit
Intensity
Degrees 2 Theta
d = 9.35 Talc
d = 4.57 Talc
d = 4.15 Goe
d = 3.12 Talc
d = 2.95 Magh
d = 2.68 Hem
d = 2.50 Talc, Hem, Goe
d = 2.42 Talc
d = 2.23 Talc
d = 1.68 Hem
1.52 Talc
1.47 Hem
A
Entisol - South
d = 9.35 Talc
d = 7.20 Kt
d = 4.68 Talc
d = 4.57 Talc
d = 4.17 Goe
d = 3.67 Hem
d = 3.35 Qtz
d = 3.12 Talc
d = 2.95 Magh
d = 2.68 Hem
d = 2.60 Talc, Goe
d = 2.49 Talc, Goe, Hem
d = 2.23 Talc, Goe
d = 2.10 Goe, Hem
d = 1.68 Hem
d = 1.52 Talc
A1
A2
A2 (550°C)
A3
Entisol - Northeast
d = 9.35 Talc
d = 7.20 Kt
d = 4.58 Talc
d = 4.17 Goe
d = 3.58 Kt
d = 3.12 Talc
d = 2.95 Magh
d = 2.68 Hem
d = 2.50 Hem, Talc, Goe
d = 2.44 Goe
d = 2.20 Talc, Hem
d = 1.69 Hem
d = 1.52 Talc
A
A (550°C)
Inceptisol - Southwest
d = 9.35 Talc
d = 7.19 Kt
d = 4.85 Gibb
d = 4.67 Talc
d = 4.37 Gibb
d = 4.15 Goe
d = 3.63 Hem, Kt
d = 3.12 Talc
d = 2.95 Magh
d = 2.67 Hem, Goe
d = 2.49 Hem
d = 2.42 Goe, Gibb
d = 2.19 Talc
d = 1.68 Hem
d = 1.52 Talc
A1
A1 (550°C)
A2
B

Fig. 5

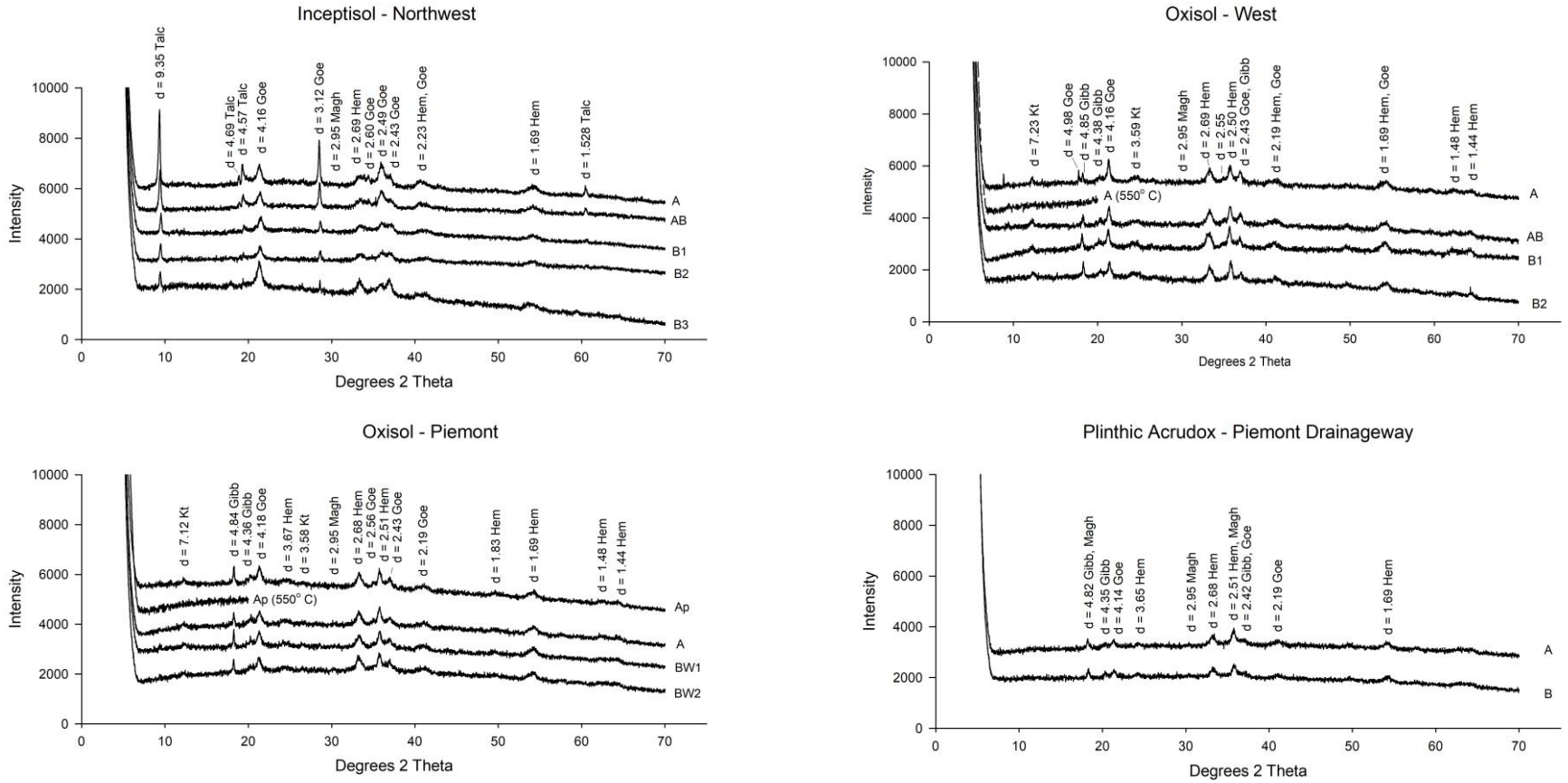
Inceptisol - Northwest
d = 9.35 Talc
d = 4.69 Talc
d = 4.57 Talc
d = 4.16 Goe
d = 3.12 Goe
d = 2.95 Magh
d = 2.69 Hem
d = 2.60 Goe
d = 2.49 Goe
d = 2.43 Goe
d = 2.23 Hem, Goe
d = 1.69 Hem
d = 1.528 Talc
A
AB
B1
B2
B3
Intensity
Degrees 2 Theta
Oxisol - West
d = 7.23 Kt
d = 4.98 Goe
d = 4.85 Gibb
d = 4.38 Gibb
d = 4.16 Goe
d = 3.59 Kt
d = 2.95 Magh
d = 2.69 Hem
d = 2.55
d = 2.50 Hem
d = 2.43 Goe, Gibb
d = 2.19 Hem, Goe
d = 1.69 Hem, Goe
d = 1.48 Hem
d = 1.44 Hem
A (550° C)
A
AB
B1
B2
Intensity
Degrees 2 Theta
Oxisol - Piemont
d = 7.12 Kt
d = 4.84 Gibb
d = 4.36 Gibb
d = 4.18 Goe
d = 3.67 Hem
d = 3.58 Kt
d = 2.95 Magh
d = 2.68 Hem
d = 2.56 Goe
d = 2.51 Hem
d = 2.43 Goe
d = 2.19 Goe
d = 1.83 Hem
d = 1.69 Hem
d = 1.48 Hem
d = 1.44 Hem
Ap (550° C)
Ap
A
BW1
BW2
Intensity
Degrees 2 Theta
Plinthic Acrudox - Piemont Drainageway
d = 4.82 Gibb, Magh
d = 4.35 Gibb
d = 4.14 Goe
d = 3.65 Hem
d = 2.95 Magh
d = 2.68 Hem
d = 2.51 Hem, Magh
d = 2.42 Gibb, Goe
d = 2.19 Goe
d = 1.69 Hem
A
B
Intensity
Degrees 2 Theta

Fig. 6.

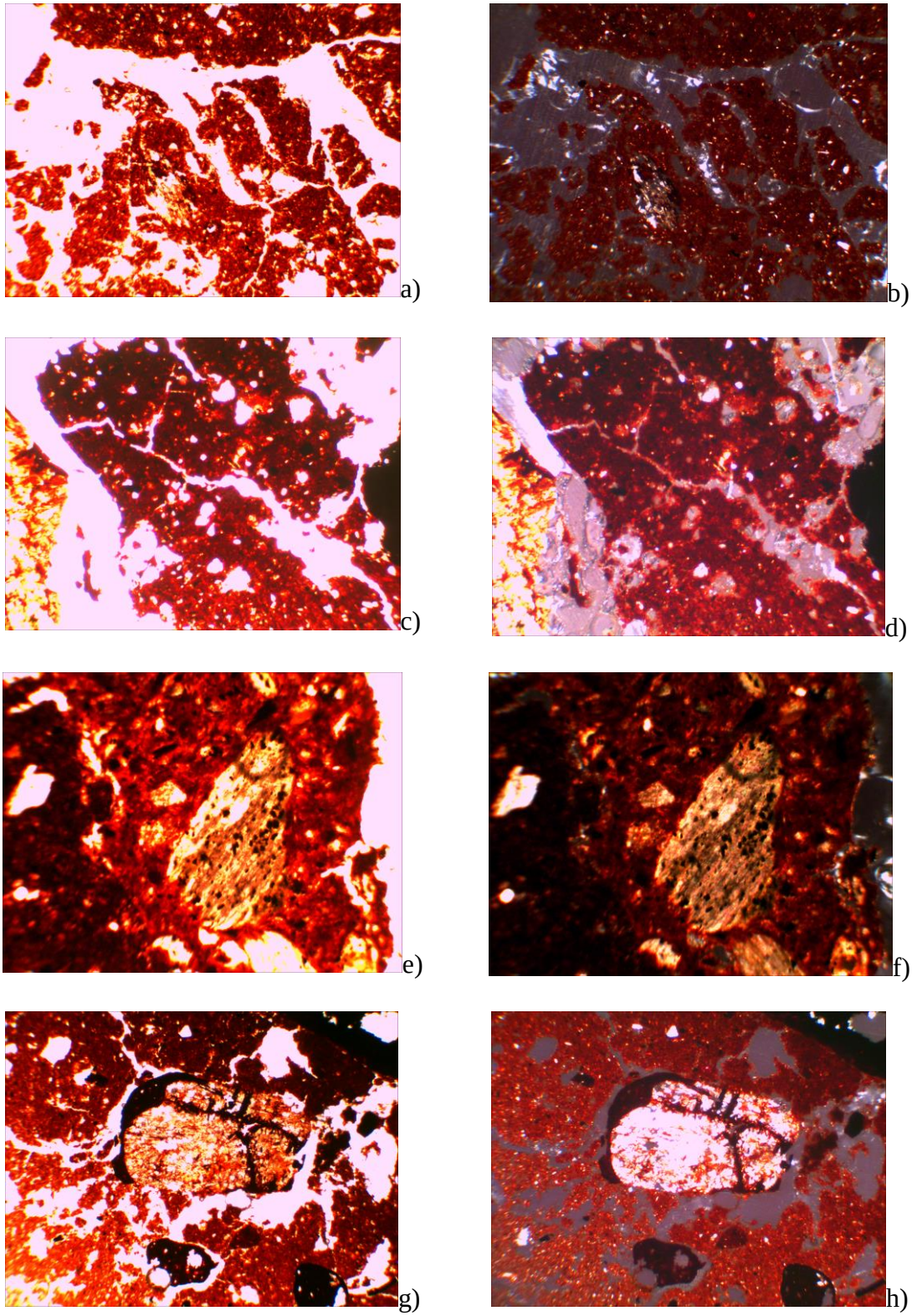

Fig 7.

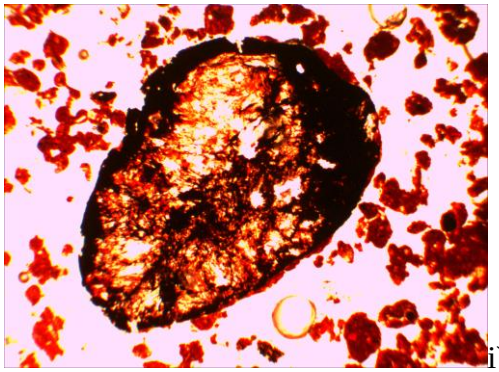
i)

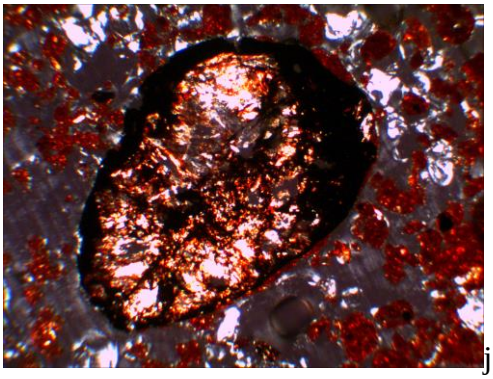
j)

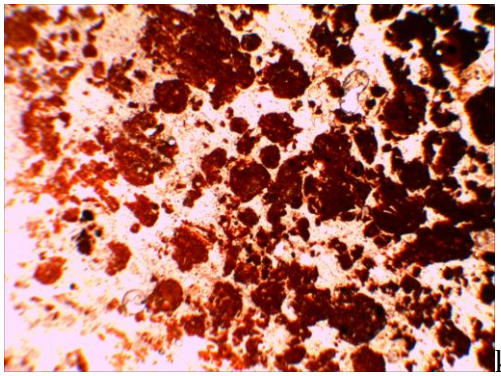
k)

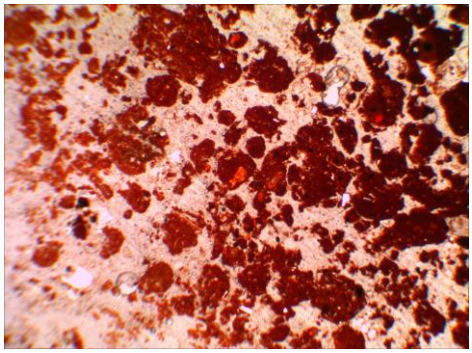
l)

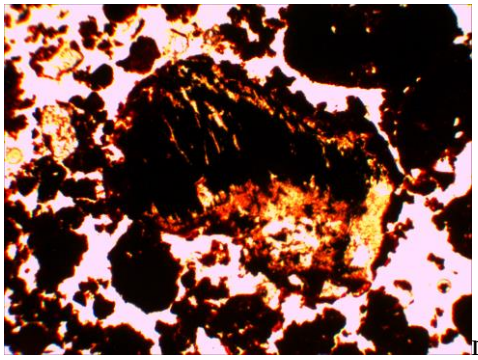
m)

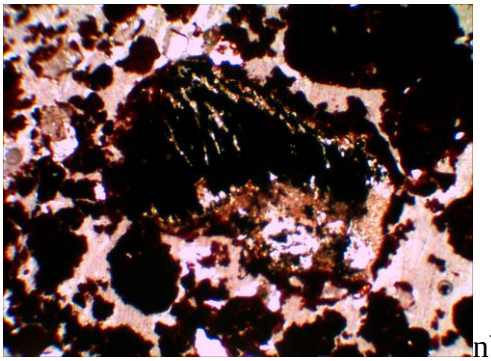
n)

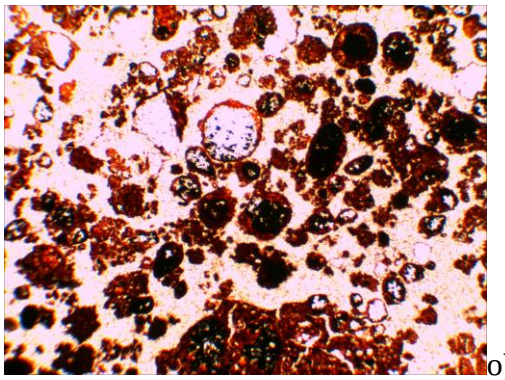
o)

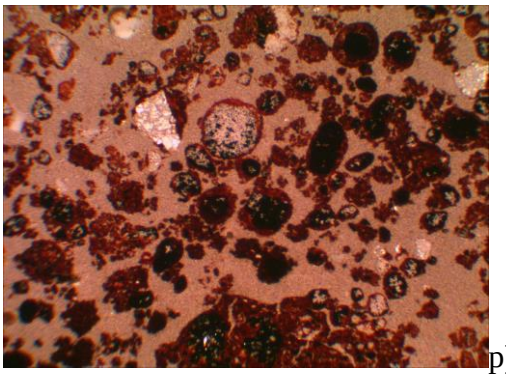
p)

Fig 7

APÊNDICES

APÊNDICE A

MATERIAIS DE ORÍGEM

Figura 8 - Materiais de origem

ESTEATITO - SERPENTINITO

SAPROLITO

TALCO

TAFONI

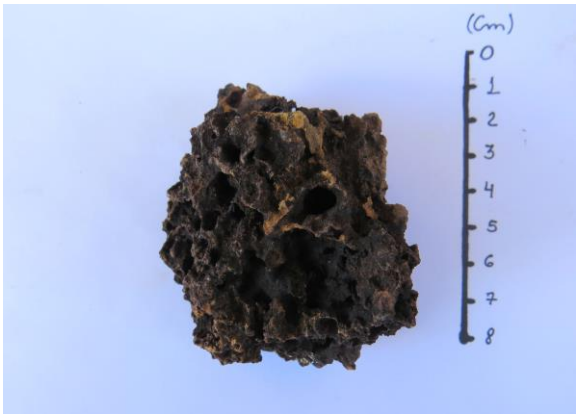

OBSIDIANA

MAGNETITA

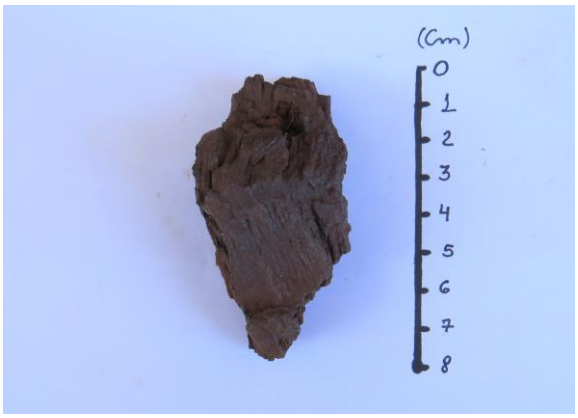

MICROMORFOLOGIA

Figura 9 - Seções delgadas da rocha esteatito-serpentinito, corte longitudinal (a, b); corte Transversal (c, d), aumento de 40 X. Luz polarizada planar (a, c), luz polarizada cruzada (b, d), Largura das imagens 2,3 mm.

ESTEATITO - SERPENINITO

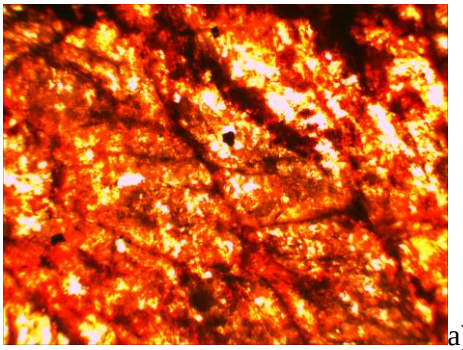
a)

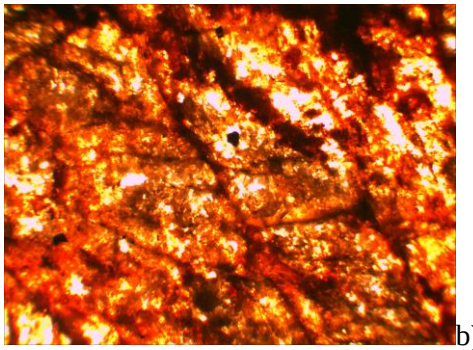
b)

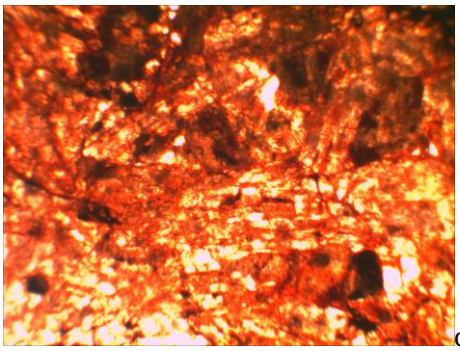
c)

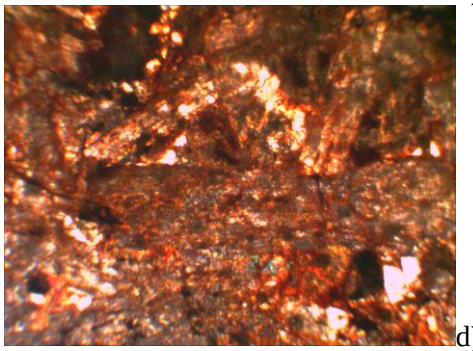
d)

Figura 10 - Seções delgadas do talco, corte longitudinal (a, b); corte transversal (c, d), aumento de 40 X a) luz polarizada planar, b) luz polarizada cruzada, largura das imagens 2,3 mm. Aumento de 100 x, c) luz polarizada planar, d) luz polarizada cruzada, largura das imagens 0,9 mm

TALCO

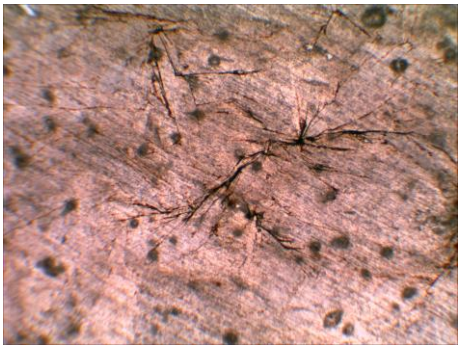

a)

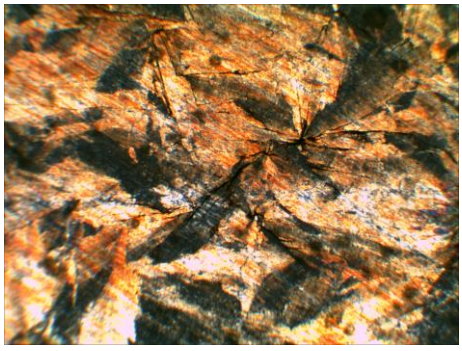

b)

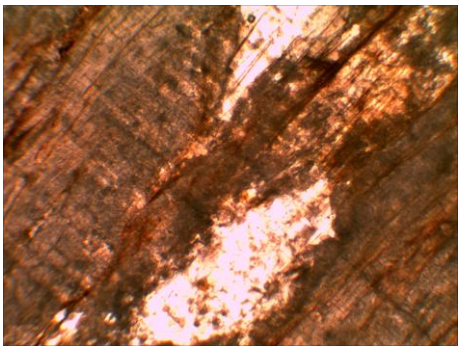

c)

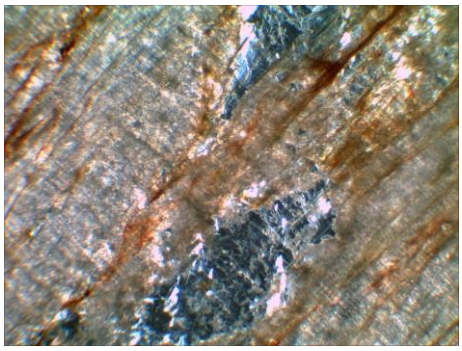

d)

Figura 11 - Seções delgadas da obsidiana, aumento de 40 X a) luz polarizada planar, b) luz polarizada cruzada, largura das imagens 2,3 mm. Aumento de 100 x, c) luz polarizada planar, d) luz polarizada cruzada, largura das imagens 0,9 mm. Notar prováveis cristais de Zeólitas (Barbosa, 1998).

OBSIDIANA

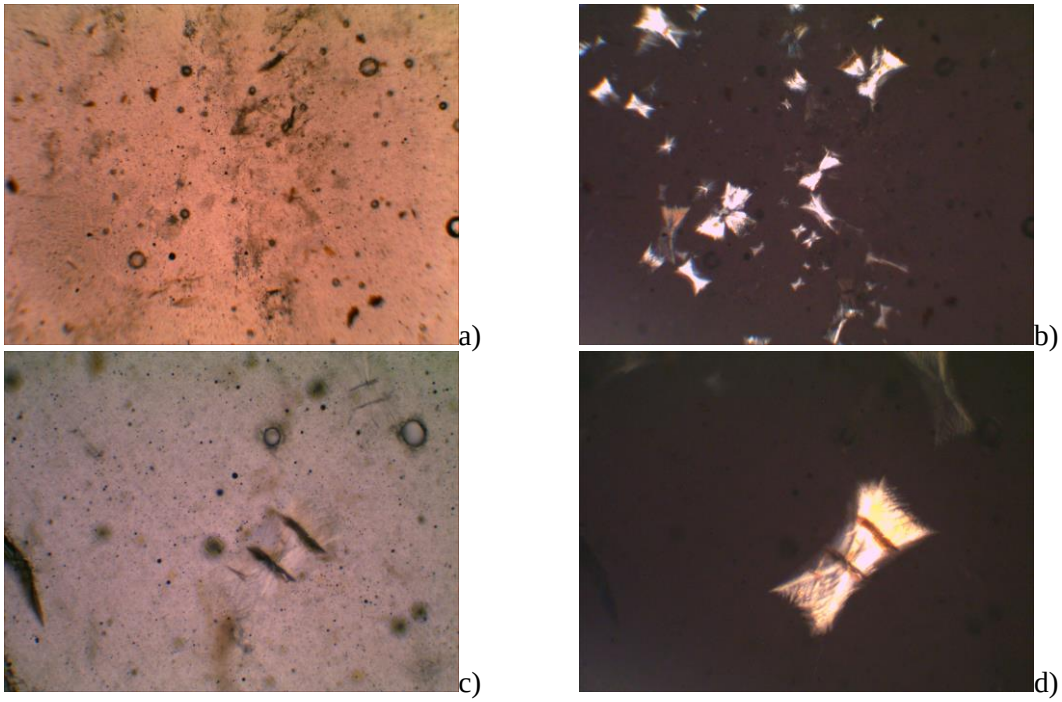

Figura 12 - Seções delgadas do tafoni, aumento de 40 X a,c) luz polarizada planar, b,d) luz polarizada cruzada, largura das imagens 2,3 mm.

TAFONI

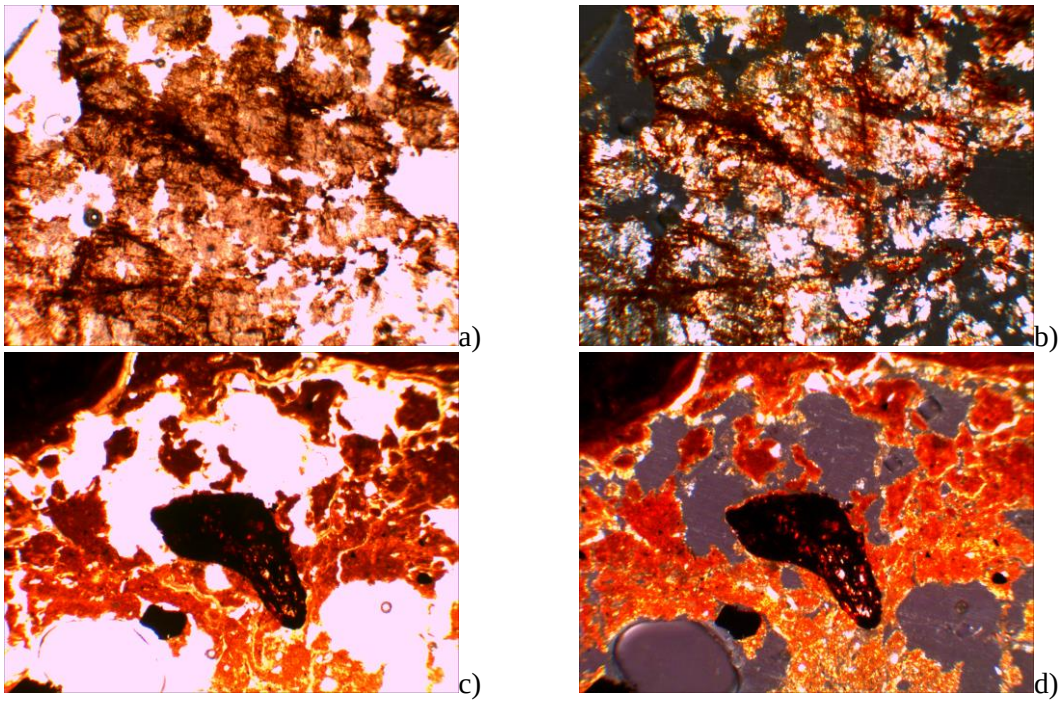

APÊNDICE B

PERFIL NEOSSOLO TOPO

DESCRIÇÃO GERAL

DATA – 21.8.2017

PROPOSTA DE CLASSIFICAÇÃO SiBCS – NEOSSOLO LITÓLICO Distrófico magnésico Tb A moderado textura argilosa fase vegetação Cerrado relevo montanhoso.

LOCALIZAÇÃO, MUNICIPIO, ESTADO E COORDENADAS – Localidade de Aureliano Mourão. Bom Sucesso – MG, 21°06'38.3" S e 44°46'09.4" W .

SITUAÇÃO DO PERFIL – Descrito e coletado em trincheira aberta no topo da montanha, sob vegetação de cerrado.

ALTITUDE – 1018 metros.

DECLIVIDADE – <5%.

LITOLOGIA – Serpentinito/esteatito.

FORMAÇÃO GEOLÓGICA – Maciço Ultramáfico do Morro das Almas. Arqueano (mais de $2.5x10^9$ anos).

MATERIAL ORIGINÁRIO – Produto da alteração da rocha supracitada.

PEDREGOSIDADE – Muito pedregosa.

ROCHOSIDADE – Muito Rochosa.

RELEVO LOCAL montanhoso.

EROSÃO – Laminar não aparente

DRENAGEM – Bem drenado.

VEGETAÇÃO PRIMÁRIA – Cerrado.

USO ATUAL – Reserva de vegetação nativa.

CLIMA – Tropical com inverno seco.

DESCRITO E COLETADO POR – Emerson F Vilela, Yuri L. Zinn e Nathan V. Almeida

DESCRIÇÃO MORFOLÓGICA

A 0 – 6 cm, bruno-avermelhado-escuro (5YR 3/4, úmido) textura argila; estrutura muito fina/pequena, granular; macia/solta, muito friável; plástica e ligeiramente pegajosa.

RAÍZES – muito finas, pouco comuns.

OBSERVAÇÕES – Campo de matacões.

Figura 13 - Foto em lupa da fração areia (2-0,05 mm) do Topo - horizonte A. Notar grãos de Talco (Brancos) e óxidos de Fe (Negros). Quadríciulado: 0.5 x 0.5 cm

Figura 14 - Seções delgadas do topo, aumento de 40 X. Saprolito revestido com material ferruginoso a) luz polarizada planar b) luz polarizada cruzada. Largura das imagens 2,3 mm

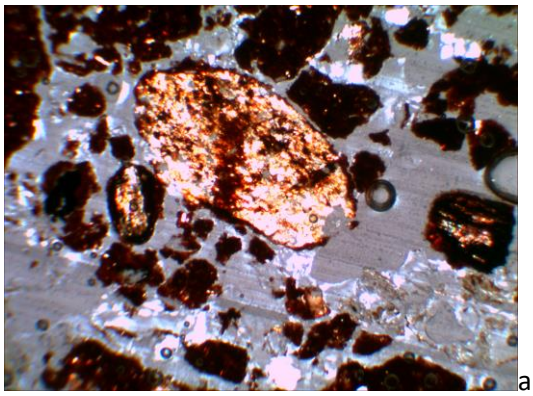
a)

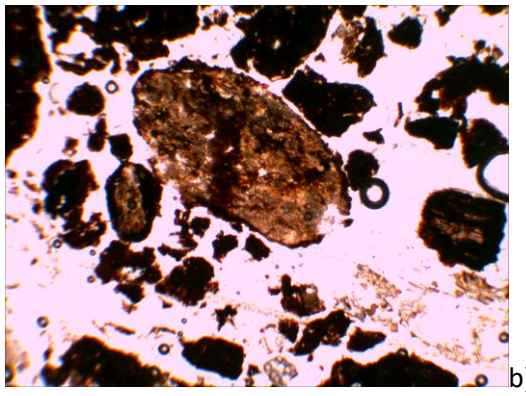
b)

Microestrutura em blocos subangulares para granular, altamente separada e parcialmente acomodada; poros planares e de empacotamento complexo; limite G/F: 21,4 µm; distribuição relativa c/f: porfírica; material grosseiro: fragmentos de rocha (438 µm), talco (85 - 1314 µm), saprolito (273 µm), magnetita fibrosa, quartzo; material orgânico: raízes vivas; micromassa vermelha nebular, trama-b: salpicada e cristalítica talco; pedofeição intrusiva: nódulos de Fe.

ANÁLISES QUÍMICAS E FÍSICAS

Horiz.	$pH_{água}$	pH_{KCl}	Al^{3+}	Ca^{2+}	Mg^{2+}	SB	T	V	CO	Prem	Areia	Argila
	1:2,5		----------$cmol_c$ Kg^{-1}----------					------%------		$mg\ L^{-1}$	----g Kg^{-1}----	
A	5,9	4,9	0,07	0,46	1,16	1,7	6,56	26,36	3.03	15.8	194	424

Teores de elementos químicos da TFSA obtidos pelo ataque sulfúrico e determinados por ICP - OES.

Hor.	SiO_2	Al_2O_3	Fe_2O_3	TiO_2	P_2O_5	MgO	Cr_2O_3	Ki	Kr	Al_2O_3/Fe_2O_3	Cr/Ni	Ti/Zr
	..... dagKg^{-1}											
A	5.56	8.03	36.82	0.45	0.13	1.56	1.71	1.18	0.30	0.34	11.1	56.6

Hor.	CaO	K_2O	MnO_2	Zn	Co	Ni	V	Zr	Cd	Pb	Ba	Ce
	..... dagKg^{-1}			..... ppm								
A	0.05	0.07	0.60	174.4	530.2	1060.5	324.5	48.0	36.2	55.9	88.3	70.3

MINERALOGIA DA FRAÇÃO AREIA

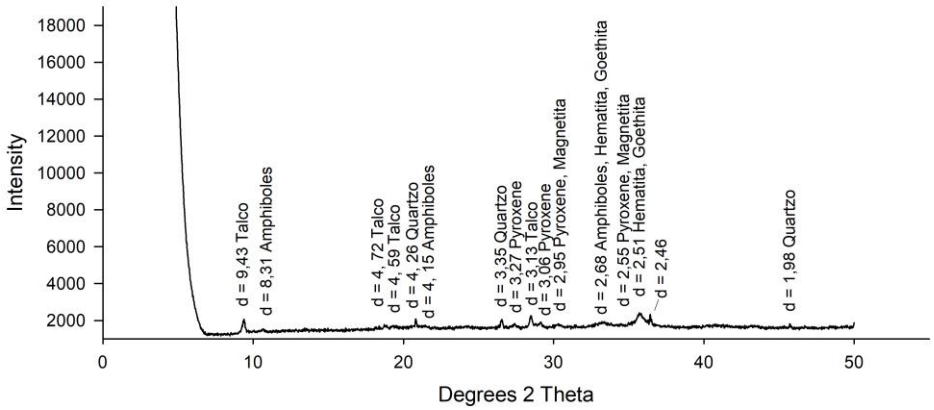

MINERALOGIA DA FRAÇÃO SILTE

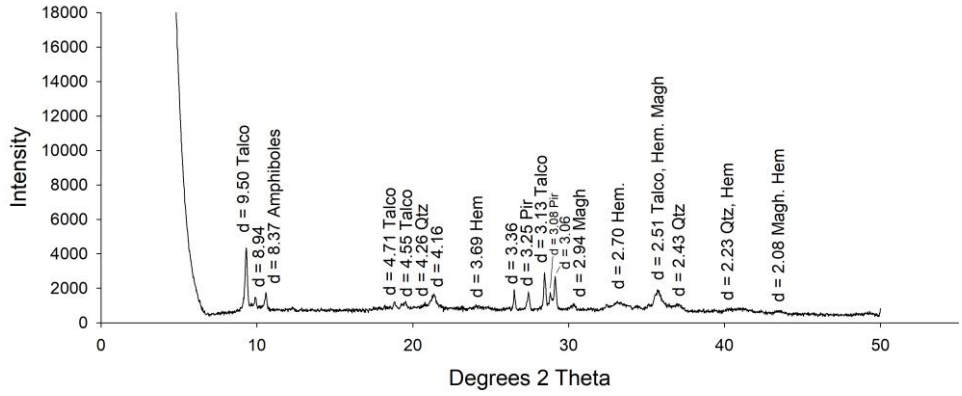

Obs. Radiação Cu-Kα. Serp = Serpentina; Qtz = quartzo; Magh =maghemita; Hem = hematita; Pir = piroxênio

APÊNDICE C

PERFIL FACE NE

DESCRIÇÃO GERAL

DATA – 21.8.2017

PROPOSTA de CLASSIFICAÇÃO SiBCS – NEOSSOLO LITÓLICO Eutrófico fragmentário magnésico Ta A moderado textura argilosa fase vegetação floresta semidecidual relevo montanhoso.

LOCALIZAÇÃO, MUNICIPIO, ESTADO E COORDENADAS – Localidade de Aureliano Mourão. Bom Sucesso – MG, 21°06'19.1" S e 44°46'01.3" W Gr.

SITUAÇÃO DO PERFIL – Descrito e coletado em barranco, em sopé de encosta, com 35 % de declive, sob vegetação de floresta com árvores entre 4 e 6 metros de altura.

ALTITUDE – 873 metros.

DECLIVIDADE – 35 %.

LITOLOGIA – Serpentinito/esteatito.

FORMAÇÃO GEOLÓGICA – Maciço Ultramáfico do Morro das Almas. Arqueano (mais de 2.5×10^9 anos).

MATERIAL ORIGINÁRIO – Produto da alteração da rocha supracitada.

PEDREGOSIDADE – Muito pedregosa.

ROCHOSIDADE –Rochosa.

RELEVO LOCAL – Forte ondulado.

EROSÃO – Laminar não aparente

DRENAGEM – Bem drenado.

VEGETAÇÃO PRIMÁRIA –Floresta semidecidual estacional.

USO ATUAL – Reserva de vegetação nativa.

CLIMA – Tropical com inverno seco.

DESCRITO E COLETADO POR – Emerson F Vilela, Yuri L. Zinn.

DESCRIÇÃO MORFOLÓGICA

A 0 – 30 cm, bruno-avermelhado-escuro (5YR 3/4, úmido); textura franca; estrutura media, granular; ligeiramente dura, muito friável; plástica e pegajosa; transição irregular e descontínua.

RAÍZES – muito finas, comuns e poucas grossas no horizonte A; poucas finas no horizonte B, tornando-se raras finas a partir de 30 cm.

OBSERVAÇÕES – Muito pedregoso, muitas raízes, magnético.

Figura 15 - Seções delgadas da face NE, aumento de 40 X.a) luz polarizada planar b) luz polarizada cruzada Largura das imagens 2,3 mm.

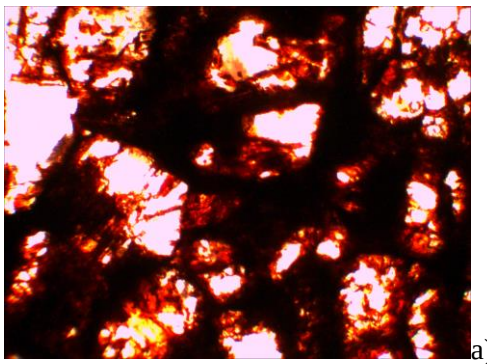

a)

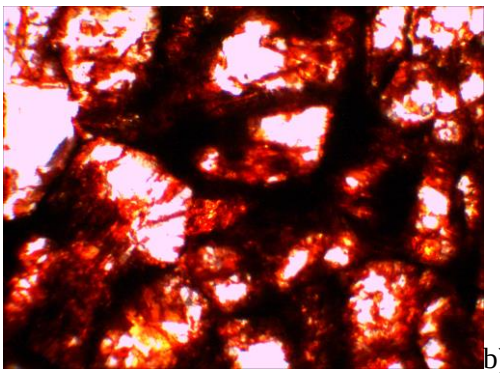

b)

Microestrutura em blocos angulares: acomodada, altamente separada; poros planares; padrão de distribuição aleatório; limite G/F: 43 µm; material grosseiro: quartzo (43 - 186 µm), saprolito, grãos opacos; micromassa vermelha; límpida, trama-b poroestriada salpicada e cristalítica Talco; pedofeição intrusiva: nódulos.

ANÁLISES QUÍMICAS E FÍSICAS

Hor.	$pH_{água}$ 1:2,5	pH_{KCl}	Al^{3+}	Ca^{2+}	Mg^{2+}	SB	T	V	CO	Prem	Areia	Argila
			----------cmol$_c$ Kg^{-1}----------					-----%-----		mgL^{-1}	----g Kg^{-1}----	
A	5,9	4,89	0,08	2,01	3,77	5,9	11,52	51,03	2.65	25.2	149	420

Teores de elementos da TFSA obtidos pelo ataque sulfúrico.

Hor.	SiO_2	Al_2O_3	Fe_2O_3	TiO_2	P_2O_5	MgO	Cr_2O_3	Ki	Kr	Al_2O_3/Fe_2O_3	Cr/Ni	Ti/Zr
	..... dagKg^{-1}.....											
A	12.05	8.38	25.13	0.46	0.11	1.37	0.94	2.45	0.84	0.52	7.07	34.92

Hor	CaO	K_2O	MnO_2	Zn	Co	Ni	V	Zr	Cd	Pb	Ba	Ce
	..... dagKg^{-1}			....ppm.....								
A	0.11	0.08	0.73	182.3	329.7	909.2	339.7	79.7	25.6	29.8	1.2	63.3

MINERALOGIA DA FRAÇÃO AREIA

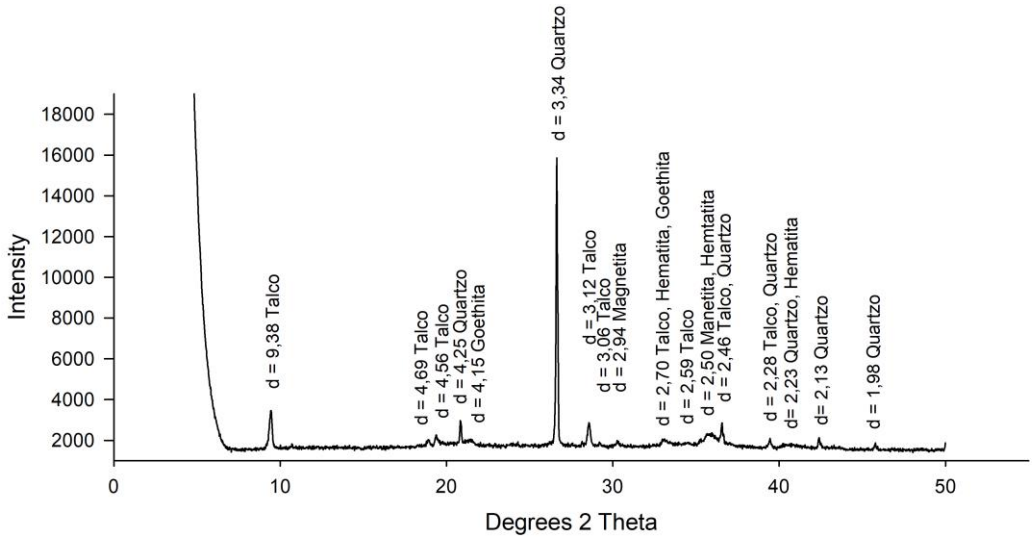

.

MINERALOGIA DA FRAÇÃO SILTE

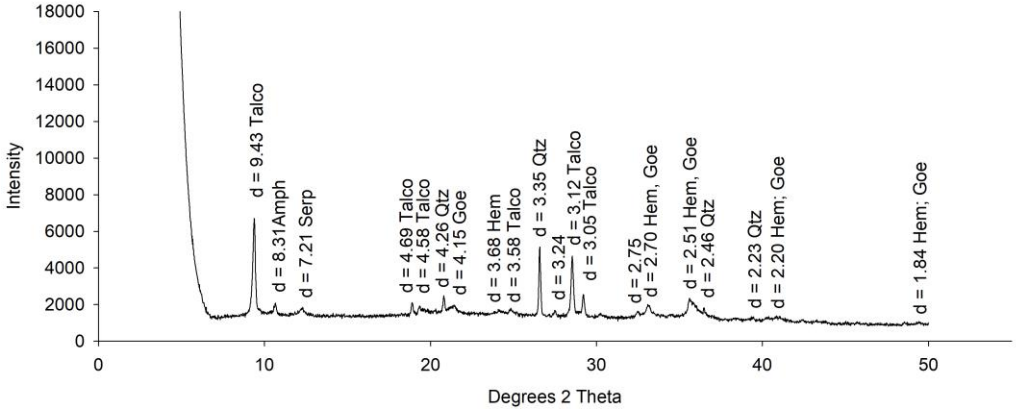

Obs. Radiação Cu-Kα. Amph = amfibólio, serp = serpentina, Qtz = quartzo, Goe = Goethita, Hem = hematita.

APÊNDICE D

PERFIL FACE SUL

DESCRIÇÃO GERAL

DATA – 13.7.2011

PROPOSTA CLASSIFICAÇÃO SiBCS NEOSSOLO LITÓLICO Eutrófico magnésico Ta A moderado textura média fase vegetação Floresta ombrófila relevo montanhoso.

LOCALIZAÇÃO, MUNICIPIO, ESTADO E COORDENADAS – Localidade de Aureliano Mourão. Bom Sucesso – MG, 21°06'53.3" S e 44°46'03.8" W Gr.

SITUAÇÃO DO PERFIL – – Descrito e coletado em trincheira aberta no sopé de encosta, com 90 % de declive, sob vegetação de floresta com árvores entre 4 e 6 metros de altura.

ALTITUDE –846 metros.

DECLIVIDADE – 90%.

LITOLOGIA – Serpentinito/esteatito.

FORMAÇÃO GEOLÓGICA – Maciço Ultramáfico do Morro das Almas. Arqueano (mais de 2.5×10^9 anos).

MATERIAL ORIGINÁRIO – Produto da alteração da rocha supracitada.

PEDREGOSIDADE – Muito pedregosa.

ROCHOSIDADE – Rochosa.

RELEVO LOCAL - Escarpado.

EROSÃO – Laminar forte

DRENAGEM – Bem drenado.

VEGETAÇÃO PRIMÁRIA – Floresta ombrófila do canyon do Rio das Mortes

USO ATUAL – Reserva de vegetação nativa.

CLIMA – Tropical com inverno seco.

DESCRITO E COLETADO POR – Emerson F Vilela, Yuri L. Zinn e Nathan V. Almeida

DESCRIÇÃO MORFOLÓGICA

A1 0 – 7 cm, franco-argilossiltoso; estrutura pequena granular; macia, friável; não plástica e não pegajosa; transição plana e abrupta.

A2 7 -21 cm, bruno avermelho (5 YR 4/3, úmido); franco-argilosa; pequena granular; macia, muito friável; ligeiramente plástica e ligeiramente pegajosa; transição plana e abrupta.

A3 21-25 cm, bruno avermelho escuro (5 YR 3/4, úmido); franco-argilosa; pequena granular; macia, muito friável; plástica e ligeiramente pegajosa

RAÍZES – finas no horizonte O e muito grossas no horizonte A2 e A3.

OBSERVAÇÕES – Ausência de saprolito e tafoni, presença de formigas e minhocas, muito rochoso, canyon do Rio das Mortes. Pedregosidade nos horizontes A2 e A3.

Figura 16 - Foto em lupa da face sul da fração areia (2-0,05 mm) do horizonte A. Notar abundância de Talco, Serpentina e Anfibólio. Quadríciulado: 0.5 x 0.5 cm

Figura 17 - Seções delgadas da face Sul-A2. Presença saprolito e magnetita aumento de 40 X. a) luz polarizada planar b) luz polarizada cruzada. Largura das imagens 2,3 mm.

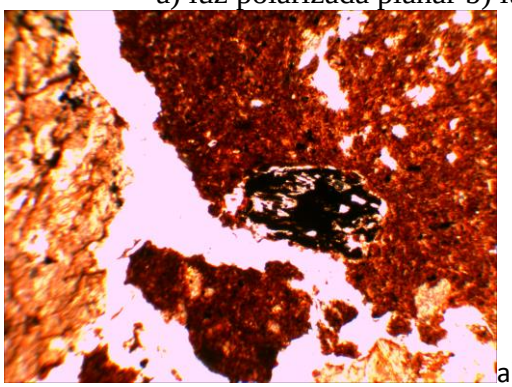
a)

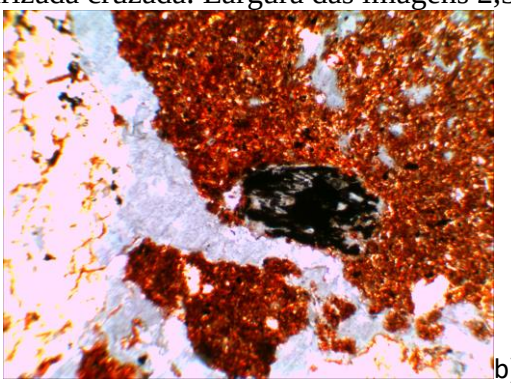
b)

Microestrutura em blocos sugangulares a angulares, altamente separada, parcialmente acomodada; poros planares; padrão de distribuição aleatório; limite G/F: 42 µm; material grosseiro: quartzo angular (42 – 214 µm), fragmentos de serpentinito (164 µm), grãos opacos, saprolito (219 µm); material orgânico: raízes; micromassa vermelha; límpida, trama-b salpicada pontilhada; pedofeição intrusiva: nódulos.

ANÁLISES QUÍMICAS E FÍSICAS

Hor.	$pH_{água}$ 1:2,5	pH_{KCl}	Al^{3+}	Ca^{2+}	Mg^{2+}	SB	T	V	CO	Prem	Areia	Argila
			----------cmol$_c$ Kg^{-1}----------					----%----		mgL^{-1}	----g Kg^{-1}-----	
A1	6,3	5,45	0,06	8,10	6,40	14	18,59	79,21	4,81	41,7	177	308
A2	5,6	4,77	0,11	2,23	4,77	7,1	13,05	54,81	3,09	36,8	253	304
A3	5,6	4,78	0,09	0,52	3,79	4,4	7,48	58,57	1,22	38,5	328	234

Teores de elementos da TFSA obtidos pelo ataque sulfúrico.

Hor.	**SiO_2**	**Al_2O_3**	**Fe_2O_3**	**TiO_2**	**P_2O_5**	**MgO**	**Cr_2O_3**	**Ki**	**Kr**	**Al_2O_3/Fe_2O_3**	Cr/Ni	Ti/Zr
	..... dagKg^{-1}											
A1	6.25	3.19	9.73	0.15	0.11	2.19	0.30	3.33	1.13	0.51	5.60	48.06
A2	6.31	2.98	11.37	0.15	0.07	2.44	0.37	3.60	1.05	0.41	5.32	50.60
A3	6.48	3.10	11.69	0.13	0.05	2.50	0.43	3.56	1.04	0.42	5.48	38.05

Hor	CaO	K_2O	MnO_2	Zn	Co	Ni	V	Zr	Cd	Pb	Ba	Ce
	..... dagKg^{-1}			....ppm.....								
A1	0.71	0.10	0.37	102.3	103.5	362.2	143.5	18.5	9.8	14.1	<LQ	33.2
A2	0.12	0.07	0.30	80.6	90.5	472.2	159.9	17.6	11.1	14.6	<LQ	31.5
A3	0.04	0.07	0.30	71.3	82.2	533.6	171.3	20.1	12.7	25.4	<LQ	30.8

MINERALOGIA DA FRAÇÃO AREIA

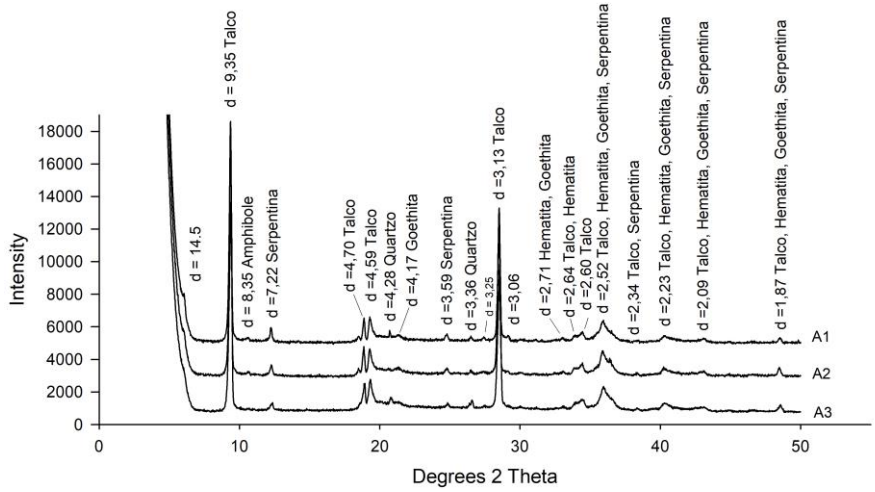

MINERALOGIA DA FRAÇÃO SILTE

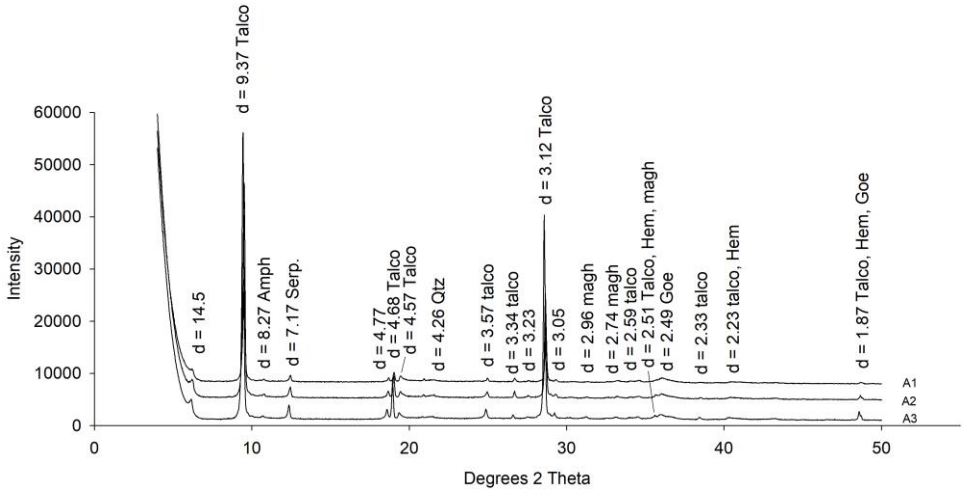

Obs. Radiação Cu-Kα. Serp = Serpentina; Qtz = quartzo; Magh =maghemita; Hem = hematita; Amph = amfibólio, Goe = Goethita, Hem = hematita.

APÊNDICE E

PERFIL SW

DESCRIÇÃO GERAL

DATA – 13.7.2017

PROPOSTA CLASSIFICAÇÃO SiBCS CAMBISSOLO HÁPLICO Tb Distroférrico magnésico, A moderado textura argilosa fase vegetação Floresta ombrófila relevo montanhoso.

LOCALIZAÇÃO, MUNICIPIO, ESTADO E COORDENADAS – Localidade de Aureliano Mourão. Bom Sucesso – MG, 21°07'00.1" S e 44°46'20.7" W Gr.

SITUAÇÃO DO PERFIL – Descrito e coletado em trincheira aberta no sopé de encosta, com 30 % de declive, sob vegetação de floresta com árvores entre 4 e 6 metros de altura.

ALTITUDE –840 metros.

DECLIVIDADE – 30%.

LITOLOGIA – Serpentinito/esteatito.

FORMAÇÃO GEOLÓGICA – Maciço Ultramáfico do Morro das Almas. Arqueano (mais de 2.5×10^9 anos).

MATERIAL ORIGINÁRIO – Produto da alteração da rocha supracitada.

PEDREGOSIDADE Moderadamente pedregosa.

ROCHOSIDADE – Ligeiramente Rochosa.

RELEVO LOCAL – Forte ondulado.

EROSÃO – sulcos profundos

DRENAGEM – Bem drenado.

VEGETAÇÃO PRIMÁRIA – Floresta ombrófila do canyon do Rio das Mortes

USO ATUAL – Reserva de vegetação nativa.

CLIMA – Tropical com inverno seco.

DESCRITO E COLETADO POR – Emerson F Vilela, Yuri L. Zinn e Nathan V. Almeida

DESCRIÇÃO MORFOLÓGICA

A1 0 – 16 cm, bruno escuro (7,5 YR 3/4, úmido), textura argilossiltosa; estrutura granular muito fino; macia, muito friável; não plástica e não pegajosa; transição plana e clara.

A2 17 – 36 cm, bruno-avermelhado-escuro (2,5 YR 3/4, úmido), argila; muito fino / pequena, granular/bloco; macia / ligeiramente dura, muito friável; plástica e ligeiramente pegajosa; transição plana e difusa.

A3 36 - 100 cm, vermelho-amarelo (5 YR 4/6, úmido), argila; muito fino / pequena, granular; macia, muito friável; plástica e pegajosa.

Figura 18 - Seções delgadas da face SW-A3. Presença de óxidos de Fe revestindo saprolito. Aumento de 40 X.a) luz polarizada planar b) luz polarizada cruzada. Largura das imagens 2,3 mm.

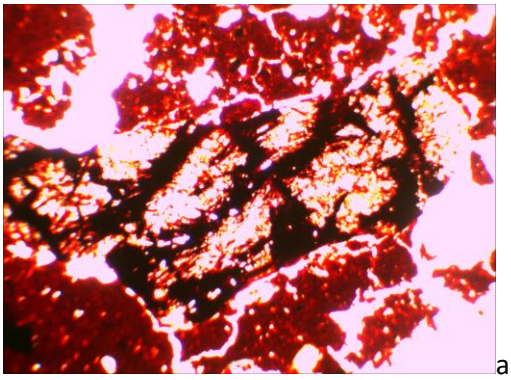
a)

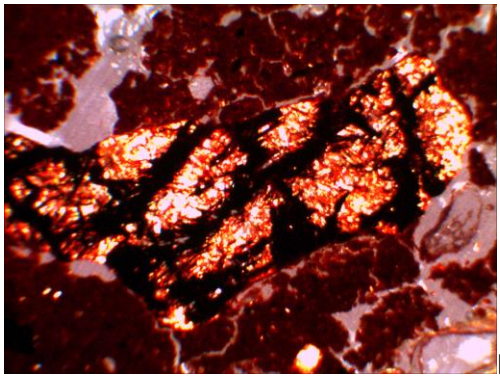
b)

Microestrutura em blocos angulares: acomodada, altamente separada; poros planares; padrão de distribuição aleatório; limite G/F: 17 µm; material grosseiro: talco (30 - 1095 µm), saprolito (186 – 2190 µm), quartzo (17 – 227 µm), fragmentos de rocha (164 – 547 µm), grãos opacos; micromassa vermelha, limpida; trama-b cristalítica talco; pedofeição intrusiva: nódulos.

ANÁLISES QUÍMICAS E FÍSICAS

Horiz.	$pH_{água}$	pH_{KCl}	Al^{3+}	Ca^{2+}	Mg^{2+}	SB	T	V	CO	Prem	Areia	Argila
	1:2,5		----------$cmol_c\ Kg^{-1}$----------					------%------		mgL^{-1}	----g Kg^{-1}----	
A1	5.70	4,94	0.07	4.77	5.47	10	14.99	69.52	4.98	33.8	114	475
A2	5.60	4,75	0.11	1.57	3.01	4.7	11.77	40.12	3.00	20.1	124	511
A3	4.70	4,47	0.18	0.10	0.57	0.7	6.36	11.39	1.61	14.7	120	464

Teores de elementos da TFSA obtidos pelo ataque sulfúrico.

Hor.	SiO_2	Al_2O_3	Fe_2O_3	TiO_2	P_2O_5	MgO	Cr_2O_3	Ki	Kr	Al_2O_3/Fe_2O_3	Cr/Ni	Ti/Zr
	..... $dagKg^{-1}$											
A1	6.41	7.30	24.58	0.38	0.12	0.77	0.95	1.49	0.47	0.47	9.39	58.51
A2	6.20	10.88	35.85	0.50	0.14	0.99	1.47	0.97	0.31	0.48	8.48	51.45
A3	6.93	9.41	30.44	0.48	0.10	0.80	1.31	1.25	0.41	0.49	9.19	51.71

Hor	CaO	K_2O	MnO_2	Zn	Co	Ni	V	Zr	Cd	Pb	Ba	Ce
	..... $dagKg^{-1}$.....			.....	.....	.....ppm.....		.....	.....	.....		
A1	0.41	0.09	0.30	120.6	240.9	657.34	243.8	38.5	24.4	30.6	5.86	44.5
A2	0.12	0.08	0.63	180.7	499.7	1185.74	370.0	58.2	35.2	38.2	<LQ	64.2
A3	0.01	0.07	0.43	122.5	381.9	971.07	323.9	55.4	31.4	31.9	<LQ	41.6

MINERALOGIA DA FRAÇÃO AREIA

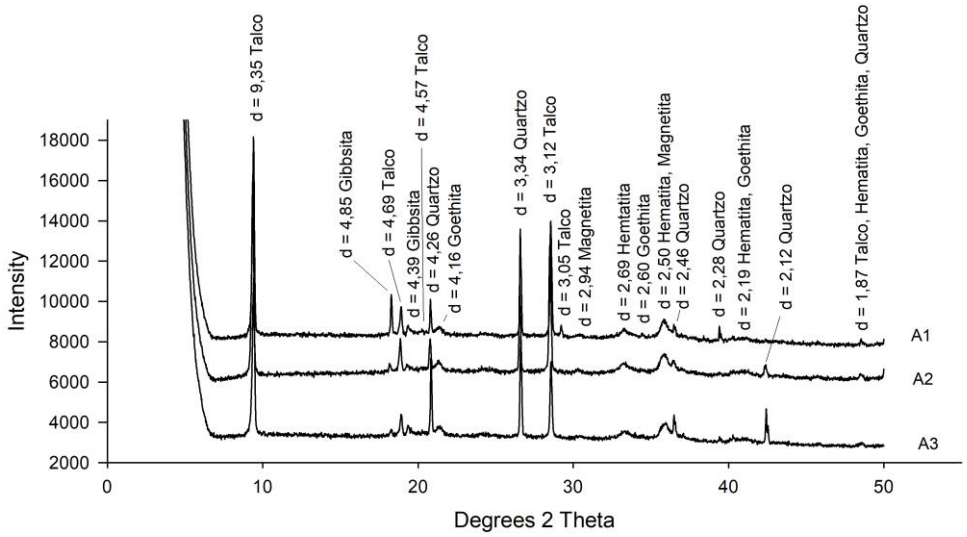

MINERALOGIA DA FRAÇÃO SILTE

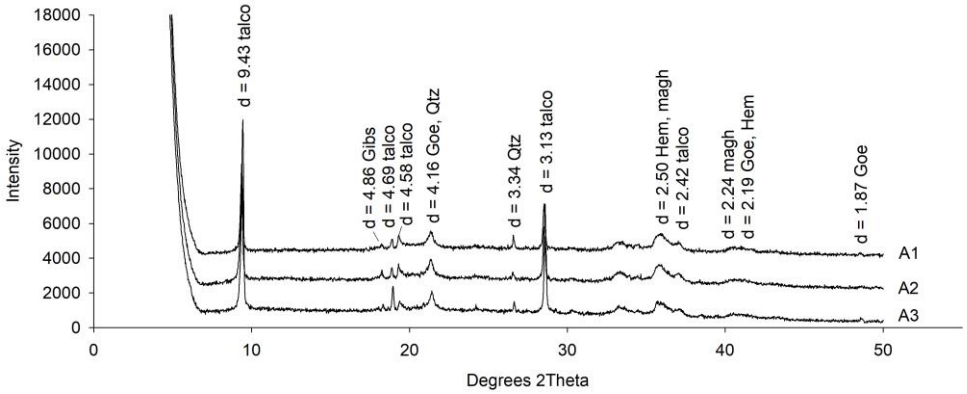

Obs. Radiação Cu-Kα. Qtz = quartzo, Gibs = gibsita, Goe = Goethita, Hem = hematita, magh = maghemita

APÊNDICE F

PERFIL NW

DESCRIÇÃO GERAL

DATA – 13.7.2017

CLASSIFICAÇÃO SiBCS CAMBISSOLO HÁPLICO Tb Distroférrico magnésico, A moderado textura argilosa fase vegetação Cerrado relevo montanhoso.

LOCALIZAÇÃO, MUNICIPIO, ESTADO E COORDENADAS – Localidade de Aureliano Mourão. Bom Sucesso – MG, 21°06'25.7" S e 44°46'17.4" W Gr.

SITUAÇÃO DO PERFIL – Descrito e coletado em barranco de corte de estrada, em terço médio de encosta, com 15 % de declive, sob vegetação de cerrado.

ALTITUDE –963 metros.

DECLIVIDADE – 15 %.

LITOLOGIA – Serpentinito/esteatito.

FORMAÇÃO GEOLÓGICA – Maciço Ultramáfico do Morro das Almas. Arqueano (mais de 2.5×10^9 anos).

MATERIAL ORIGINÁRIO – Produto da alteração da rocha supracitada.

PEDREGOSIDADE Pedregoso.

ROCHOSIDADE – Rochoso.

RELEVO LOCAL – Montanhoso.

EROSÃO – Laminar

DRENAGEM – Bem drenado.

VEGETAÇÃO PRIMÁRIA – Cerrado.

USO ATUAL – Reserva de vegetação nativa.

CLIMA – Tropical com inverno seco.

DESCRITO E COLETADO POR – Emerson F Vilela, Yuri L. Zinn.

DESCRIÇÃO MORFOLÓGICA

A 0 – 16 cm, bruno escuro (7,5 YR 3/4, úmido), textura argilosa; estrutura muito fino/médio, granular; ligeiramente dura, muito friável; ligeiramente plástica e ligeiramente pegajosa; transição plana e abrupta.

AB 16 – 57 cm, bruno avermelhado escuro (5 YR 3/3, úmido), argilosa; muito fino, granular; ligeiramente dura, muito friável; ligeiramente plástica e pegajosa; transição plana e abrupta.

B1 57 – 105 cm, vermelho escuro (2,5 YR 3/6, úmido), argilosa; médio, granular; ligeiramente dura, muito friável; ligeiramente plástica e ligeiramente pegajosa; transição plana e gradual.

B2 105 – 150 cm, vermelho-amarelo (5 YR 4/6, úmido), argilosa; muito fino/médio, granular; muito dura, muito friável; plástica e pegajosa; transição plana e gradual.

B3 150+ cm, bruno forte (7,5 YR 4/6, úmido), argilosa; pequena, granular; muito dura, muito friável; ligeiramente plástica e ligeiramente pegajosa.

Figura 19 - Seções delgadas da face NW-B. Presença de óxidos de Fe revestindo saprolito. aumento de 40 X.a) luz polarizada planar b) luz polarizada cruzada. Largura das imagens 2,3 mm

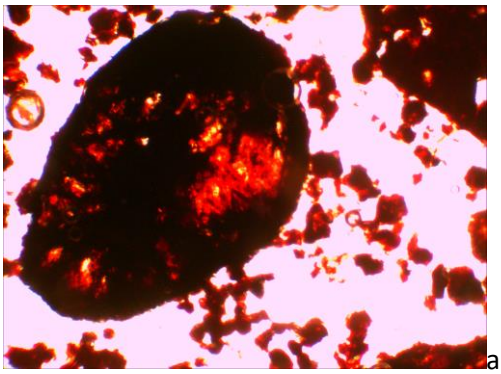
a)

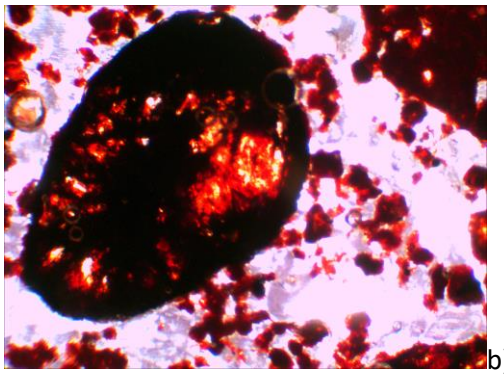
b)

NW AB _ Microestrutura blocos subangulares; altamente separada; acomodada; poros planares e canais**;** padrão de distribuição aleatório; limite G/F: 17 µm; distribuição relativa c/f: porfírica; material grosseiro: saprolito (128 - x µm), quartzo subangular (17 – 383 µm); material orgânico não observado; micromassa: vermelha, límpida; trama-b cristalítica talco; pedofeição intrusiva: nódulos.
NW B1 _ Microestrutura granular; altamente separado; poros de empacotamento compostos; padrão de distribuição aleatório: limite G/F: 17 µm; distribuição relativa G/F porfírica aberta; material grosseiro: quartzo subangular (17 - 214 µm), saprolito (300), fragmentos de talco e serpentina (85 - 328 µm), micromassa vermelha; trama-b salpicada pontilhada, límpida; pedofeição intrusiva: nódulos de Fe.

ANÁLISES QUÍMICAS E FÍSICAS

Horiz.	$pH_{água}$ 1:2,5	pH_{KCl}	Al^{3+}	Ca^{2+}	Mg^{2+}	SB	T	V	CO	Prem	Areia	Argila
			----------$cmol_c$ Kg^{-1}----------					-----%-----		mgL^{-1}	----g Kg^{-1}-----	
A	5,7	4.81	0.11	1.30	2.47	3.9	9.53	41.45	2.81	23.1	153	492
AB	5,8	5.06	0.04	0.10	0.99	1.2	4.8	24.64	1.58	18.1	230	430
B1	5,8	6.72	0.00	0.10	0.23	0.3	1.7	20.34	0.37	3.1	109	571
B2	6,2	6.93	0.00	0.10	0.32	0.4	1.82	23.64	0.15	3.9	128	493
B3	6,7	6.77	0.00	0.10	0.42	0.5	1.92	27.62	0.19	1.3	141	577

Teores de elementos químicos da TFSA obtidos pelo ataque sulfúrico, determinados por ICP - OES.

Hor.	SiO_2	Al_2O_3	Fe_2O_3	TiO_2	P_2O_5	MgO	Cr_2O_3	Ki	Kr	Al_2O_3/Fe_2O_3	Cr/Ni	Ti/Zr
	..... dagKg^{-1}.....											
A	5.50	5.14	24.41	0.23	0.11	1.16	0.93	1.82	0.45	0.33	8.29	46.26
AB	4.88	5.76	29.51	0.22	0.10	1.12	1.33	1.44	0.34	0.31	10.08	34.14
B1	4.39	8.04	33.23	0.24	0.08	0.65	1.27	0.93	0.25	0.38	6.97	41.04
B2	4.10	6.88	32.75	0.21	0.07	0.54	1.36	1.01	0.25	0.33	6.76	39.08
B3	5.51	6.86	42.73	0.21	0.07	0.59	2.12	1.37	0.27	0.25	5.41	35.72

Hor	CaO	K_2O	MnO_2	Zn	Co	Ni	V	Zr	Cd	Pb	Ba	Ce
	..... dagKg^{-1}			....ppm.....								
A	0.07	0.08	0.28	137.5	177.5	765.2	200.8	29.3	22.4	30.2	2.5	32.2
AB	0.03	0.07	0.42	119.6	251.8	899.7	240.4	38.2	29.2	25.7	0.8	36.2
B1	0.02	0.07	0.32	112.9	260.4	1243.9	257.9	34.5	32.6	30.4	2.6	69.0
B2	0.01	0.07	0.32	104.1	255.6	1378.2	233.9	32.6	31.8	25.9	0.7	41.2
B3	0.03	0.07	0.72	138.2	446.6	2678.0	277.9	35.1	43.8	43.0	3.5	40.1

MINERALOGIA DA FRAÇÃO AREIA

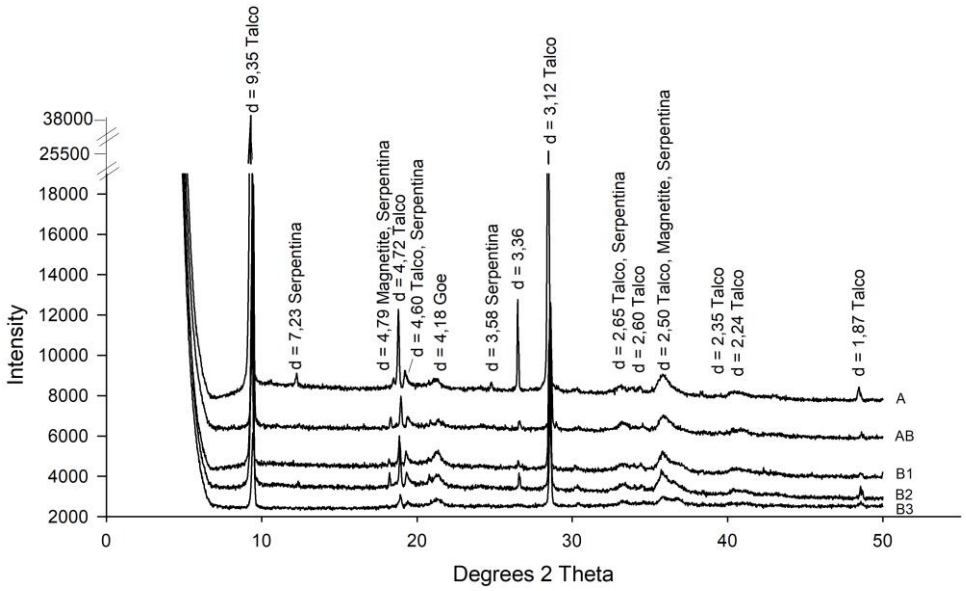

MINERALOGIA DA FRAÇÃO SILTE

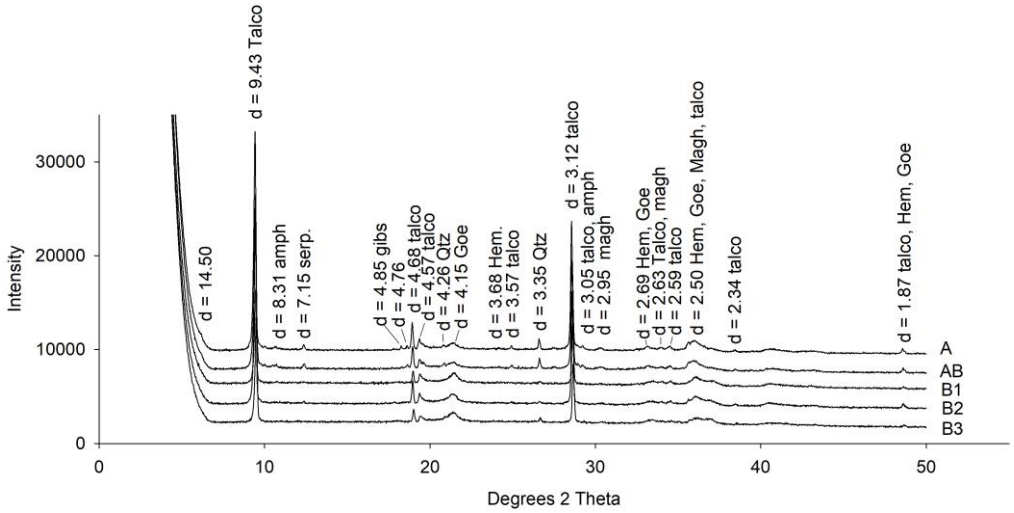

Obs. Radiação Cu-Kα. Serp = Serpentina; Qtz = quartzo; Magh =maghemita; Hem = hematita; Pir = piroxênio, amph = anfibólio.

APÊNDICE G

PERFIL FACE W

DESCRIÇÃO GERAL

DATA – 13.7.2017

PROPOSTA CLASSIFICAÇÃO SiBCS Latossolo Vermelho Perférrico A moderado textura argilosa fase vegetação Cerrado/Pastagem relevo montanhoso.

LOCALIZAÇÃO, MUNICIPIO, ESTADO E COORDENADAS – Localidade de Aureliano Mourão. Bom Sucesso – MG, 21°06'45.5" S e 44°46'22.9" W.

SITUAÇÃO DO PERFIL – Descrito e coletado em trincheira aberta em solo sob pastagem, com 14 % de declive.

ALTITUDE –947 metros.

DECLIVIDADE – 14 %.

LITOLOGIA – Serpentinito/esteatito.

FORMAÇÃO GEOLÓGICA – Maciço Ultramáfico do Morro das Almas. Arqueano (mais de 2.5×10^9 anos).

MATERIAL ORIGINÁRIO – Produto da alteração da rocha supracitada.

PEDREGOSIDADE Pedregosa.

ROCHOSIDADE – Rochosa.

RELEVO LOCAL – Montanhoso.

EROSÃO – Laminar

DRENAGEM – Bem drenado.

VEGETAÇÃO PRIMÁRIA – Cerrado.

USO ATUAL – Pastagem.

CLIMA – Tropical com inverno seco.

DESCRITO E COLETADO POR – Emerson F Vilela, Yuri L. Zinn. Nathan V. Almeida

DESCRIÇÃO MORFOLÓGICA

A 0 – 15 cm, vermelhado escuro acinzentado (10 R 3/2, úmido), textura argilosiltosa; estrutura pequena/media, granular; macia, muito friável; plástica e pegajosa; transição plana e difusa.

AB 15 – 95 cm, bruno avermelhado escuro (2,5 YR 2,5/4, úmido), argilosiltosa; pequena/media, granular; macia, muito friável; plástica e pegajosa; transição plana e difusa.

B1 95 – 110 cm, vermelho escuro (10 R 3/3, úmido), argila; médio, granular; macia, muito friável; plástica e ligeiramente pegajosa; transição plana e difusa.

B2 110 – 170 cm, bruno avermelhado escuro (2,5 YR 2,5/4, úmido), muito argilosa, médio, granular; macia, muito friável; plástica e pegajosa.

Figura 20 - Foto em lupa da face W na fração areia (2-0,05 mm) do horizonte AB. Notar pouco talco, muitos grãos de óxidos de Fe e Quartzo. Quadríciulado: 0.5 x 0.5 cm

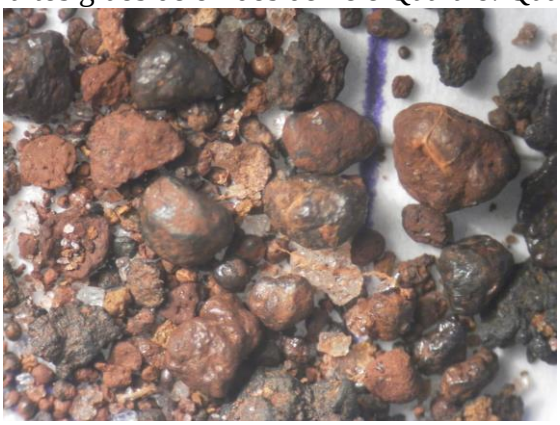

Figura 21. Seções delgadas da face W-B. Presença de óxidos de Fe revestindo saprolito. aumento de 40 X. a) luz polarizada planar b) luz polarizada cruzada. Largura das imagens 2,3 mm

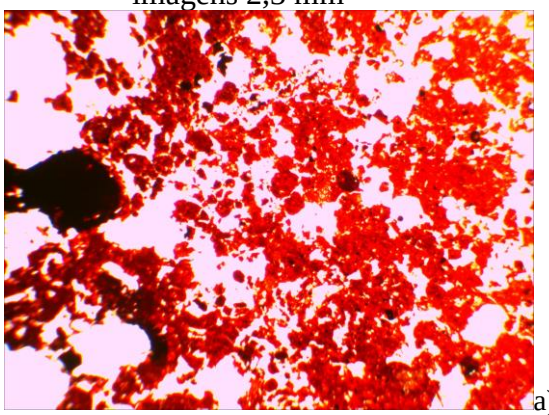

a)

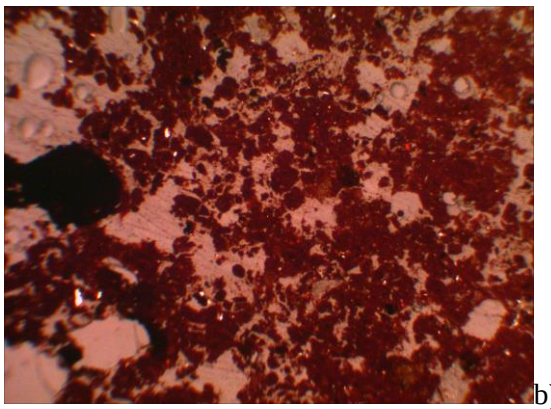

b)

ANÁLISES QUÍMICAS E FÍSICAS

Horiz.	$pH_{água}$ 1:2,5	Al^{3+}	Ca^{2+}	Mg^{2+}	SB	T	V	CO	Prem	Areia	Argila
		----------$cmol_c\ Kg^{-1}$----------					-----%-----		mgL^{-1}	-----g Kg^{-1}-----	
A	6.18	0.00	1.89	1.59	3.6	6.25	58	1.90	9.8	95	402
AB	5.77	0.03	0.36	0.29	0.7	3.28	21	1.35	4.7	84	463
B1	6.61	0.03	0.10	0.11	0.2	1.93	12	0.50	1.2	93	574
B2	6.86	0.03	0.17	0.27	0.5	2.1	22	0.33	1.5	91	642

Teores de elementos químicos da TFSA obtidos pelo ataque sulfúrico e determinados por ICP - OES.

Hor.	SiO_2	Al_2O_3	Fe_2O_3	TiO_2	P_2O_5	MgO	Cr_2O_3	Ki	Kr	Al_2O_3/Fe_2O_3	Cr/Ni	Ti/Zr
	..... $dagKg^{-1}$											
A	7.69	3.20	46.02	0.48	0.13	0.18	1.97	4.08	0.40	0.11	8.40	35.13
AB	7.38	3.34	47.86	0.48	0.12	0.13	1.98	3.75	0.37	0.11	9.13	35.65
B1	7.49	3.84	51.83	0.47	0.13	0.09	1.97	3.31	0.34	0.12	10.60	29.04
B2	7.36	4.00	51.44	0.47	0.14	0.08	1.90	3.13	0.34	0.12	10.12	27.01

Hor	CaO	K_2O	MnO_2	Zn	Co	Ni	V	Zr	Cd	Pb	Ba	Ce
	..... $dagKg^{-1}$			....ppm.....								
A	0.11	0.09	0.67	205.3	532.2	1602.8	531.0	82.5	46.7	55.3	53.7	72.2
AB	0.02	0.08	0.56	175.5	473.8	1481.8	543.8	81.1	46.7	51.7	29.4	61.6
B1	0.05	0.08	0.43	224.7	315.0	1274.3	599.6	97.3	49.1	48.6	2.5	59.1
B2	0.03	0.09	0.57	199.6	372.8	1282.4	596.2	103.5	49.2	62.4	0.4	74.7

MINERALOGIA DA FRAÇÃO AREIA

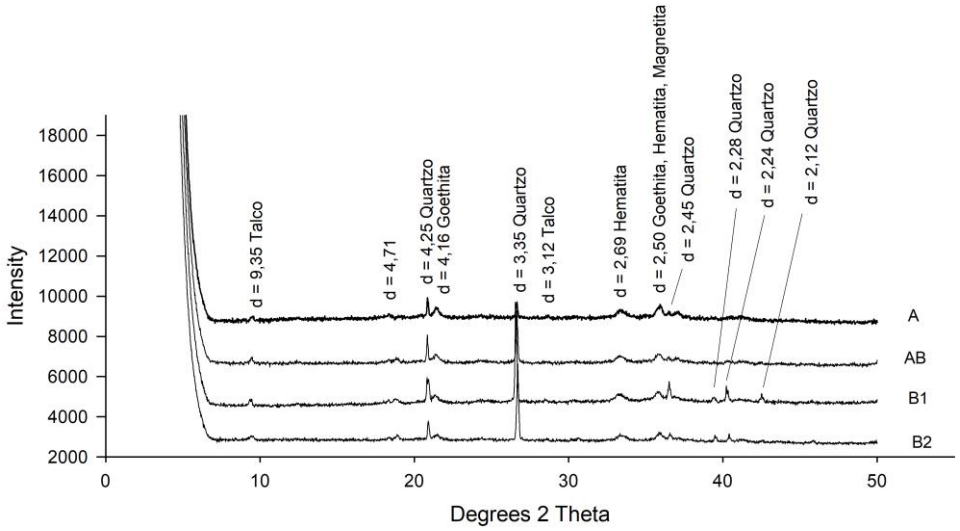

MINERALOGIA DA FRAÇÃO SILTE

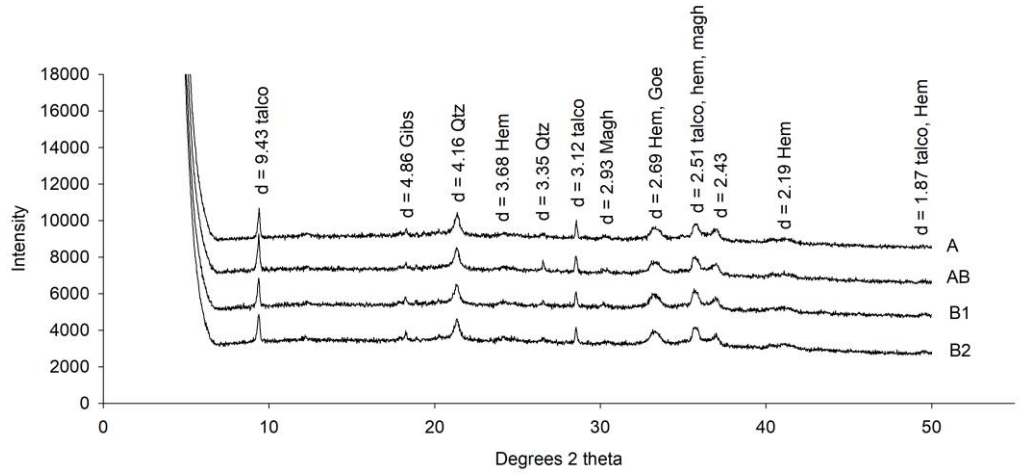

Obs. Radiação Cu-Kα. Serp = Serpentina; Qtz = quartzo; Magh =maghemita; Hem = hematita; Gibs = Gibsita

APÊNDICE H

PERFIL PIEMONTE

DESCRIÇÃO GERAL

DATA – 13.7.2017

PROPOSTA CLASSIFICAÇÃO SiBCS Latossolo Vermelho Perférricos Tb A moderado textura argilosa fase vegetação pastagem relevo montanhoso.

LOCALIZAÇÃO, MUNICIPIO, ESTADO E COORDENADAS – Localidade de Aureliano Mourão. Bom Sucesso – MG, 21°06'00.6" S e 44°46'18.1" W.

SITUAÇÃO DO PERFIL – Descrito e coletado em barranco de corte de estrada em solo sob pastagem, com 20 % de declive.

ALTITUDE –898 metros.

DECLIVIDADE – 20 %

LITOLOGIA – Serpentinito/esteatito.

FORMAÇÃO GEOLÓGICA – Maciço Ultramáfico do Morro das Almas. Serra de bom Sucesso. Supergrupo Minas. Arqueano (mais de 2.5×10^9 anos).

MATERIAL ORIGINÁRIO – Produto da alteração da rocha supracitada.

PEDREGOSIDADE – Não observado.

ROCHOSIDADE – Não observado.

RELEVO LOCAL – Ondulado.

EROSÃO – Laminar

DRENAGEM – Bem drenado.

VEGETAÇÃO PRIMÁRIA – Vegetação savânica conjugada a floresta semidecidual estacional.

USO ATUAL – Pastagem.

CLIMA – Tropical com inverno seco.

DESCRITO E COLETADO POR – Emerson F Vilela, Yuri L. Zinn

DESCRIÇÃO MORFOLÓGICA

Ap 0 – 5 cm, Bruno avermelhado escuro (2,5 YR 2,5/4, úmido), --------- ; muito fina/pequena, granular; macia/solta, muito friável; plástica e ligeiramente pegajosa; transição plana e difusa.

A2 6 – 36 cm, bruno avermelhado escuro (2,5 YR 2,5/4, úmido), francoargilosa; muito fina/pequena, granular; macia, muito friável; plástica e ligeiramente pegajosa; transição plana e difusa.

B1 36 – 140 cm, bruno avermelhado escuro (2,5 YR 2,5/4, úmido), francoargilosa; muito fina/pequena, granular; macia/solta, muito friável; plástica e ligeiramente pegajosa; transição plana e difusa.

B2 140 – 200+ cm, vermelho muito escuro-acinzentado (10 R 2,5/2, úmido), francoargilosa; muito fina/pequena, granular; ligeiramente dura, muito friável; plástica e ligeiramente pegajosa.

Figura 22. Foto em lupa da face Piemonte-BW1na fração areia (2-0,05 mm) do horizonte A2. Notar grãos alongados de magnetita fibrosa.

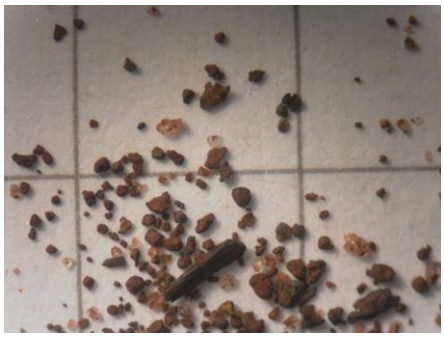

Figura 23 - Seções delgadas da face Piemonte-BW1. Presença de óxidos de Fe revestindo saprolito. aumento de 40 X.a) luz polarizada planar b) luz polarizada cruzada. Largura das imagens 2,3 mm

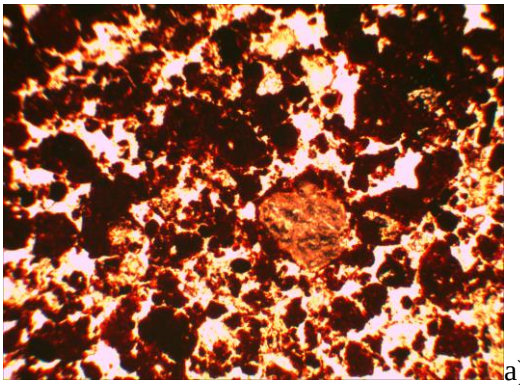
a)

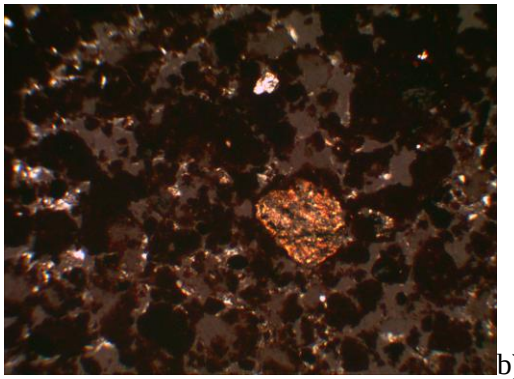
b)

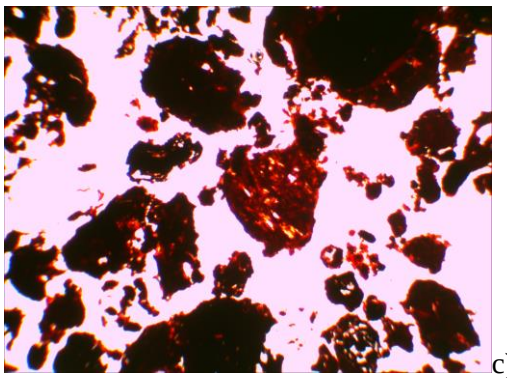
c)

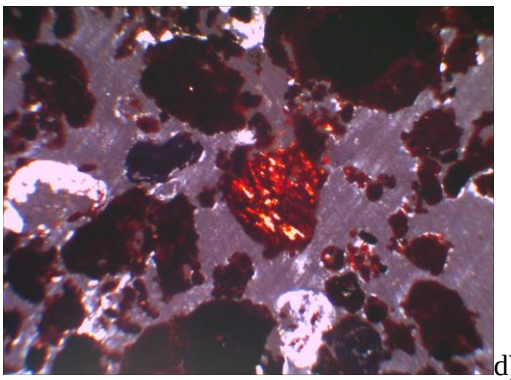
d)

Piemonte A1 _ Microestrutura granular, alta a fracamente separada, padrão de arranjamento aleatório; poros de empacotamento compostos; padrão de distribuição aleatório; limite G/F: 30 µm; distribuição relativa G/F: porfírica; material grosseiro: quartzo subangular, pequenos grãos opacos; material orgânico não observado; micromassa vermelha; nebular, trama-b granoestriada e cristalítica talco, pedofeição intrusiva: nódulos de Fe.

Piemonte BW1 _ Microestrutura granular; poros de empacotamento; limite G/Fa) : 25 µm ; distribuição relativa G/F: porfírica aberta; trama não diferenciada; material grosseiro: fragmentos de rocha intemperizada, quartzo subangular (25 – 328 µm diâmetro), fragmentos de serpentinito (109 – 438 µm diâmetro), saprolito de serpentinito (0,76 – 1,53 µm), pequenos grãos opacos; material orgânico: não observado; micromassa: vermelha e amarelo, límpida; pedofeição intrusiva: nódulos, com efervescência em peróxido de hidrogênio.

ANÁLISES QUÍMICAS E FÍSICAS

Horiz.	$pH_{água}$ 1:2,5	pH_{KCl}	Al^{3+}	Ca^{2+}	Mg^{2+}	SB	T	V	CO	Prem	Areia	Argila
			----------cmol$_c$ Kg^{-1}----------					----%----		mgL^{-1}	-----g Kg^{-1}-----	
Ap	5.30	5.30	0.40	1.61	1.33	3.1	7.11	43	2.63	13.2		
A2	6.30	5.42	0.03	1.73	0.35	2.1	5.75	37	2.77	5.6	330	348
Bw1	6.20	6.10	0.03	0.24	0.28	0.5	2.69	20	1.31	2.9	292	390
Bw2	6.60	6.54	0.05	0.12	0.20	0.3	2	17	0.56	2.7	313	410

Teores de elementos químicos da TFSA obtidos pelo ataque sulfúrico e determinados por ICP - OES.

Hor.	SiO_2	Al_2O_3	Fe_2O_3	TiO_2	P_2O_5	MgO	Cr_2O_3	Ki	Kr	Al_2O_3/Fe_2O_3	Cr/Ni	Ti/Zr
	..... dagKg^{-1}											
AP	5.00	12.46	50.67	0.49	0.16	0.40	2.50	0.68	0.19	0.39	4.55	39.94
A2	5.19	3.45	59.86	0.47	0.17	0.38	2.78	2.56	0.21	0.09	4.41	31.30
BW1	4.35	12.31	54.48	0.49	0.13	0.39	2.66	0.60	0.16	0.35	3.94	39.68
BW2	4.44	12.30	56.88	0.49	0.13	0.34	2.79	0.61	0.16	0.34	4.75	39.44

Hor	CaO	K_2O	MnO_2	Zn	Co	Ni	V	Zr	Cd	Pb	Ba	Ce
	..... dagKg^{-1}			....ppm.....								
Ap	0.07	0.09	0.50	279.8	490.6	3756.4	451.7	72.8	51.0	60.3	5.0	49.1
A2	0.07	0.09	0.76	272.5	693.4	4312.0	548.1	89.8	59.9	69.9	4.1	99.9
BW1	0.02	0.08	0.81	287.6	748.6	4624.3	491.5	73.7	54.8	59.7	16.7	55.9
BW2	0.01	0.09	0.59	265.2	668.1	4012.8	510.7	73.9	55.3	63.0	3.4	68.9

MINERALOGIA DA FRAÇÃO AREIA

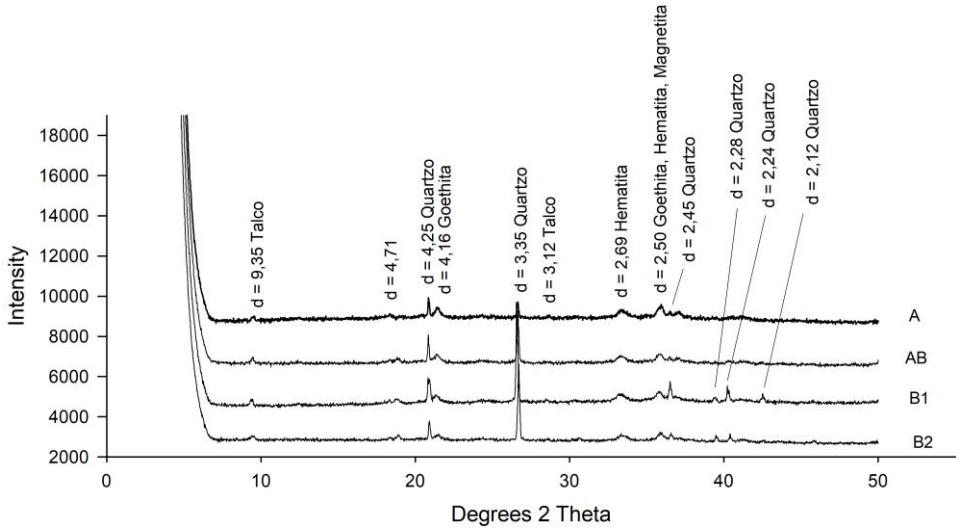

MINERALOGIA DA FRAÇÃO SILTE

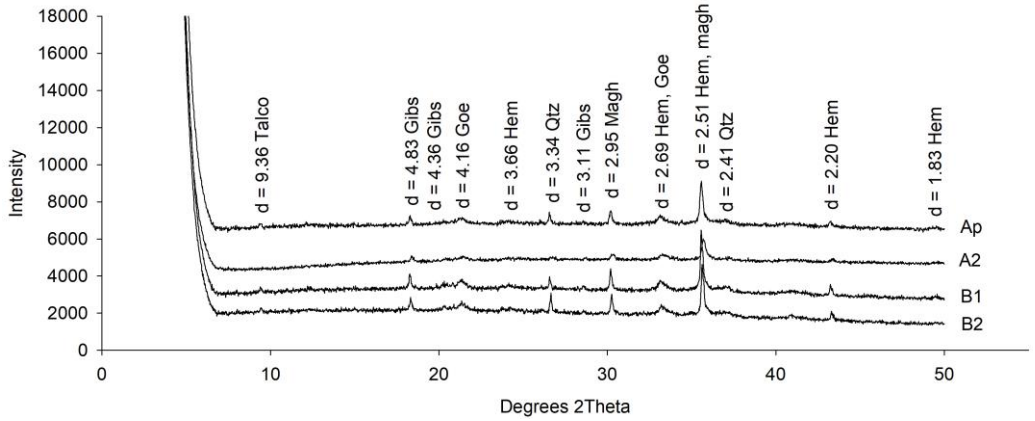

Obs. Radiação Cu-Kα. Serp = Serpentina; Qtz = quartzo; Magh =maghemita; Hem = hematita; Gibs = Gibsita

APÊNDICE I

PERFIL PLINTOSSOLO

DESCRIÇÃO GERAL

DATA – 13.7.2011

PROPOSTA DE CLASSIFICAÇÃO SiBCS – Plintossolo Pétrico concrecionário Tb A moderado textura média fase vegetação savânica conjugada a floresta semidecidual estacional relevo montanhoso.

LOCALIZAÇÃO, MUNICIPIO, ESTADO E COORDENADAS – Localidade de Aureliano Mourão. Bom Sucesso – MG, 21^{O}06'15" S e 44º45"20' W Gr.

SITUAÇÃO DO PERFIL – Descrito e coletado em trincheira aberta em terço médio de encosta, sob vegetação de floresta com árvores entre 4 e 6 metros de altura.

ALTITUDE – 909 metros.

DECLIVIDADE – 16%.

LITOLOGIA – Serpentinito/esteatito.

FORMAÇÃO GEOLÓGICA – Maciço Ultramáfico do Morro das Almas. Serra de bom Sucesso. Supergrupo Minas. Arqueano (mais de 2.5 x 10^9 anos).

MATERIAL ORIGINÁRIO – Produto da alteração da rocha supracitada.

PEDREGOSIDADE – Muito pedregosa.

ROCHOSIDADE – Muito rochosa.

RELEVO LOCAL – Linha de drenagem do piemonte.

EROSÃO – Laminar fraca e sucos

DRENAGEM – não descrito.

VEGETAÇÃO PRIMÁRIA – Vegetação savânica conjugada a floresta semidecidual estacional.

USO ATUAL – Reserva de vegetação nativa.

CLIMA – Tropical com inverno seco.

DESCRITO E COLETADO POR – Marla A. Araujo, Yuri L. Zinn e Alessandro V. Pedroso

DESCRIÇÃO MORFOLÓGICA

A 0 – 8 cm, vermelho muito escuro acinzentado (10 R 2,5/2, úmido); textura franco-siltoso; estrutura não coerente pequena granular; solta, muito friável; cerosidade fraca e rara; não plástica e não pegajosa; transição plana e gradual.

B 8 -100 cm+, vermelho muito escuro acinzentado (5 R 2,5/3, úmido); franco; não coerente pequena granular; solta, muito friável; ligeiramente plástica e não pegajosa;transição plana e gradual.

RAÍZES – muito finas, comuns e poucas grossas no horizonte A; poucas finas no horizonte B, tornando-se raras finas a partir de 60 cm.

OBSERVAÇÕES – Muito cascalho e calhaus ao longo do perfil

Figura 24 - Foto em lupa do Plintossolo fração areia (2-0,05 mm) do horizonte B. Notar quase exclusividade de nódulos de óxidos de Fe

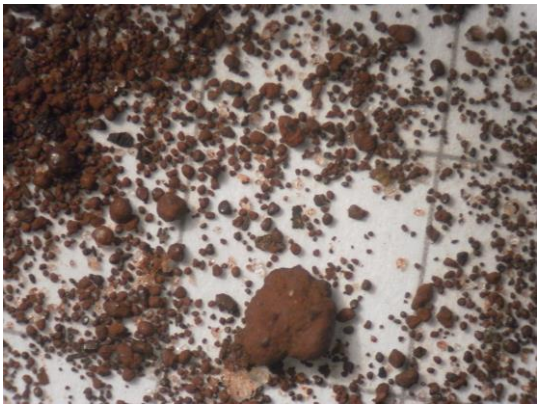

.

Figura 25 - Seções delgadas Plintossolo - B. Presença de óxidos de Fe revestindo saprolito. aumento de 40 X.a) luz polarizada planar b) luz polarizada cruzada. Largura das imagens 2,3 mm

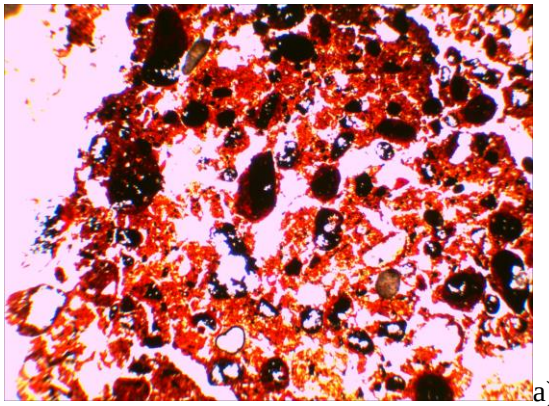
a)

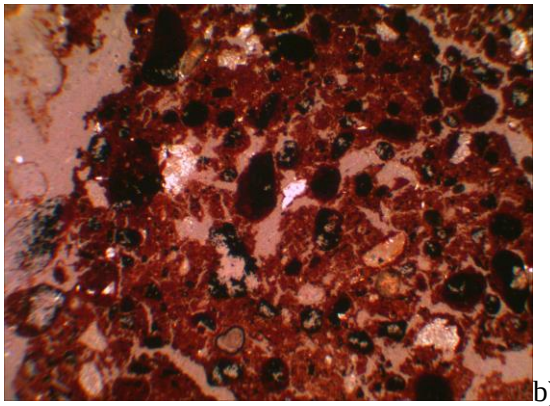
b)

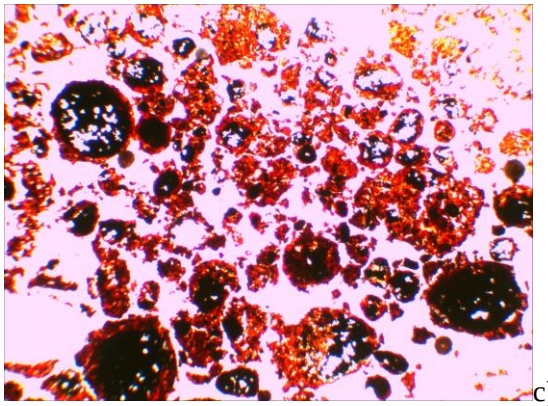
c)

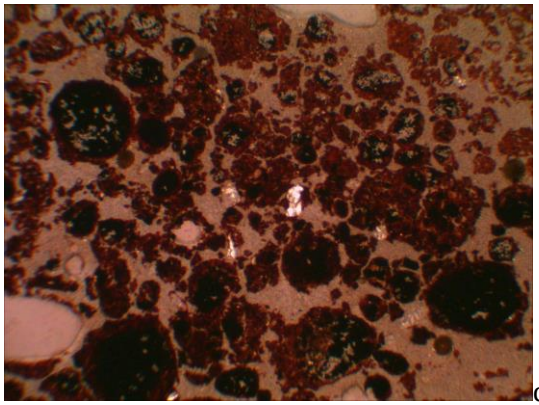
d)

ANÁLISES QUÍMICAS E FÍSICAS

Horiz.	$pH_{água}$	pH_{KCl}	Al^{3+}	Ca^{2+}	Mg^{2+}	SB	T	V	CO	Prem	Areia	Argila
	1:2,5		----------$cmol_c\ Kg^{-1}$----------					-----%-----		mgL^{-1}	-----g Kg^{-1}-----	
A	5,1	5,4	0,2	0,3	1,3	1,7	6,7	26,2		11.7	510	183
B	5,8	6,1	0,1	0,1	0,2	0,3	2,5	12,7		1.3	446	181

Teores de elementos químicos da TFSA obtidos pelo ataque sulfúrico e determinados por ICP - OES.

Hor.	SiO_2	Al_2O_3	Fe_2O_3	TiO_2	P_2O_5	MgO	Cr_2O_3	Ki	Kr	Al_2O_3/Fe_2O_3	Cr/Ni	Ti/Zr
	..... $dagKg^{-1}$.....											
A	2.32	7.86	50.30	0.42	0.12	0.94	3.69	0.50	0.10	0.25	6.42	55.59
Bc	1.64	9.39	65.59	0.48	0.12	0.94	4.96	0.30	0.05	0.22	7.04	51.33

Hor	CaO	K2O	MnO_2	Zn	Co	Ni	V	Zr	Cd	Pb	Ba	Ce
	..... $dagKg^{-1}$			....ppm.....								
A	0.01	0.08	0.76	8.2	342.2	733.9	3934.2	323.2	45.5	51.7	63.7	6.7
B	0.01	0.07	0.99	193.0	435.6	874.7	4820.5	380.8	56.6	64.0	67.6	8.3

MINERALOGIA DA FRAÇÃO AREIA

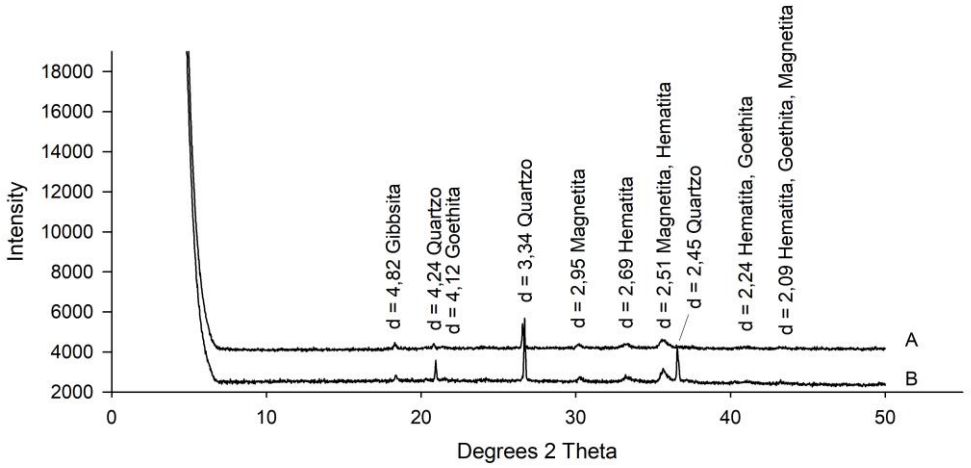

MINERALOGIA DA FRAÇÃO SILTE

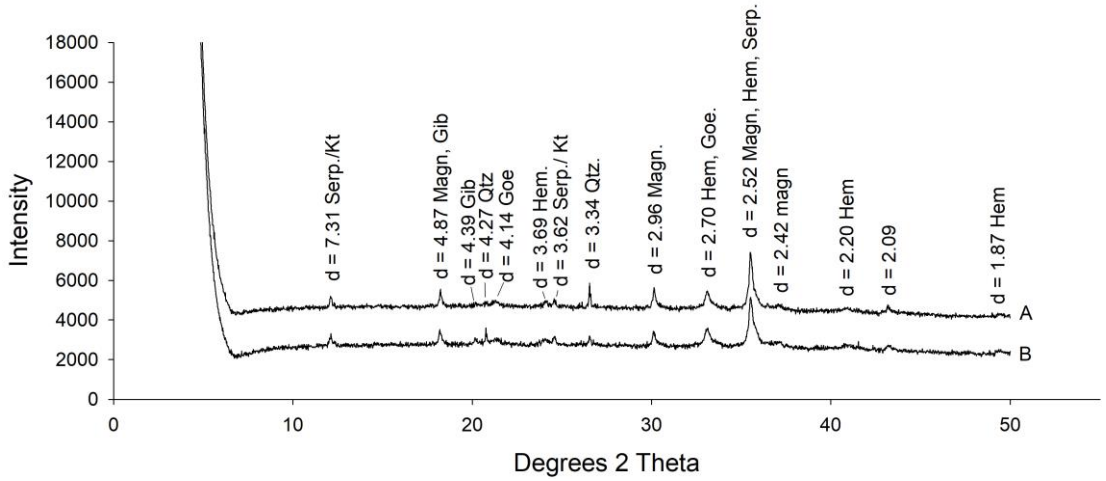

Obs. Radiação Cu-Kα. serp = serpentina, Kt = caulinita, Qtz = quartzo, Goe = Goethita, Hem = hematita, Gbs = Gibsita

Tabela 9. Susceptibilidade magnética em alta (X-HF) e baixa frequência (X-LF) e teor de maghemita (Mh) nas frações TFSA, areia, silte e argila do solos.

			----------TFSA----------			----------Areia----------			----------Silte----------			----------Argila----------			
			X-LF	X-HF	X-FD	X-LF	X-HF	X-FD	X-LF	X-HF	X-FD	X-LF	X-HF	X-FD	Mh
			$(m^3.kg^{-1}).10^{-6}$		%	$(m^3.kg^{-1}).10^{-6}$		%	$(m^3.kg^{-1}).10^{-6}$		%	$(m^3.kg^{-1}).10^{-6}$		%	$g.Kg^{-1}$
TOPO/RL	A	0-6	63.7	58.7	7.9	86.7	84.2	2.9	49.5	46.2	6.6	77.1	67.6	12.3	77.1
NE / RL	A	0-30	39.1	36.3	7.0	52.5	51.1	2.7	28.3	27.2	3.9	56.5	50.5	10.7	56.5
S / RL	O	0-7	11.5	10.7	6.8	19.0	18.4	3.1	19.5	17.7	9.4	18.6	15.8	15.4	18.6
	A1	7-21	11.1	10.3	7.2	11.3	11.2	1.1	10.7	10.3	4.4	19.6	16.7	14.6	19.6
	A2	21-25	9.7	8.9	8.4	6.8	6.6	2.7	6.4	6.3	1.3	22.2	18.5	16.5	22.2
SW / LVA	O	0-16	30.8	28.4	7.9	54.3	52.2	3.8	43.1	39.3	8.8	46.7	40.2	14.0	46.7
	A	17-36	41.8	38.1	8.8	52.2	49.7	4.7	47.6	43.2	9.2	48.4	41.9	13.4	48.4
	B	36-100	43.7	39.7	9.3	50.9	48.8	4.2	40.1	38.1	5.1	51.8	44.6	13.9	51.8
NW / LVA	A	0-16	33.4	30.6	8.5	36.3	35.4	2.5	27.6	26.5	4.1	38.6	33.4	13.3	38.6
	AB	16-57	37.4	34.4	8.0	37.7	36.5	3.1	28.1	27.1	3.7	39.5	34.3	13.0	39.5
	B1	57-105	26.3	23.9	9.0	44.0	42.1	4.4	19.9	18.0	9.4	29.3	25.0	14.8	29.3
	B2	105-150	24.9	22.9	8.2	37.8	36.9	2.4	18.0	16.6	7.4	25.3	21.5	15.0	25.3
	B3	150+	28.0	25.5	8.9	38.6	37.6	2.6	18.5	16.9	8.4	31.3	26.4	15.7	31.3
W / LV	A	0-15	56.8	51.1	9.9	57.7	52.6	8.8	59.9	54.4	9.1	61.3	53.0	13.5	61.3
	AB	15-95	62.0	55.6	10.3	45.3	42.3	6.8	63.8	59.7	6.4	64.6	56.1	13.2	64.6
	B1	95-110	68.5	60.9	11.0	43.4	40.9	5.7	66.7	61.4	7.9	68.7	59.7	13.1	68.7
	B2	110-170+	72.6	64.6	11.1	42.9	40.7	5.2	69.9	63.9	8.5	76.3	66.3	13.1	76.3
Piemonte/LV	AP	0-5	156	151	3.2	192	189	1.2	192	187	2.6	76.0	65.3	14.0	76.0
	A2	6-36	156	150	3.7	173	168	2.8	177	171	3.1	70.0	60.8	13.2	70.0
	BW1	36-140	175	169	3.5	186	183	1.6	200	194	2.9	95.8	82.9	13.4	95.8
	BW2	140-200+	168	162	3.6	177	172	2.6	195	189	3.0	88.1	77.5	12.1	88.1
Plintossolo	A	0-8	207	201	2.8	231	226	2.0	236	228	3.2	173	155	10.6	173
	B	8-100	210	204	3.0	229	229	0.1	221	212	4.1	160	142	11.3	160